2012

Synthesis And Photoluminescence (Pl) Of Gold (I) And Silver (I) Metal Complexes With 1-Methylbenzimidazole Diphenylphosphine (Mbdp): Potential Sensing Applications For Volatile Organic Compounds

Darkus Elizabeth Jenkins
North Carolina Agricultural and Technical State University

SYNTHESIS AND PHOTOLUMINESCENCE (PL) OF GOLD (I) AND SILVER (I) METAL COMPLEXES WITH 1-METHYLBENZIMIDAZOLE DIPHENYLPHOSPHINE (MBDP): POTENTIAL SENSING APPLICATIONS FOR VOLATILE ORGANIC COMPOUNDS

Darkus Elizabeth Jenkins

North Carolina A&T State University

A dissertation submitted to the graduate faculty

in partial fulfillment of the requirements for the degree of

DOCTOR OF PHILOSOPHY

Department: Energy and Environmental Systems

Major: Energy and Environmental Systems (Inorganic Chemistry)

Major Professor: Dr. Zerihun Assefa

Greensboro, North Carolina

2012

School of Graduate Studies
North Carolina Agricultural and Technical State University

This is to certify that the Doctoral Dissertation of

Darkus Elizabeth Jenkins

has met the dissertation requirements of
North Carolina Agricultural and Technical State University

Greensboro, North Carolina
2012

Approved by:

Dr. Zerihun Assefa Major Professor	Dr. Julius Harp Committee Member
Dr. Alex Williamson Committee Member	Dr. Joost de Gouw Committee Member
Dr. Keith Schimmel Department Chairperson	Dr. Sanjiv Sarin Associate Vice Chancellor for Research and Graduate Dean

Biographical Sketch

Darkus Elizabeth Jenkins was born on January 16, 1982, in Savannah, Georgia. She graduated from the Savannah Arts Academy in 2000. She received the Bachelor of Science degree in Chemistry from Savannah State University in 2004 and the Master of Science degree in Chemistry from North Carolina Agricultural and Technical State University in 2007. She is a candidate for the Ph.D. in Energy and Environmental Systems.

Acknowledgments

I would like to thank God for health, strength, and sanity. I wish to express my sincere gratitude to Dr. Zerihun Assefa for motivating independence, cultivating a critical thinker, and molding a scientific researcher. The assistance provided during the period of investigation and writing of this dissertation has been greatly appreciated. Much appreciation is shown to the Department Chairperson, Dr. Keith Schimmel. Special thanks are given to my research advisory committee members Dr. Alex Williamson, and Dr. Julius Harp, Dr. Joost de Gouw. Thank you to the faculty of the Department of Chemistry at North Carolina Agricultural and Technical State University for the additional help required to complete my goals. A special thanks to Cynthia Day and Tanya Pinder at Wake Forest University. Thank you to Dr. Bruce Noll at Bruker AXS. I am overwhelmingly grateful for my best friend, Junia Selby; he has provided an invaluable amount of support during this process. I would also like to thank Seporal Jenkins, Willie and Eleanor Bynes, and a host of family and friends for their support. Thank you to the Department of Chemistry (NCAT) support staff, Ms. C. Mayo, Mr. J. King, and C. Wilson. This project was supported by the National Oceanic and Atmospheric Administration Educational Partnership Program award number NA06OAR4810187.

Table of Contents

List of Figures

List of Tables

List of Symbols

VOC	Volatile Organic Compound
tht	Tetrahydrothiophene
THF	Tetrahydrofuran
HOMO	Highest occupied molecular orbital
LUMO	Lowest unoccupied molecular orbital
MLCT	Metal to ligand charge transfer
LMCT	Ligand to metal charge transfer
MMLCT	Metal – metal to ligand charge transfer
LMMCT	Ligand to metal - metal charge transfer
TPA	1, 3, 5-triaza-7-phosphadamantane
PL	Photoluminescence
PPh_3	Triphenylphosphine
Å	Angstrom
n-Bu_4N^+	Tetrabutylammonium
$BzimPh_2P$	(1-benzyl-2-imidazolyl)diphenylphosphine
MBDP	1-methylbenzimidazole diphenylphosphine
nBuLi	*n*-Butyllithium
DCM	Dichloromethane
^1H	Proton NMR
^{31}P	Phosphorus NMR
UV	Ultraviolet
Vis	Visible

IR	Infrared
NMR	Nuclear magnetic resonance
TMS	Tetramethylsilane
MHz	Megahertz
g	Gram
mL	Milliliters
ppm	Parts per million
DFT	Density Functional Theory
TD-DFT	Time-dependent Density Functional Theory
nm	Nanometer
cm^{-1}	Wavenumber
$CDCl_3$	Deuterated chloroform
CD_3CN	Deuterated acetonitrile

Abstract

Volatile organic compound(s), VOC(s), detection have become a highly demanding area of research due to potential harmful effects to the ecosystem. The search for methods of VOC sensor devices has led to the examination of photoluminescence and photoluminescent materials such as metal complexes. Their luminescent properties markedly with phosphine and/or nitrogen based ligands, bridging ligands, have the ability to accommodate metal atoms with short metal – metal distances. It is of great interest to accomplish short metal interactions as the photoluminescent properties can be altered. We show the synthesis and structural characterization of the bridging ligand, 1-methylbenzimidazole diphenylphosphine. We examined the coordination mode of this ligand to gold (I) and silver (I) metals. The structure of the mononuclear gold (I) complex, a gold (I) dimer, as well as a silver (I) dimer complex were observed in non-polymeric form with notable differences around the metal center. It was also shown the bringing together of two silver dimers by a second bridging ligand, diphenylphosphonic acid, to form a silver tetranuclear complex. The electronic properties of the ligand and metal complexes were also described. The tetranuclear complex displayed temperature dependent photoluminescence when excited by long-wave radiation. Finally, we explored the sensitivity of the dimer gold (I) complex to acetonitrile. Here, we show the synthesis, X-ray crystallography, characterization, and photoluminescence of the ligand, mononuclear complex, dimers of gold (I) and silver (I) complexes, and the tetranuclear complex.

CHAPTER 1

Introduction

The wealth of knowledge in inorganic chemistry has offered to the area of metal complexation a variety of utilities. The development of applications that range from medicinal processes, water treatment methods, to sensor technologies are a small amount of examples in this field of science. It is well known that chemical sensor technology has employed such materials including nanomaterials [1], polymers [2], or metal complexes [3], all having varied physical and chemical properties making them suitable for sensing devices.

1.1. Chemical Sensors

The use of chemical sensors has been found to be useful in a number of areas, of particular interest is in the area of environmental pollutants. One class of environmental pollutant is volatile organic compounds (VOCs). These compounds have relatively high vapor pressures allowing them to escape into the atmosphere in a gaseous state where they can potentially participate in gaseous atmospheric reactions that could lead ozone production of ozone. Albeit, ozone in the stratosphere is useful in protecting the earth's surface from harmful UV radiation, tropospheric ozone is of danger to humans and the ecosystem. Acetonitrile (CH_3CN), a VOC, can be found in the atmosphere and is a major byproduct of biomass burning. Acetonitrile has an atmospheric lifetime of just 1 year, and dissolves primarily in waters. Methods for detection of these types of compounds are of great interest. The development of useful materials for chemical sensors could lead to their potential use in real-time applications.

Roberts and coworkers [4] noted the evolution of harmful isocyanic acid (HCNO) from biomass burning, tobacco smoke, and the combustion of coal/fuels. This study helped to understand the mode of this VOC escape into the atmosphere and its potential links to smoke-

related health issues. Through a series of experiments they were able to show that the sources of HCNO produced enough emissions to negatively impact humans. Albeit this work was not used to quantify the health effects of HCNO, it provided a route to the pathways that lead to production of HCNO and derivatives, including CH_3CN; and also how they can participate in biological processes or cross sensitive membranes that result in carbamylation of proteins, atherosclerosis, cataracts, or rheumatoid arthritis. Moreover, it was also suggested that in developing countries in which small indoor fires are used for warming or cooking the levels of HCNO need to be closely monitored due to the potential health effects. For this reason a sensing device needs to be developed. Furthermore, a non-specific sensor with capabilities of detecting several compounds such as HCNO and its derivatives would be of great use in developing countries.

The types of developmental processes for new sensors are just as important as the end products, fully functional sensors. It is well known that various sensors use different mechanisms to work including infrared [5] and/or microwave energy monitoring, pH monitoring variations [6], and various luminescence [7, 8] techniques. An example of the current technology is vapochromicity, a color change is seen while monitoring luminescence with concomitant exposure to the vapor of an organic solvent or VOC. A sensor using this method works by exposing a substance of known luminescence properties to small amounts of VOC(s), and monitoring the change in luminescent properties visually or by instrumentation.

In a communication published by Kato[9] and coworkers, the vapochromic behavior of a platinum (II) complex is described. X-ray quality crystals were grown from an acetonitrile/ethanol solution yielding head-to-head (*syn*) and head-to-tail (*anti*) isomers. The complex encompassed a platinum dinuclear center with short metal-metal distances of 2.923 and

2.997 Å for the *syn* and *anti* form of the complex, respectively. The isomers are both luminescent and described spectroscopically. It is also of interest to note that the *syn* isomer crystals appeared dark red at room temperature and when exposed to air, the color of the crystals lighten over a period of several hours. The darkening and lightening of the crystals was noted as being reversible. The vapochromism was seen when the complex was introduced to acetonitrile or ethanol vapor causing a change to the luminescence by over 100 nm in the *syn* isomer only. Other spectroscopic techniques including infrared (IR) and proton nuclear magnetic spectroscopy (^{1}H NMR) also indicated that acetonitrile or ethanol were present after vapor exposure. In addition to luminescence shifting or color change, other properties such as increasing or diminishing luminescence are known markers of vapochromism. This can also be seen in examples of other transition metal complexes including platinum [10, 11], ruthenium [12, 13], zinc [14], iridium [15], or gold [16, 17].

It is noteworthy to mention that the central theme of the changes in the photophysical properties are due to changes in inter- and intramolecular metal-metal interactions and/or highest occupied molecular orbital (HOMO) – lowest unoccupied molecular orbital (LUMO) gap differences. The fundamental knowledge is that such properties can be explained by quantum mechanics. The relativistic effects can be seen by examining the frontier molecular orbitals experimentally, as well as, theoretically. It offers a greater understanding of how center metal ion(s) and ligand(s) share electrons and energy in the ground and excited states while also explaining other electronic properties. Some of the electronic properties can then be characterized by which entity, metal or ligand, is dominating in transferring energy through the sharing process described as metal-to-ligand (MLCT) or ligand-to-metal (LMCT) charge transfer. Moreover, those metal complexes that have at minimum two metal ion interactions offer

more interesting transitions. Due to the close proximity of the metals, usually they participate in a charge transfer with each other as well as with the ligand via MMLCT or LMMCT, thereby varying the intensity of the photophysical properties. It is fascinating to exploit different material's chemical properties to increase or decrease the HOMO-LUMO gap further changing their photophysical properties.

When considering gold (I) metal complexes that employ tertiary phosphine ligands, the consequence of the electronic transitions are usually of $\pi \rightarrow \pi^*$, although other transitions are known. This is a direct result of the molecule consisting of at least one conjugated double bond, as conjugation governs this type of electronic transition. It has long been studied the effects of the phosphine ligand on charge transfer in gold (I) metal systems. Almost two decades have passed since Forward [18] and co-workers discussed the topic. In their work they used a zero π-system tertiary phosphine, 1, 3, 5-triaza-7-phosphadamantane phosphine (TPA) and a thiolate ligand, to investigate the Au – Au distances and emission energies. The first comment made by the authors was that the use of the TPA ligand was due to sterics and size, and the second comment was that this ligand has no π-system that evolves from intraligand transitions. This work discussed points surrounding no correlation between emission energy and Au-Au distances. One major point was made regarding the expected low energy representation which not only came from the complexes containing short multinuclear Au units, but also from the complexes with mononuclear Au (I) units. Lifetime measurements supported their conclusions of phosphorescent assignment. Finally, by changing the TPA ligand to triphenylphosphine (PPh_3) a shift from phosphorescence to fluorescence was observed.

1.2. Gold (I) Complexes

The aggregation of gold (I) ions to other gold (I) ions in metal complexes with short

distances, usually less than the sum of their van der Waals radii, is of great interest due to the unusual and unpredictable chemical and physical behavior these compounds display. Researchers have extensively attempted to produce these types of products for a number of uses. The importance of these types of compounds to our research is their photophysical properties. Gold (I) complexes usually exhibit very intensive photoluminescence (PL). The variation in the type of ligand used or the number of metal ions, homo- or hetero-nuclear, present are never exactly the same so no one conclusion can be drawn about gold (I) complexes and photoluminescence [19]. Moreover, the science behind the design of such complexes affords the drive for continued research in this area.

Gold metal complexes have been extensively studied for decades to learn about their photophysical properties. Due to this extensive work with gold, much is known including gold ions exhibits characteristic broad-band luminescent profile [20-26]. Moreover, aurophilicity is the widely accepted term derived to describe the short distances, shorter than the van der Waals radii (~3.7 Å), between gold ions [27, 28]. The aurophilic behavior of gold complexes, bringing gold ions within 2.8 – 3.3 Å of each other, often intensifies the luminescence and can be explained relativitistically. This type of luminescent performance offers gold complexes as a qualifying material for chemical sensors.

King [24] and coworkers provided theoretical and luminescence studies of gold (I) metal-metal interactions in 1989. Since that time, the quantity of research in the area of gold (I) luminescence has continued to grow exponentially. In a communication, the Eisenberg group [20] discussed preliminary findings supporting the reversible luminescence of a linear chain dinuclear gold (I) complex upon interaction of VOCs. They found that upon exposing the crystalline material to air, it lost its orange color and luminescence emission. It was only when

exposure to polar aprotic solvent vapors such acetonitrile or acetone that the color and luminescence properties returned.

More recently, Arvapally [29] and coworkers provided a detailed study of the photophysics and theory of $M[Au(SCN)_2]$ where M is a series of differing salts of n-Bu_4N^+, potassium, rubidium, or cesium. The solid-state luminescence studies conducted by varying the temperatures in the range of 4 – 295 K showed that for all compounds, there are broad emission bands and the energy gaps between excitation and emission is fairly large. They resolved through the phenomenon of simultaneous fluorescence and phosphorescence by using time-resolved luminescence spectroscopy. Finally, the aurophilic, Au-Au emission, is a result of gold-gold bonding excimer occurrence with ligand reorganization. This aids in developing materials for the purpose of having short gold-gold distances.

Most recent, the Laguna [30] group has taken the d^{10} metal-metal interaction to another level by examining the relationship of gold (I) and copper (I). They explored the tetranuclear Au (I) – Cu (I) cluster formation, as well as photophysical and theoretical works. The mixed-metal systems have Au-Cu distances of 2.9565, 2.9538, and 2.9278 for complexes with methyl-4-ethynylbenzoate, alkynyl, and 1-ethynyl-4-methoxybenzene ligands, respectively. The luminescent profiles of the complexes have been characterized as phosphorescent with lifetimes ranging from 0.95 to 8.0 μs and are dependent on the alkynyl ligands.

The behavior of the gold (I) varies vastly. It can be seen that despite the multitude of research in the area of gold chemistry, no definitive conclusion can be made about the mechanism of action for metal – metal interactions. Again, King showed that the Au-Au metal interaction controls the luminescent behavior whereas Laguna showed that ligands control the luminescence profile. Regardless of the mode of luminescence one central idea can be concluded

from this survey, these gold (I) compounds are highly stable at room temperature. If molecular oxygen proved to be a quencher of the luminescence the viability of these types of metal complexes as sensors would be very low. It is here that we choose to further explore gold (I) metal complexes in regard to their optical properties for potential use in optoelectronic devices. Moreover, it is of great interest to further explore the group 11 metals for this purpose, as they too have shown to have interesting photophysical properties.

1.3. Ligands

Phosphines ligands are well known for their ability to coordinate to a gold (I) center. Due to their steric effects and π-acceptor, tertiary phosphines are one of the most studied groups of ligands for gold (I) complexes. Over the past four decades attention has been given to bifuntional ligands with regards to bringing to metal atoms in close proximity[31-34]. In particular, interest has been given to the N,P-type ligand. These ligands follow the Lewis soft acid/base chemistry when coordinating with group 11 metals. Although N is to some extent a lesser soft base than P, (N is a stronger σ-donor and poorer π-acceptor than P) its ability to bind with gold (I) metal ions is well documented [35-39]. Due to relativistic effects for the gold, it is the strong σ-donor properties that support the complexation with N. The ability to bring two gold (I) atoms in close proximity is a goal for many research groups because of the fascinating photoluminescence these types of compounds reveal; a property necessary for making photoluminescent chemical sensors.

The bridging N,P ligands not only coordinate as a monodentate ligand, it also has the ability to structurally act as a bidentate ligand. This multi-mode of coordination has proven to bring homo- and heteronuclear atoms together with short distances. These ligands are thought to offer stability for metal – metal interactions. It is also worth mentioning that the scope of search for this type of ligand should be extended beyond gold (I) complexes, developments in the

literature divulge a host of metal complexes with interesting structures and chemical properties. For example, the lighter metals of group 11 possess the same abilities to coordinate two or more metal atoms in close proximity to each other. There a number of interesting structures of Cu (I) and Ag (I) with N,P ligands [31, 34, 40-43]. These compounds also have interesting luminescent properties, hence further supporting the desire for using this type of ligand.

To demonstrate the strengths of this type of ligand, Burini and co-wokers have extensively studied the N,P type ligand of (1-benzyl-2-imidazolyl)diphenylphosphine ($BzimPh_2P$) to understand the behavior of coordination with various metal systems. They examined this ligand with gold (I), silver (I), copper (I), rhodium (I), iridium (I), mercury (II), zinc (II), and cadmium (II) metal ions. They were able to utilize the monodentate and bidentate feature of the $BzimPh_2P$. In the gold (I) chloride structure, the coordination is monodentate with a near linear geometry P-Au-Cl bond. It is also interesting that they were able to show intermolecular Au – Au distances of 3.306 Å. Through continued work Bachechi along with Burini and co-workers, the X-ray crystal structure of silver complex with the same ligand. Although dinuclear silver (I) interactions were not the result of this work, interesting geometries around the metal ion were observed.

It is clear that an environmental change response system is a necessity. With the potential threat of forest fires releasing a source of acetonitrile into the atmosphere, a rapid response method of detection is needed. For such devices, the variant luminescent profile of a number of metal complexes offers one such solution to a materials need. The versatility of gold (I) complexes and its group members silver (I) and copper (I), lends to the idea that they are suitable for handling the task. They are often found to be stable during and after exposure to the atmosphere, also at room temperature, as well as, having interesting luminescent properties.

Furthermore, it is of great importance to design materials that can host two metal ions in close proximity to each other. To accomplish the task, it is here that we provide viable options for a host in the form of ligands capable of having one or more binding site(s). In addition these ligands should offer support to enhancing the luminescence intensity of the newly designed metal complexes. The final product should have exploitable solvent dependent properties that can be useful in a sensor-type device.

CHAPTER 2

Experimental

2.1. General Procedures

2.1.1. Chemicals. All reactions were carried out by modified or standard Schlenk techniques under dinitrogen (N_2) at room temperature unless otherwise noted. Tetrahydrothiophene gold (I) chloride (thtAuCl) was prepared as described in the literature [44]. Silver tetrafluoroborate ($AgBF_4$), silver hexafluorophosphate ($AgPF_6$), silver trifluoromethanesulfonate ($AgCF_3SO_3$), 1-methylbenzimidazole (MBDP), n-butyllithium (nBuLi), and chlorodiphenylphosphine (PPh_2Cl) were commercially available from the Sigma-Aldrich or Fisher Scientific companies and used without further purification. All solvents (tetrahydrofuran (THF), acetonitrile (CH_3CN), dichloromethane (DCM), diethyl ether (Et_2O), chloroform ($CHCl_3$), and hexanes were degassed using an N_2 purge or used as received.

2.1.2. Physical measurements. The infrared (IR) spectra were collected using potassium bromide (KBr) pellets on a Shimadzu IRPrestige21 Fourier-Transform infrared spectrophotometer, over the range 4000-400 cm^{-1}. The ultraviolet and visible (UV-Vis) spectra was collected using a Shimadzu UV-2401PC UV-Vis spectrometer. The proton (^1H) and phosphorus (^{31}P) nuclear magnetic resonance (NMR) spectra were recorded on a 300 MHz Varian NMR 300 – 411149 FT-NMR spectrometer. Chemical shifts (δ ppm) were reported relative to an internal standard, tetramethylsilane (TMS) for ^1H, while 85% phosphoric acid (H_3PO_4) was used as an external standard for ^{31}P NMR in $CDCl_3$ (if no other solvent is stated). The ^{31}P-NMR spectra were obtained using a 300 MHz Bruker 300 and 300 MHz Varian NMR 300 – 411149 FT-NMR spectrometer. Solid steady-state excitation and emission spectra were collected at 77 K and 298 K on a Photon Technology International PTI model 810/814

Photomultiplier Detection System.

2.2. Synthesis

2.2.1. Preparation of 1-methylbenzimidazole diphenylphosphine (MBDP) (1). To a 250 mL Schlenk flask, (6.6085 g, 50 mmol) 1-methylbenzimidazole is added to 100 mL THF. The solution is allowed to stir until the solid has dissolved. The solution is cooled to -78 ºC in acetone/dry ice bath. To the solution (31.25 mL, 50 mmol) n-BuLi is added slowly. The reaction is allowed to stir for 1 hour. Chlorodiphenylphosphine (9ml, 50mmol) is added drop-wise. The solution is allowed to warm to room temperature and stirred for 3hours. The solvent is evacuated by vacuum to yield an orange foamy product. To this Et_2O and H_2O (50mL each) is added and the organic layer is collected. The Et_2O is removed under vacuum to produce an oily product. The product is sonicated for 10 minutes in warm hexanes. A cloudy layer is formed, collected, and allowed to cool. X-ray quality crystals are produced.

2.2.2. Preparation of tetrahydrothiophene gold (I) chloride and MBDP (2). The thtAuCl (0.0654 g, 0.20 mmol) is dissolved in 10 mL THF in a 25 ml round-bottom flask. The ligand, **1**, (0.0645 g, 0.20 mmol) is added and allowed to stir for 3 hours. The solution is concentrated under vacuum to approximately 3 mL. The solution is layered with 4 mL Et_2O. The flask is placed in the freezer overnight. X-ray quality crystals are formed.

2.2.3. Preparation of gold (I) tetrafluoroborate and MBDP (3). In a 25 mL round-bottom flask, thtAuCl (0.0654 g, 0.20 mmol) is dissolved in 10 mL CH_3CN. The $AgBF_4$ (0.0397 g (0.20 mmol) is added to the flask and stirred for 5 minutes. A white precipitate forms then the solution is filtered through a pad of Celite®. To the filtrant, the ligand, MBDP (0.0645 g, 0.20 mmol) is added and allowed to stir for 3 hours. The solution is concentrated under vacuum to

approximately 3 mL. The solution is layered with Et_2O then the flask is placed in the freezer. After 4 days, X-ray quality crystals are formed.

2.2.4. Preparation of silver tetrafluoroborate and MBDP (4). This reaction is completed with the lights off. In a 25 mL round-bottom flask covered with aluminum foil, $AgBF_4$ (0.0397 g (0.20 mmol) is dissolved in 10 mL CH_3CN. To the solution MBDP (0.0645 g, 0.20 mmol) is added and allowed to stir for 3 hours. The solution is concentrated under vacuum to approximately 3 mL then layered with Et_2O. The flask is placed in the freezer. X-ray quality crystals are formed.

2.2.5. Preparation of silver trifluoromethanesulfonate and MBDP (5). This reaction is completed with the lights off. In a 25 mL round-bottom flask covered with aluminum foil $AgCF_3SO_3$ (0.05234 g (0.20 mmol) is dissolved in 10 mL THF. To the solution MBDP (0.0645 g, 0.20 mmol) is added and allowed to stir for 3 hours. The solution is filtered through a pad of Celite®, followed by concentration under vacuum to approximately 3 mL followed by layering with Et_2O. The flask is placed in the freezer. After 4 days, X-ray quality crystals are formed.

2.2.6. Preparation of silver tetrafluoroborate, tetrahydrothiophene gold (I) chloride, and MBDP (6). This reaction is completed with the lights off. A 25 mL round-bottom flask is covered with aluminum foil. To the flask thtAuCl (0.0645g (20 mmol) and $AgBF_4$ (0.0794 g (0.40 mmol) are dissolved in 15 mL CH_3CN. After 5 min the solution is filtered through a pad of Celite®, collecting AgCl. To the solution MBDP (0.1900 g, 0.20 mmol) is added and allowed to stir for 3 hours. The solution is concentrated under vacuum to approximately 3 mL then layered with Et_2O. The flask is placed in the freezer. A white solid is formed.

2.2.7. Preparation of silver hexafluorophosphate, tetrahydrothiophene gold (I) chloride, and MBDP (7). This reaction is completed with the lights off. A 25 mL round-bottom

flask is covered with aluminum foil. To the flask $AgPF_6$ (0.0126 g (0.20 mmol) is dissolved in 10 mL CH_3CN. To the solution MBDP (0.0645 g, 0.20 mmol) is added and allowed to stir for 3 hours. The solution is concentrated under vacuum to approximately 3 mL then layered with Et_2O. The flask is placed in the freezer. A white solid is formed.

2.3. X-ray Crystallography

2.3.1. Data collection of 1. A colorless crystal of MBDP with the dimensions of 0.05 mm x 0.50 mm x 0.50 mm mounted was used for X-ray crystallographic analysis. Data collection temperature was -73°C. The integration of the data yielded a total of 8036 reflections to a maximum θ angle of 25.08° (0.84 Å resolution). The constants for the triclinic unit cell are a = 9.574(2) Å, b = 9.904(3) Å, c = 10.513(3) Å, α = 74.215(7)°, β = 67.172(7)°, γ = 70.346(7)°, V = 853.7(4) $Å^3$ the space group to be P -1, with Z = 2. They are based upon the refinement of the XYZ-centroids of 3787 reflections above 20.0 I/σ(I) with $2.21° \leq \theta \leq 25.04°$. Data were corrected for absorption effects with SADABS using the multiscan technique. The ratio of minimum to maximum apparent transmission is 90.5:100. The average residual for symmetry equivalent reflections is R_{int} = 2.66% and R_σ = 2.83%.

The final anisotropic full-matrix least-squares refinement on F_o^2 with 209 variables converged at R_1 = 4.50% for the observed data and wR_2 = 13.81% for all data. The goodness-of-fit was 1.036. The largest peak on the final difference electron density synthesis was 0.77 $e^-/Å^3$ and the deepest hole was -0.17 $e^-/Å^3$ with an RMS deviation of 0.04 $e^-/Å^3$. On the basis of the final model, the calculated density is 1.235 g/cm^3 and F(000) = 334.

2.3.2. Data collection of 2. A specimen of **2**, approximate dimensions 0.050 mm x 0.050 mm x 1.000 mm, was used for the X-ray crystallographic analysis. The integration of the data using a monoclinic unit cell yielded a total of 14408 reflections to a maximum θ angle of 25.07 °

(0.84 Å resolution), of which 3323 were independent (average redundancy 4.336, completeness = 99.6 %, R_{int} = 10.81 %, R_{sig} = 8.52 %) and 2552 (76.80 %) were greater than $2\sigma(F^2)$. The final cell constants of a = 15.650(3) Å, b = 7.4736(12) Å, c = 17.493(3) Å, β = 113.462(5)°, volume = 1876.9(6) $Å^3$, the space group P 1 21/c 1, with Z = 4, are based upon the refinement of the XYZ-centroids of reflections above 20 σ(I). Data were corrected for absorption effects using the multi-scan method (SADABS). The ratio of minimum to maximum apparent transmission was 0.325. The calculated minimum and maximum transmission coefficients (based on crystal size) are 0.0456 and 0.6884.

The final anisotropic full-matrix least-squares refinement on F^2 with 228 variables converged at R1 = 8.20 %, for the observed data and wR2 = 23.35 % for all data. The goodness-of-fit was 1.110. The largest peak in the final difference electron density synthesis was 5.790 $e^-/Å^3$ and the largest hole was -2.966 $e^-/Å^3$ with an RMS deviation of 0.325 $e^-/Å^3$. On the basis of the final model, the calculated density was 1.942 g/cm^3 and F(000), 1048 e^-.

2.3.3. Data collection of 3. Colorless needle-like crystals of **3** were grown from acetonitrile and ether, approximate dimensions 0.200 mm x 0.500 mm x 0.600 mm, was used for the X-ray crystallographic analysis. A total of 1080 frames were collected. The total exposure time was 1.50 hours. The integration of the data using a monoclinic unit cell yielded a total of 20345 reflections to a maximum θ angle of 25.04° (0.84 Å resolution), of which 4076 were independent (average redundancy 4.991, completeness = 98.8 %, R_{int} = 5.48 %, R_{sig} = 3.83 %) and 3376 (82.83 %) were greater than $2\sigma(F^2)$. The final cell constants of a = 8.9993(8) Å, b = 19.6166(18) Å, c = 13.4484(12) Å, β = 100.966(2) °, volume = 2330.8(4) $Å^3$, the space group $P2_1/n$, with Z = 4, are based upon the refinement of the XYZ-centroids of 7694 reflections above 20 σ(I) with 5.049 ° < 2θ < 49.88 °. The ratio of minimum to maximum apparent transmission

was 0.559. The calculated minimum and maximum transmission coefficients (based on crystal size) are 0.1134 and 0.3597.

The final anisotropic full-matrix least-squares refinement on F^2 with 291 variables converged at R1 = 2.64 %, for the observed data and wR2 = 6.99 % for all data. The goodness-of-fit was 0.981. The largest peak in the final difference electron density synthesis was 1.225 $e^-/Å^3$ and the largest hole was -0.808 $e^-/Å^3$ with an RMS deviation of 0.146 $e^-/Å^3$. On the basis of the final model, the calculated density was 1.833 g/cm^3 and F(000), 1240 e^-.

2.3.4. Data collection of 4. A colorless needle-like specimen of **4**, approximate dimensions 0.200 mm x 0.400 mm x 0.600 mm, was used for the X-ray crystallographic analysis. A total of 1080 frames were collected. The total exposure time was 1.50 hours. The integration of the data using a triclinic unit cell yielded a total of 12591 reflections to a maximum θ angle of 25.09 ° (0.84 Å resolution), of which 4657 were independent (average redundancy 2.704, completeness = 97.8 %, R_{int} = 4.21 %, R_{sig} = 4.54 %) and 4096 (87.95 %) were greater than $2\sigma(F^2)$. The final cell constants of $\underline{a}$ = 10.5423(10) Å, $\underline{b}$ = 10.7638(10) Å, $\underline{c}$ = 12.3530(12) Å, α = 88.592(3) °, β = 73.097(3) °, γ = 84.422(3) °, volume = 1334.8(2) $Å^3$, the space group P -1, with Z = 1 are based upon the refinement of the XYZ-centroids of 5987 reflections above 20 σ(I) with 4.491 ° < 2θ < 49.89 °. Data were corrected for absorption effects using the multi-scan method (SADABS). The ratio of minimum to maximum apparent transmission was 0.704. The calculated minimum and maximum transmission coefficients (based on crystal size) are 0.6259 and 0.8465.

The final anisotropic full-matrix least-squares refinement on F^2 with 320 variables converged at R1 = 3.37 %, for the observed data and wR2 = 10.40 % for all data. The goodness-of-fit was 1.114. The largest peak in the final difference electron density synthesis was 0.874 $e^-/Å^3$ and the largest hole was -0.425 $e^-/Å^3$ with an RMS deviation of 0.097 $e^-/Å^3$. On the basis of

the final model, the calculated density was 1.478 g/cm^3 and F(000), 598 e$^-$.

2.3.5. Data collection of 5. A specimen of **5**, approximate dimensions 0.200 mm x 0.300 mm x 0.400 mm, was used for the X-ray crystallographic analysis. The integration of the data using a monoclinic unit cell yielded a total of 132869 reflections to a maximum θ angle of 26.02 ° (0.81 Å resolution), of which 14158 were independent (average redundancy 9.385, completeness = 99.2 %, R_{int} = 16.01 %, R_{sig} = 12.19 %) and 9076 (64.11 %) were greater than 2σ(F^2). The final cell constants of a = 20.973(2) Å, b = 14.8853(13) Å, c = 24.206(3) Å, β = 106.566(3) °, volume = 7243.2(12) Å^3, the space group P 1 21/n 1, with Z = 4 are based upon the refinement of the XYZ-centroids of reflections above 20 σ(I). The calculated minimum and maximum transmission coefficients (based on crystal size) are 0.6272 and 0.7829.

The final anisotropic full-matrix least-squares refinement on F^2 with 868 variables converged at R1 = 7.63 %, for the observed data and wR2 = 24.69 % for all data. The goodness-of-fit was 1.277. The largest peak in the final difference electron density synthesis was 3.142 e$^-$/Å^3 and the largest hole was -1.560 e$^-$/Å^3 with an RMS deviation of 0.401 e$^-$/Å^3. On the basis of the final model, the calculated density was 1.692 g/cm^3 and F(000), 3664 e$^-$.

2.4. Computational Details

2.4.1. Computational procedures. The Gaussian ’09 software package [45] was used for theoretical calculations at the Density Functional Theory (DFT) level. Geometry optimizations and frequency calculations were computed with Becke three-parameter exchange with the Perdew−Wang 1991 correlation (B3PW91). The excitation energies and oscillator strengths were performed using the optimized structures of **1** and **2** without any consideration for solvent by time-dependent (TD)-DFT with B3PW91. The LANL2DZ effective core potentials and valence basis set were used to describe the valence electrons of gold. Phosphorus, carbon, and hydrogen

were described with 6-31+G*, 6-31G*, and 6-31G basis sets, respectively. Molecular isodensity diagrams (Isovalues: 0.02 atomic units) of molecular orbital estimations were created using the GaussView 5 software (Gaussian Inc.).

CHAPTER 3

Mononuclear Gold (I) Complex with the MBDP Ligand

3.1. Structure and Photoluminescence (PL) Studies for MBDP (1)

3.1.1. Structural analysis. Although, the ligand has been previously synthesized [46], there are no known reports regarding the X-ray crystal structure, electronic properties, or theoretical data. Modification to the synthesis of 1-methylimidazole diphenylphosphine [41] by changing the starting material to 1-methylbenzimidazole and chlorodiphenylphosphine lead to the successful production of the desired ligand MBDP. The ligand has a phosphorus atom attached to the carbon number 2 as well as two phenyl-rings as seen in Figure 3.1. It is also noteworthy to mention that the key feature of this ligand is that it is bidentate, having the nitrogen and phosphorus positions available for binding to metal centers, hence the desire for usage. The MBDP ligand crystallizes in a triclinic space group, the X-ray crystal structure and refinement data can be found in Table 3.1. The complete X-ray Crystallographic data can be found in Appendix A.

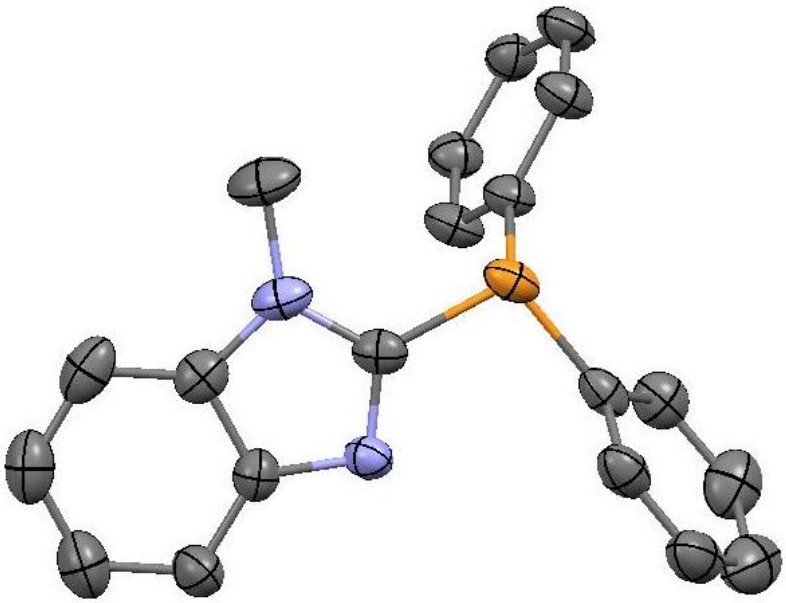

Figure 3.1. Thermal ellipsoid of the 1-methylbenzimidazole diphenylphosphine (MBDP) ligand.

Table 3.1

Data collection and structure refinement for MBDP

Empirical formula	$C_{20}\ H_{18}\ N_2\ P$	
Formula weight	317.33	
Temperature	200(2) K	
Wavelength	0.71073 Å	
Crystal system	Triclinic	
Space group	P -1	
Unit cell dimensions	a = 9.574(2) Å	α = 74.215(7)°
	b = 9.904(3) Å	β = 67.172(7)°
	c = 10.513(3) Å	γ = 70.346(7)°
Volume	853.7(4) $Å^3$	
Z	2	
Density (calculated)	1.235 Mg/cm^3	
Absorption coefficient	0.162 mm^{-1}	
F(000)	334	
Crystal size	0.05 x 0.50 x 0.50 mm^3	
Theta range for data collection	2.13 to 25.08°	
Index ranges	-11<=h<=11, -11<=k<=11, -12<=l<=12	
Reflections collected	8036	
Independent reflections	2973 [R(int) = 0.0266]	
Completeness to theta = 25.08°	97.60%	
Absorption correction	Multiscan	
Max. and min. transmission	0.9920 and 0.8980	
Refinement method	Full-matrix least-squares on F^2	
Data / restraints / parameters	2973 / 0 / 209	
Goodness-of-fit on F^2	1.036	
Final R indices [I>2sigma(I)]	R1 = 0.0450, wR2 = 0.1306	
R indices (all data)	R1 = 0.0528, wR2 = 0.1381	
Largest diff. peak and hole	0.768 and -0.169	

The packing diagram of MBDP looking down the a-axis is seen in Figure 3.2, the ligand looks as if it packs in the shape of an L and 7 within the unit cell. The overall average phosphorus-carbon length is approximately 1.827 Å. The average bond angle of the P-C-P type is 101.71˚. Selected bond lengths and averages for this ligand are detailed in Table 3.2.

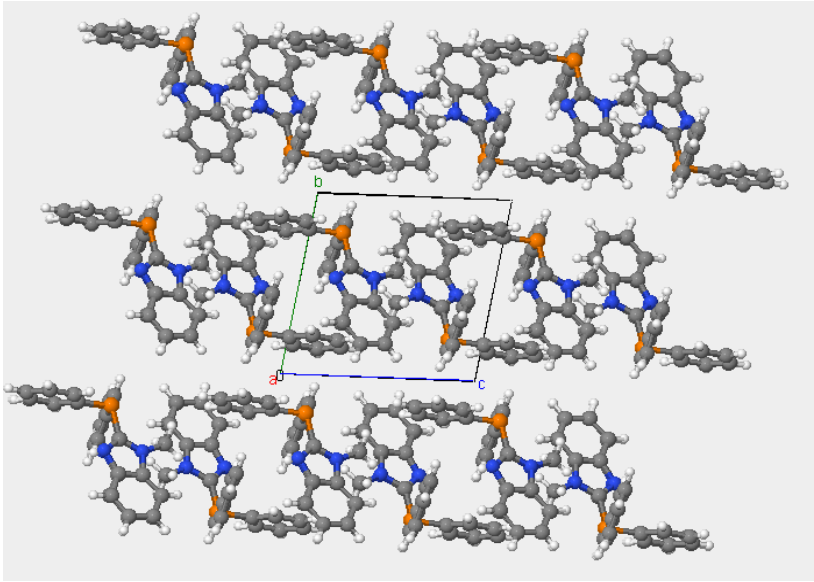

Figure 3.2. Packing diagram of MBDP.

Table 3.2

Selected bond lengths and bond angles for MBDP

Bond length (Å)	
P1-C9	1.817(4)
P1-C15	1.830(3)
P1-C1	1.833(3)
N2-C1	1.311(4)
Bond Angles	
C9-P1-C15	103.98(14)
C9-P1-C1	100.03(14)
C15-P1-C1	101.13(14)
C1-N2-C2	104.8(3)

3.1.2. Characterization and PL studies. The methylbenzimidazole was characterized using ^{31}P and ^{1}H NMR in $CDCl_3$ at room temperature. The initial ^{31}P NMR collected providing a single peak at -26.164 ppm. While using the standard phosphoric acid, corrections to the baseline were needed. It was adjusted by 0.584 ppm providing the corrected signal at -25.58 ppm. For accuracy recordings, additional recordings were collected on two different NMR spectrometers as well as on numerous occasions; essentially the same signal was provided in some instances the small amounts of diphenylphosphonic acid, less than 10%, were observed. This differs from the original reported synthesis by 1.68 ppm which is qualitatively and statistically in good relation. The ^{1}H NMR shows signals 3.6.

The absorbance bands seen at 203, 272, and 290 nm in the absorption spectra (Figure 3.3) corresponds to molar extinction coefficients for each band was calculated to be 174000, 46000, and 51200 M^{-1} cm^{-1} (respectively) is suggestive of a $\pi \rightarrow \pi^*$ electronic transition. To further examine and ensure proper assignment of the electronic properties, we will compare these values with the theoretical data.

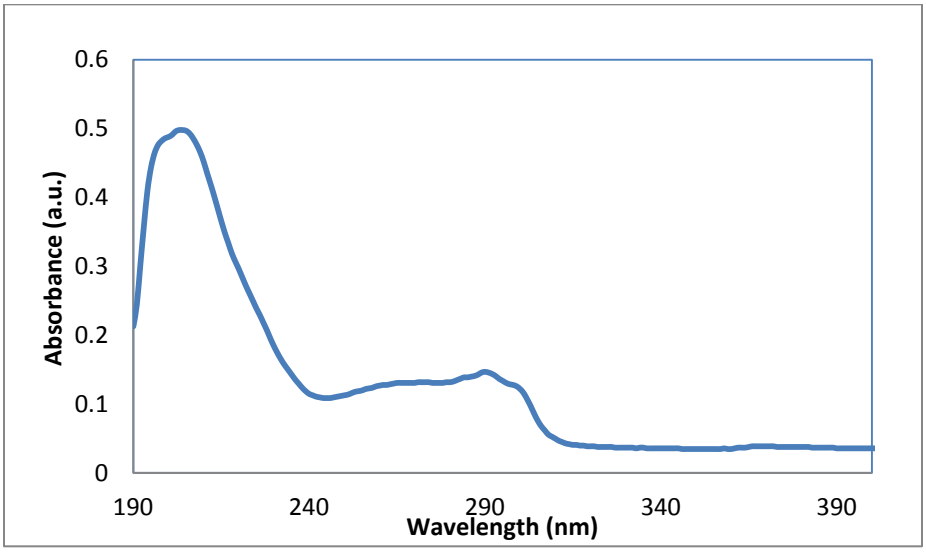

Figure 3.3. UV-Vis spectra of the MBDP Ligand.

The excitation spectrum for the MBDP ligand, while monitoring the emission at 445 nm, is broad, ranging from 280 to 400 nm. The excitation maximizes at 309 nm with a second, smaller broad band at 346 nm. The emission profile for the ligand is also broad with several vibronic components seen while monitoring the emission range from 240 to 580 nm with excitation at 311 nm. The approximate average spacing of ~917.66 cm^{-1} corresponds to a peak found on the IR spectrum at 924.88 cm^{-1}. Figure 3.4 shows the overlap of the excitation and emission spectra for MBDP. After complete comparison of the absorption and emission profiles the nature of luminescent profile is fluorescent considering the relatively small Stokes shift between the absorption and emission bands. The detail of the excitation profile will be used when comparing the metal complexes. One hypothesis to be tested is that the luminescence is ligand centered. We will examine the metal complexes to prove or disprove this notion.

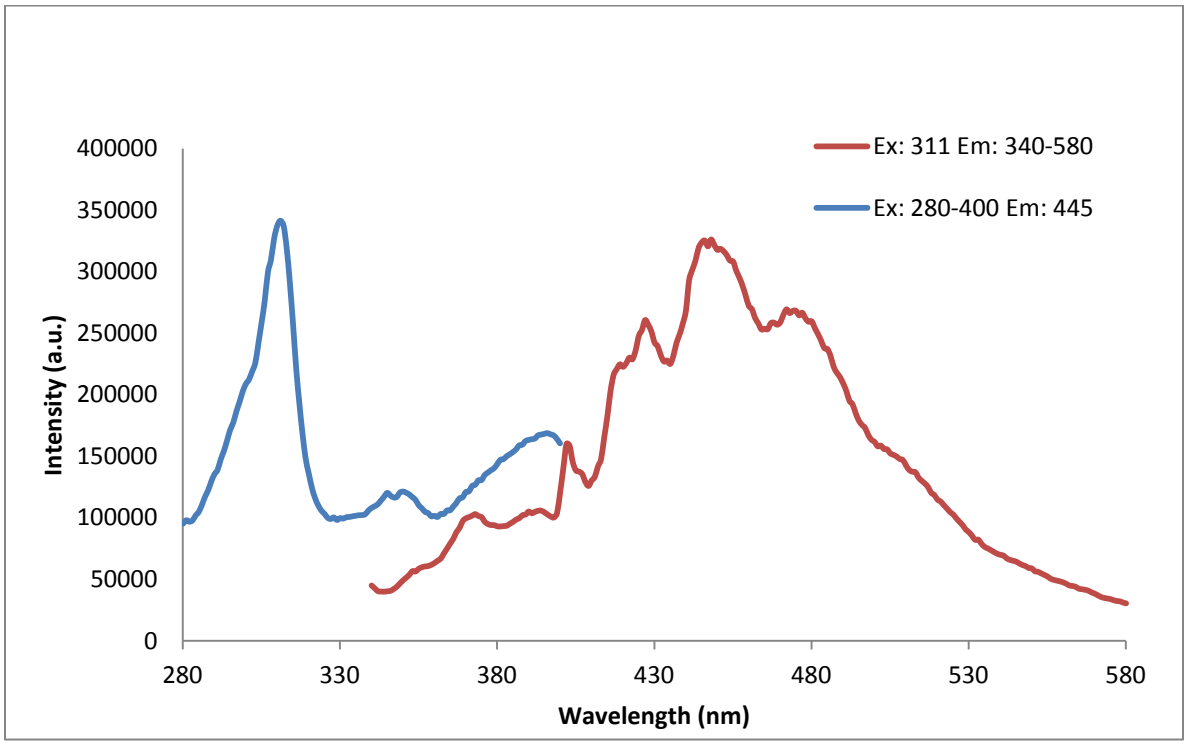

Figure 3.4. Excitation (blue) and emission (red) profile of MBDP

3.1.3. Theoretical calculations. The theoretical data was compared to the X-ray crystal structure of the ligand. It was determined that the geometry optimized structure was in good agreement with the X-ray crystal structure. Table 3.3 provides a short summary of the bond lengths and bond angles of the ligand. The length for the P1-C1 bond is slightly shorter by ~0.045 Å. This further supports the successful identification of the X-ray crystal structure of the ligand.

Table 3.3

Comparison of structural features from the X-ray crystal structure and theoretical data

	X-ray Crystal Data	Theoretical Data
Bond Angle (˚)		
C9-P1-C15	103.98	102.24
C15-P1-C1	101.13	101.86
C9-P1-C1	100.03	101.86
N1-C1-P1	122.23	121.13
N2-C1-P1	124.63	127.16
Bond Length (Å)		
P1-C9	1.81	1.89
P1-C1	1.83	1.83
P1-C15	1.83	1.89
N1-C1	1.37	1.40
N2-C1	1.31	1.33

The frequency keyword was used to compute the vibrational frequencies for the MBDP ligand with no imaginary frequencies calculated. The GaussView 5 transformed the data to provide an IR spectrum and also automation of the vibrations. Comparison of the frequencies to the collected IR shows comparable data. The vibronic component seen in the luminescence spectra was calculated to correspond to a frequency at ~918cm^{-1}. A calculated peak from the

theoretical work at 911 cm^{-1} was animated to show there is bending and stretching motion within the 1-methylbenzimidazole ring and some bending motion from a few of the hydrogen atoms on the phenyl rings.

Further analysis using the TD-DFT data revealed a total of three excited energy states seen in Figure 3.5, the theoretical UV-Vis spectrum. The first state corresponds to the electronic transition from orbital 78 to orbital 79 with total contribution of 97.78 % calculated from the coefficient of the microstate as defined by Gaussian [45]. The second excited state consists of contributions from orbitals 78 to 80 and the third excited state with contributions from the orbitals 76 to 84 and 77 to 79. These singly excited states are within range of comparison to the experimental spectrum seen in Figure 3.3. Although not exact, we can see that the theoretical calculations of the UV-Vis spectrum are similar to the experimental spectrum. Namely, the peak at 263 nm is similar to that of the 272 nm peak in the experimental. The calculated epsilon for this peak is within in range, 10^4.

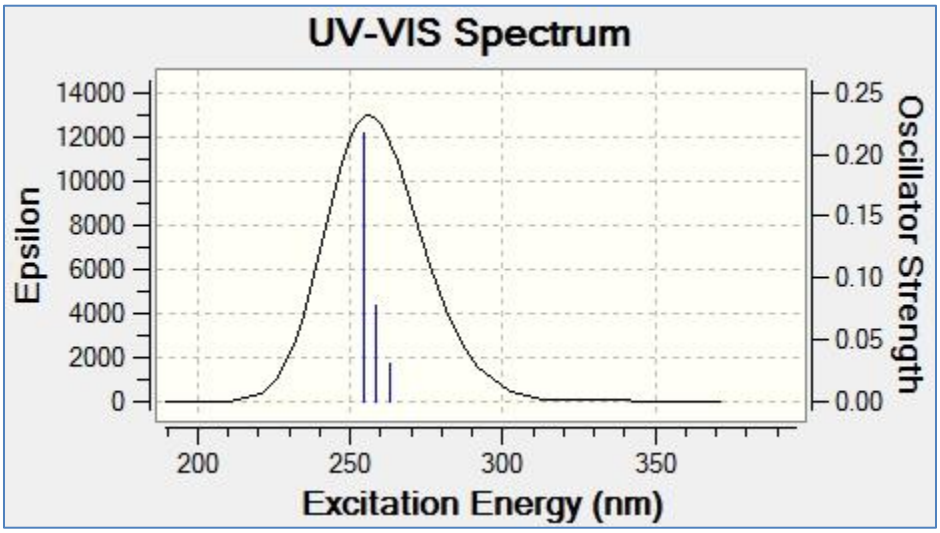

Figure 3.5. The theoretical UV-Vis spectrum of MBDP.

The population analysis for this ligand is provided in Table 3.4. There are a total of 78 occupied orbitals and 162 virtual orbitals (estimation of unoccupied orbitals). The HOMO orbital

(78 orbital) consists of contribution from the P (53.05 %), N (9.28 %), and C (37.67 %), having the phosphorus with the largest contributor. Whereas, the first virtual orbital i.e. the LUMO orbital consists of P (7.76 %), N (14.90 %), and C (77.50 %), has mainly carbon contribution. To fully grasp the molecular orbital contributions, visual representation for the LUMO+ 2, LUMO+1, LUMO, HOMO, HOMO-1, and HOMO-2 are shown by orbital correlation diagrams in Figures 3.6 – 3.10, respectively. These figures coincide with the values given in Table 3.4. The striking feature seen from these figures is the transition from the occupation of the benzimidazole portion of the ligand to the phenyl rings. This is seen in the occupied as well as the unoccupied orbitals. This offers support to conceptualize the transition from $\pi \rightarrow \pi^*$, which is believed to govern the electronic properties of this ligand.

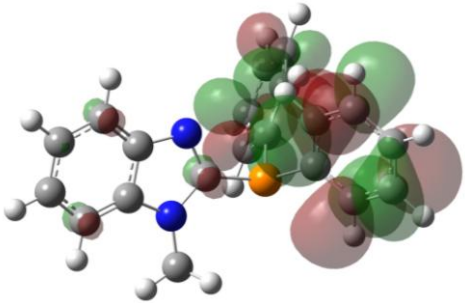

Figure 3.6. The orbital correlation diagram of LUMO+2, molecular orbital 81 (isovalue plot = 0.02).

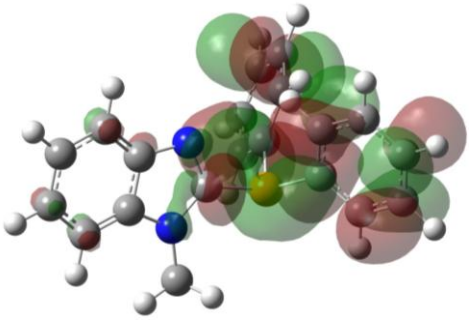

Figure 3.7. The orbital correlation diagram of LUMO+1, molecular orbital 80 (isovalue plot = 0.02).

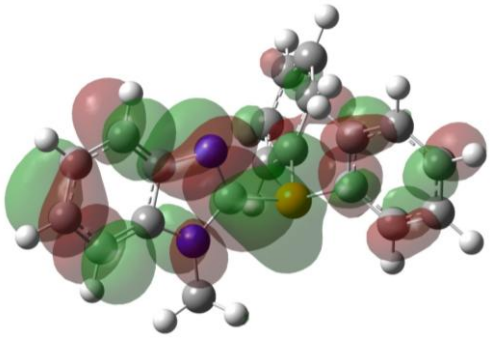

Figure 3.8. The orbital correlation diagram of LUMO orbital, molecular orbital 79 (isovalue plot = 0.02).

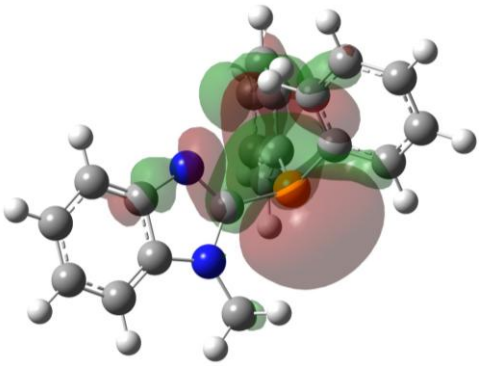

Figure 3.9. The orbital correlation diagram of HOMO, molecular orbital 78 (isovalue plot = 0.02).

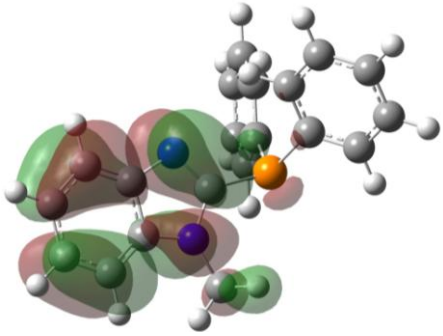

Figure 3.10. The orbital correlation diagram of HOMO-1, molecular orbital 77 (isovalue plot = 0.02).

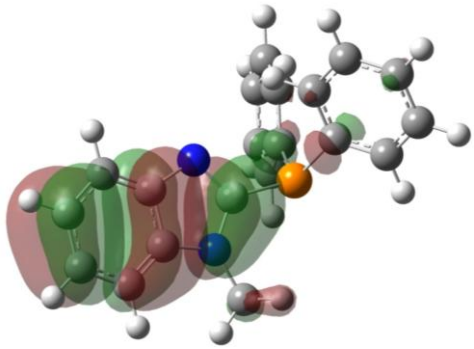

Figure 3.11. The orbital correlation diagram of HOMO-2, molecular orbital 76 (isovalue plot = 0.02).

Table 3.4

Orbital/atomic contribution for MBDP

Contributions (%)				**Component (%) Contributions**		
Orbital	**P**	**N**	**C**	**P**	**N**	**C**
81	1.78	0	98.22	1.78px	0	1.73s, 64.40px, 28.44py, 3.85pz
80	6.96	1.37	91.67	1.50s, 5.46px	1.73px	9.20s, 57.66px, 12.02py, 12.79pz
79	7.76	14.9	77.5	7.76py	14.90py	9.44s, 6.13px, 54.48py, 7.29pz
HOMO-LUMO GAP						
78	53.05	9.28	37.67	17.34s, 35.71pz	4.96s, 4.32px	10.23s, 16.97px, 4.55py, 5.91pz
77	0	40.43	59.57	0	40.43py	59.57py
76	0	12.45	87.55	0	12.45py	87.55py
75	0	51.12	48.88	0	13.81s, 24.48p	19.31s, 8.47px, 21.03pz
74	0	0	100	0	0	71.74px, 4.25py, 24.01pz

3.2. Structural and PL Studies of Au(MBDP)Cl (2)

3.2.1. Structural analysis. The gold (I) chloride complex with the MBDP ligand (1:1 molar ratio) was prepared in THF at room temperature for 3 hours. Layering with Et_2O yielded colorless crystals in 95% yield. The X-ray crystal structure of **2**, shown in Figure 3.12, has the gold (I) atom bound to the phosphorus atom of the ligand. The X-ray crystallographic details are given in Table 3.5. For the complete X-ray Crystallographic data see Appendix B. The complex crystallizes in a monoclinic system in the $P2_1/c$ space group. Figure 3.13 is the packing diagram of **2** looking down the b-axis showing P-Au-Cl arrangement affected by the pi-stacking of the phenyl rings within the unit cell. Several attempts to gain gold-gold interactions by increasing the molar ratio of the thtAuCl from 1 to 2 failed resulting in the decomposition of the gold material. The only product obtained was that of **2**.

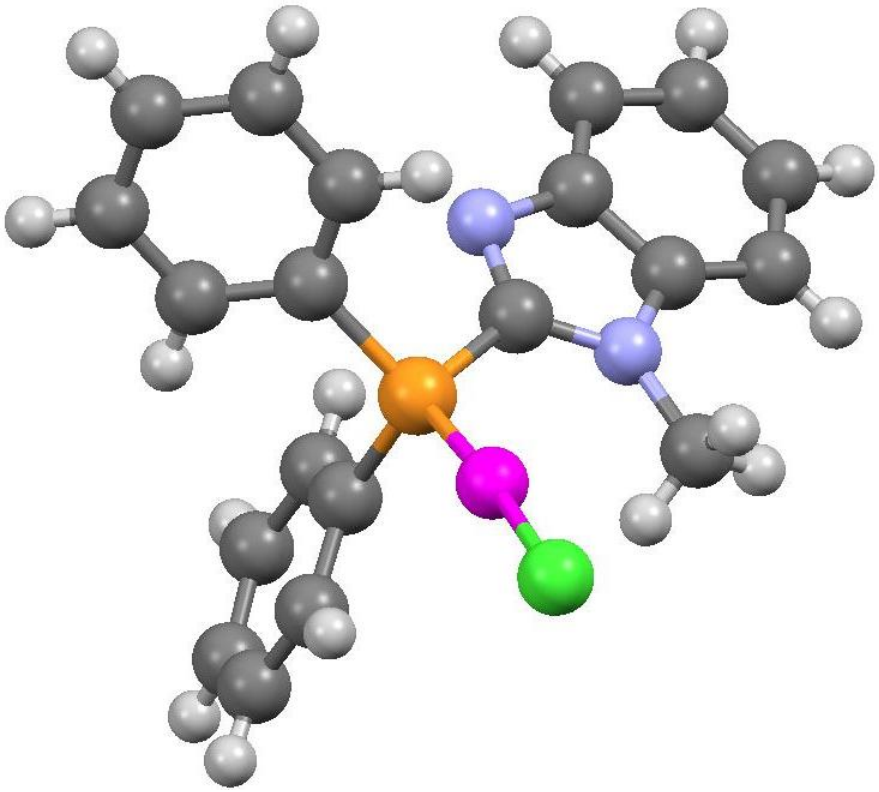

Figure 3.12. The X-ray crystal structure of **2.**

Table 3.5

*X-ray crystallographic data for **2***

Chemical formula	$C_{20}H_{17}AuClN_2P$	
Formula weight	548.74	
Temperature	200(2) K	
Wavelength	0.71073 Å	
Crystal size	0.050 x 0.050 x 1.000 mm	
Crystal system	monoclinic	
Space group	P 1 21/c 1	
Unit cell dimensions	a = 15.650(3) Å	α = 90°
	b = 7.4736(12) Å	β = 113.462(5)°
	c = 17.493(3) Å	γ = 90°
Volume	1876.9(6) $Å^3$	
Z	4	
Density (calculated)	1.942 Mg/cm^3	
Absorption coefficient	8.070 mm^{-1}	
F(000)	1048	
Theta range for data collection	1.42 to 25.07°	
Index ranges	-18<=h<=18, -8<=k<=8, -20<=l<=20	
Reflections collected	14408	
Independent reflections	3323 [R(int) = 0.1081]	
Absorption correction	multi-scan	
Max. and min. transmission	0.6884 and 0.0456	
Structure solution technique	direct methods	
Structure solution program	SHELXS-97 (Sheldrick, 2008)	
Refinement method	Full-matrix least-squares on F^2	
Refinement program	SHELXL-97 (Sheldrick, 2008)	
Function minimized	$\Sigma\, w(Fo^2 - Fc^2)^2$	
Data / restraints / parameters	3323 / 0 / 228	
Goodness-of-fit on F2	1.11	
Final R indices	2552 data; I>2σ(I)	R1 = 0.0820, wR2 = 0.2230
	all data	R1 = 0.0989, wR2 = 0.2335
Weighting scheme	$w=1/[\sigma^2(Fo^2)+(0.0947P)^2+95.0646P]$	
	where $P=(Fo^2+2Fc^2)/3$	
Extinction coefficient	0.0003(3)	
Largest diff. peak and hole	5.790 and -2.966 $eÅ^{-3}$	
R.M.S. deviation from mean	0.325 $eÅ^{-3}$	

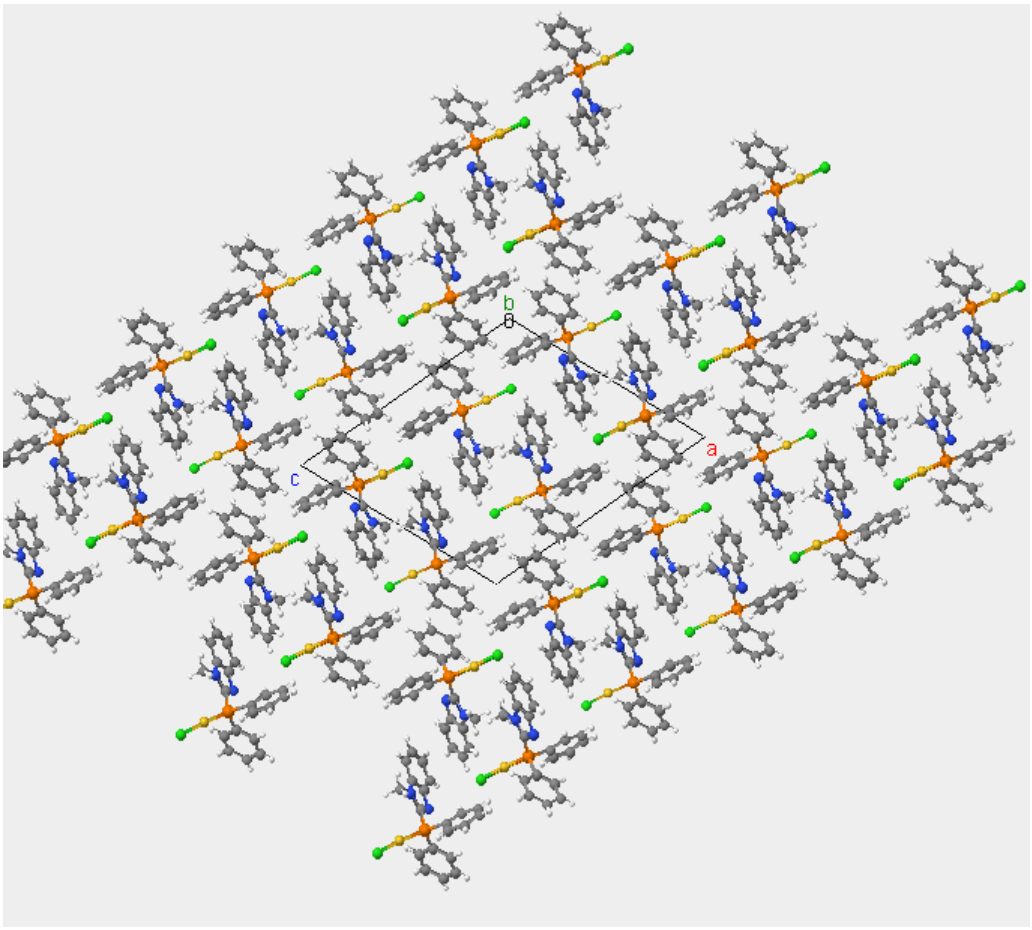

Figure 3.13. The packing diagram of **2**.

The P-Au-Cl bond angle is less than five away from perfect linearity at 175.9˚, slightly smaller angle than most P-Au-Cl type angles. This near linear geometry is expected of gold (I) complexes. However, Burini [34] and co-workers explained that this deviation from the norm can be assigned to packing in the unit cell. The shortest intermolecular Au (I) – Au (I) distance is 7.47 Å, this is too large for aurophilic assignment. The P-Au bond is 2.225 Å whereas the Au-Cl bond is slightly longer measuring 2.279 Å. The bond distances are comparable to the work of Catalano and Horner [42]. They reported bond distances for P-Au and Au-Cl as 2.227Å and 2.293 Å, respectively, while using the 1-methylimidazole diphenylphosphine ligand. Selected bond angles and distances for **2** can be found in Table 3.6.

3.2.2. Characterization and PL studies. The complex **2** was characterized by NMR, IR, UV-Vis, and photoluminescence. The ^{1}H NMR spectrum collected in $CDCl_3$ has a similar profile with the ligand with the following peaks 3.98 (s, 1H), 7.33 – 7.54 (m, 5H), 7.58 – 7.60 (m, 6H), and 7.70 – 7.83 (m, 5H). The ^{31}P NMR revealed a single peak at 14.59 ppm.

Table 3.6

*Selected Bond Angles and Bond Lengths for **2***

	Bond Length (Å)
Au1-P1	2.23(5)
Au1-Cl1	2.28(5)
P1-C2	1.79(2)
P1-C16	1.80(2)
P1-C9	1.80(19)
	Bond Angle (˚)
P1-Au1-Cl1	175.96(19)
C2-P1-C16	101.9(9)
C2-P1-C9	103.4(9)
C16-P1-C9	106.8(9)
C2-P1-Au1	118.2(7)
C16-P1-Au1	112.3(6)
C9-P1-Au1	113.1(7)

The absorbance spectrum for **2** can be found in Figure 3.14. The concentration was diluted to 10^{-5} M to see well resolved peaks at 199, 275, and 291 nm. The peaks seen here are similar to **1** lending to the notion that there is an electronic transition that originates from the ligand. This can be due to the changes in the system, the metal. The calculated molar extinction coefficient has some shift to 32000 M^{-1} cm^{-1}. This shift suggests there may be metal contribution in the transition. In addition, the shoulder seen at 229 nm is not seen in the ligand and has a molar extinction coefficient of 11699 M^{-1} cm^{-1}. The other two peaks seen at 275 and 291 nm has

molar extinction coefficients of 5375 and 5692 M^{-1} cm^{-1}, respectively. The overall shape of the absorbance spectra are relatively the same as the ligand. An overlap of the ligand, **1**, and the metal complex, **2**, can be seen in Figure 3.15.

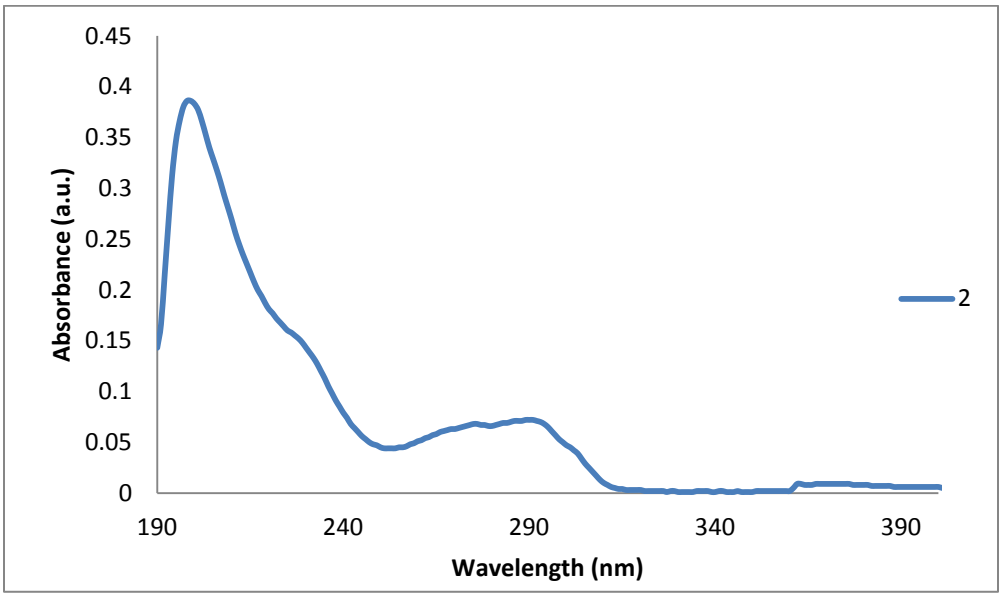

Figure 3.14. The UV-Vis spectrum of **2**.

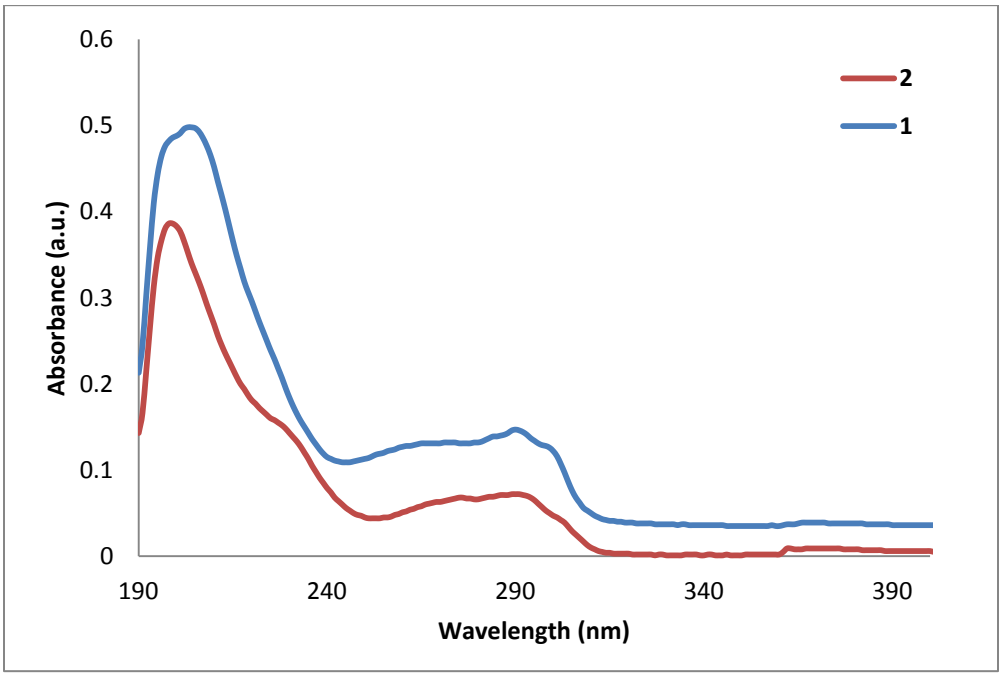

Figure 3.15. The UV-Vis spectra overlap of the ligand (**1)** and gold complex (**2**).

The photoluminescence steady-state excitation and emission of **2** were collected at liquid nitrogen temperature. While monitoring the emission at 448 nm, the excitation spectrum for **2** ranging from 280 to 430 nm is similar in profile to the free ligand. The excitation maximizes at 325 nm with seven vibronic components at 305, 314, 325, 345, 357, 367, and 377 nm. The average band gap is 1040.47 cm^{-1}. The emission profile for **2** is also broad with several vibronic components seen while monitoring the emission range from 350 to 620 nm with excitation at 325 nm. Those vibronic components are 412, 429, 453, 481, 514, and 551 nm having an average band gap of 1226 cm^{-1}. Figure 3.16 is the overlap of the excitation and emission profile for the **2** complex.

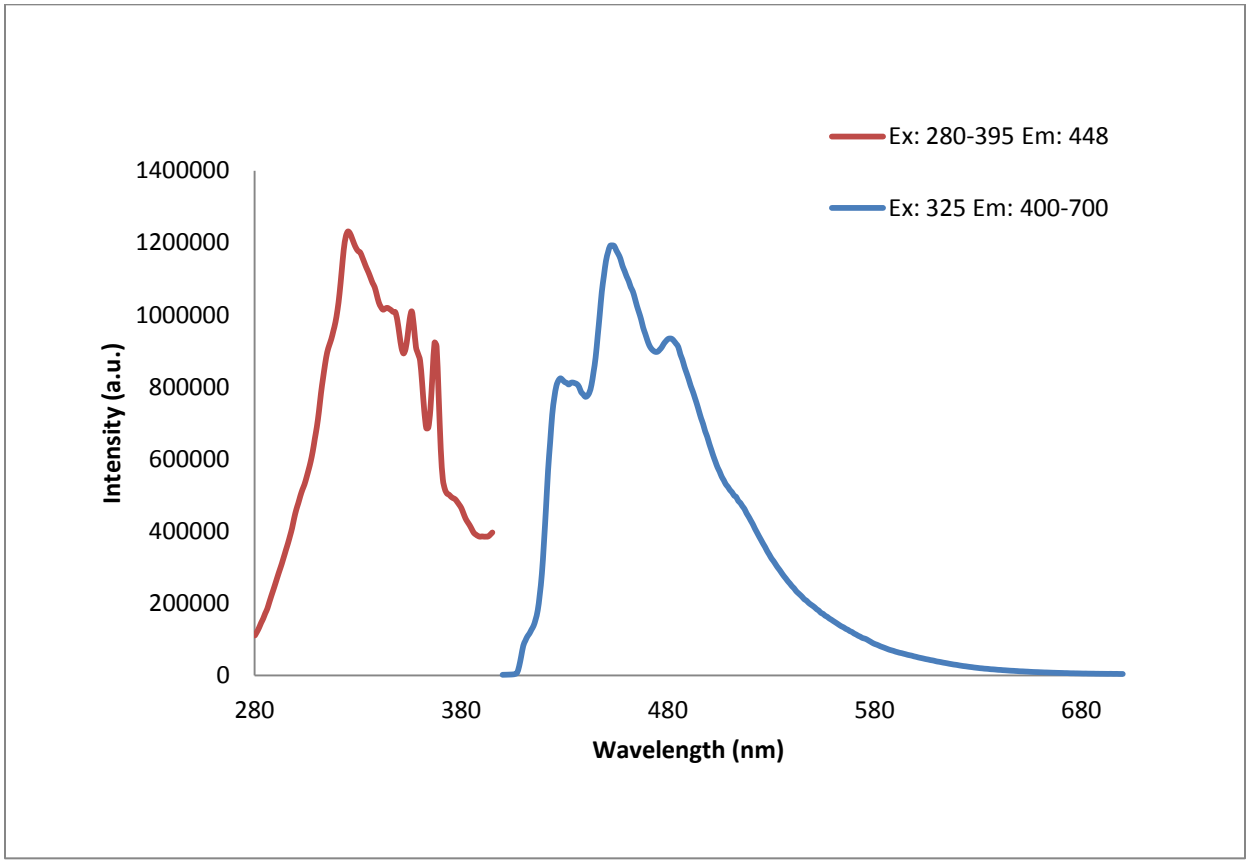

Figure 3.16. The Excitation (red) and Emission (blue) spectral overlap of the gold complex (**2**).

While monitoring the emission, a trend is seen in the spectra. The relative intensity changes as the fixed excitation changes, using 325, 346, 355, 367, and 377 nm corresponding to the vibrational band found in the excitation profile. The shape of the spectra profile appears the same, although the intensities decrease as you move away from the optimal excitation point as can be seen in Figure 3.17. The vibrational modes are generated within the benzimidazole portion of the ligand. Combination of the excitation and emission band gap average spacing is ~1133 cm^{-1}. This average spacing suggests electronic transitions to a π* orbital, thus providing evidence that the excitation and emission is ligand centered. It is clear that **2** absorb radiation between 200 and 395 nm when comparing the absorption and the excitation. The overall shape of the spectra is similar to each other, although the absorption and excitation spectra are not shown as overlaps to due scaling. To verify this hypothesis, the electronic properties of this complex is studied theoretically and compared to the ligand.

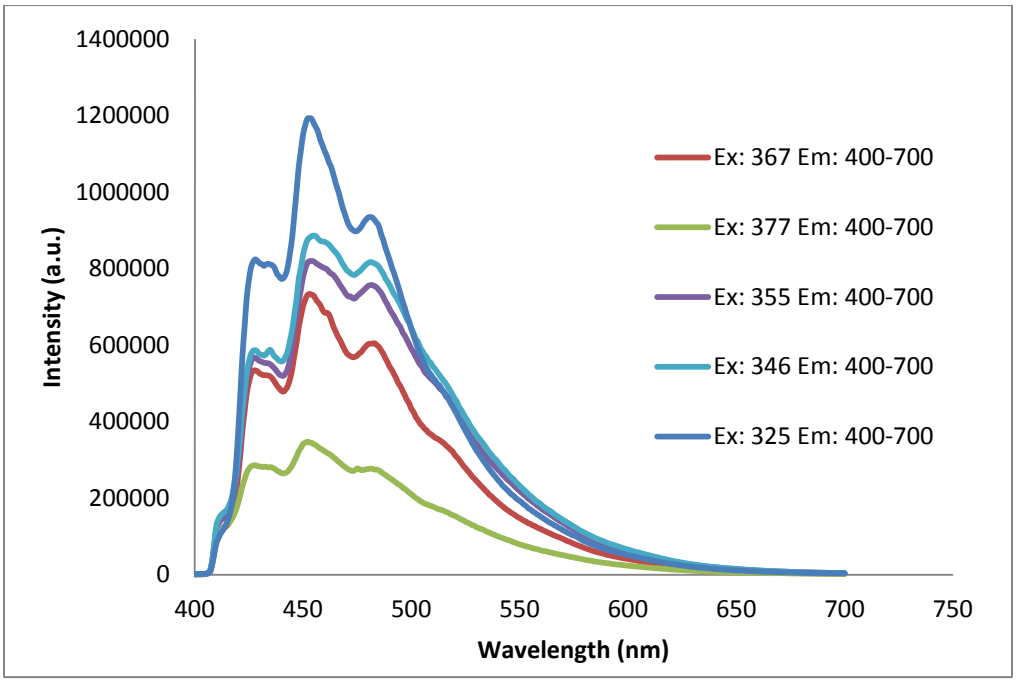

Figure 3.17. Monitoring the emission intensity of the gold complex (**2**) while varying the excitation.

3.2.3. Theoretical calculations. For a better understanding of the structural and electronic properties of the gold (I) metal and ligand interaction, we carried out DFT calculations. The first issue to address is the structure. We optimized the geometry to obtain values for bond lengths and angles. Table 3.7 is a list of the selected bond lengths and angles for comparison with the X-ray crystal structure and the optimized geometry structure. The bond lengths for the theoretical structure appear to be slightly longer than the X-ray structure. The bond angles obtained from the calculations are slightly larger than the actual structure. The near linear P-Au-Cl bond angle for the theoretical calculated structure follows the expected trend for gold (I) chloride complexes. It is interesting to see these differences. However, the values are still within an acceptable range.

Table 3.7

Comparison of selected bond angles and bond lengths

MBDP	**X-Ray**	**Theoretical**
Bond Angle (˚)		
P-Au-Cl	175.96	179.26
P-Au-C	101.90	111.10
P-Au-C	103.40	111.10
P-Au-C(im)	118.20	117.40
Bond Length (nm)		
Au-Cl	2.28	2.37
P-Au	2.23	2.36
P-C	1.80	1.87
P-C	1.80	1.87
P-C(im)	1.79	1.86

Secondly, frequency and time dependent calculations to obtain vibrational and electronic singlet transition data were conducted. Mentioned earlier, the vibronic components found in the photoluminescence spectra that have an average spacing of 1133.57 cm^{-1}. This is spacing is within range of acceptance with a calculated frequency at 1133.52 cm^{-1}. When this peak was animated in the GaussView software package it displayed bending and stretching from the benzimidazole portion of the ligand with minor H stretching on the two phenyl rings. No motion was observed from the P-Au-Cl bonds. Moreover, this is strong evidence to assign the ligand centered excitation and emission. We viewed the excitation energies from the TD-DFT calculations to obtain the UV-Vis spectrum, seen in Figure 3.18.

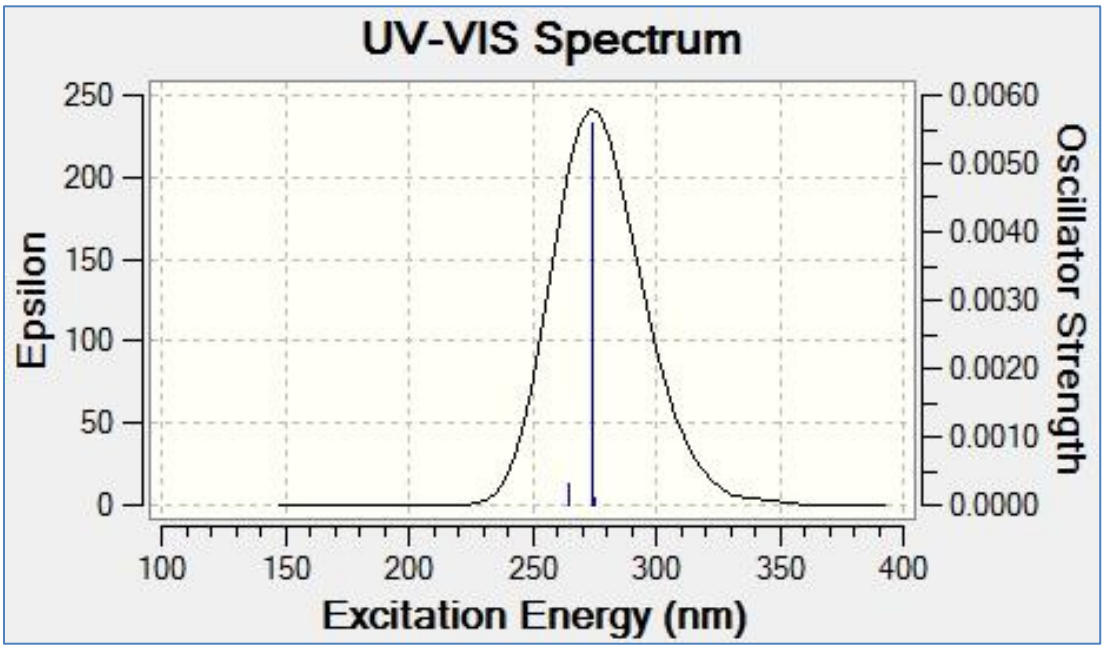

Figure 3.18. Theoretical UV-Vis spectrum of **2**.

It also provided information regarding the electronic transitions that occurred from the HOMO to the LUMO. The HOMO-LUMO gap, MO 91 and MO 92 respectively, from the theoretical calculations was approximately 40167 cm^{-1}. There were three excited states that should participate in the transition. The first was between MO 90 to MO 92 with a signal at

275.16 nm. The next was from MO 91 to MO 92 with a signal at 274.65 nm. Finally the third coming from MO 91 to MO 93 and MO 91 to MO 97 with a signal at 264.90 nm. The last contains two microstate transitions that contribute to the 264.90 nm. The MO 91 to MO 93 microstate contribution is 96% and the MO 91 to MO 97 contributes 2.5% to the transition.

When compared to the experimental data there is a slight red shift in the excitation energies. This is more than likely due to calculated gold participation in these transitions. A better explanation comes from the MO contribution seen in Table 3.8. The HOMO orbital 91 has mainly contributions from the Au d_{xz} (30 %) and Cl p_z (60 %) whereas the LUMO is totally p-orbital from C and P (p_x – 11.5 %, p_y – 4.5 %, and p_z – 48 % remaining percentage given to s-orbital) ligand centered. This further infers the presence of the $\pi \rightarrow \pi^*$ transition.

Table 3.8

Partial Molecular Orbital Contributions in the Ground State

Contributions (%)				**Component (%) Contributions**		
Orbitals	**Cl**	**Au**	**Ligand**	**Cl**	**Au**	**Ligand**
94	5	15.63	79.37	1.42s, 3.58px	11.19s, 3.17p, 3.21p	3.49s, 21.77px, 16.32py, 37.79pz
93		2.29	97.71		2.29s	11.41s, 20.04px, 49.71py, 16.55pz
92			100			11.52s, 4.50px, 11.7py, 72.28pz
HOMO-LUMO GAP						
91	69.29	30.7		69.29pz	30.70d	
90	77.17	16.54	6.28	35.29px, 41.88py	16.54d	6.28s
89			100			100pz

The predicted orbital occupation for these transitions can be seen in Figures 3.19 – 3.24 labeled as LUMO+2, LUMO+1, LUMO, HOMO, HOMO-1, HOMO-2, respectively, provide a great deal of information regarding the electronic transition of the gold complex (**2**). Starting with LUMO+2 shows the contributions from the Au, Cl, and phenyl rings. The LUMO+1 donation comes from the benzimidazole and phenyl ring portions of the ligand with minor Au participation. The LUMO is 100 % ligand centered whereas the filling of the HOMO is Au-Cl centered. The HOMO-1 is composed of majority Au-Cl contributions with some *s* contribution also. Finally, the HOMO-2 is totally ligand centered. As expected with these π-type systems. We will see how these orbital contributions participate in the metal complex.

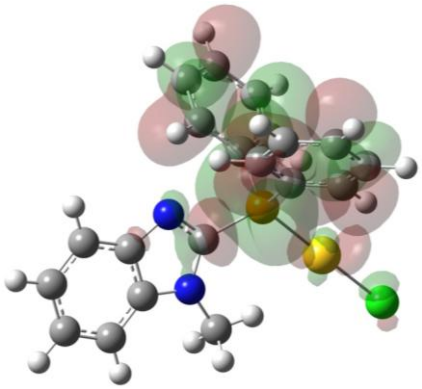

Figure 3.19. The orbital correlation diagram of LUMO+2, molecular orbital 94 (isovalue plot = 0.02).

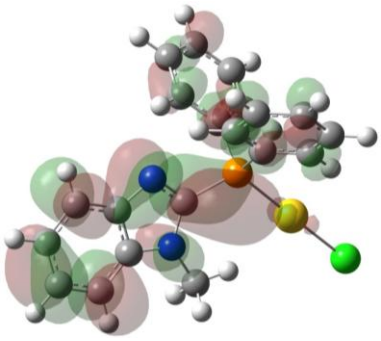

Figure 3.20. The orbital correlation diagram of LUMO+1 molecular orbital 93 (isovalue plot = 0.02).

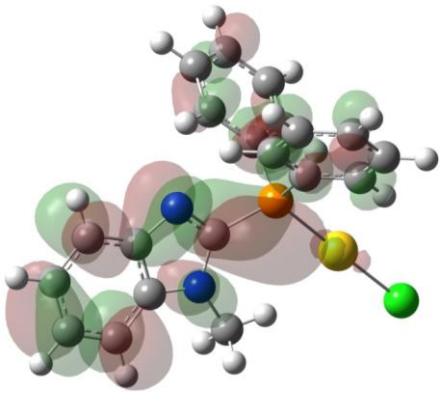

Figure 3.21. The orbital correlation diagram of LUMO molecular orbital 92 (isovalue plot = 0.02).

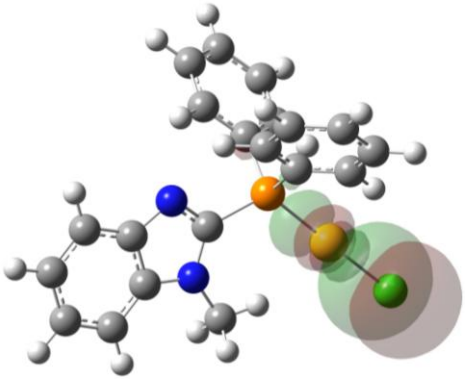

Figure 3.22. The orbital correlation diagram of HOMO molecular orbital 91 (isovalue plot = 0.02).

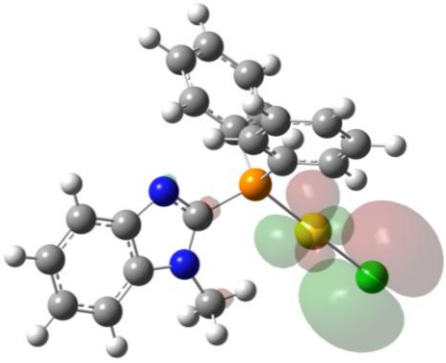

Figure 3.23. The orbital correlation diagram of HOMO-1 molecular orbital 90 (isovalue plot = 0.02).

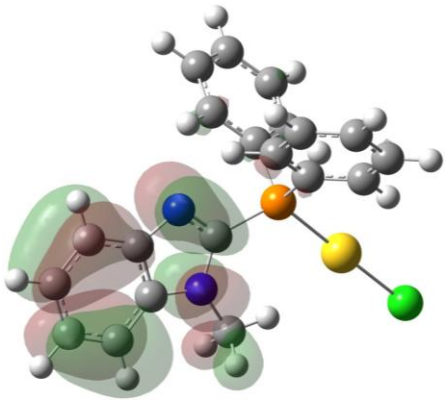

Figure 3.24. The orbital correlation diagram of HOMO-2 molecular orbital 89 (isovalue plot = 0.02).

CHAPTER 4

Characterization and PL Studies of Dinuclear and Tetranuclear Gold (I) and Silver (I) Complexes with the MBDP Ligand

4.1. Structural and PL Studies of Dinuclear Gold (I) Complex with MBDP Ligand (3)

4.1.1. Structural analysis. The gold (I) tetrafluoroborate complex was prepared by reaction of thtAuCl, **1**, and $AgBF_4$ in a 1:1:1 molar ratio in CH_3CN at room temperature. The byproduct, AgCl, precipitated immediately and was collected after formation by filtration through a pad of Celite. The filtrant was allowed to stir for 3 hours followed by a reduction in volume using high pressure vacuum. Layering with Et_2O yielded crystals in 80 % yield. The collected crystals appeared to have a pink colored tint to them. The color coating disappears when coated with Paratone-N oil rendering colorless crystals. The X-ray crystal structure of **3**, shown in Figure 4.1, is of a dinuclear gold (I) system with two ligands coordinated through the phosphorus and nitrogen atoms.

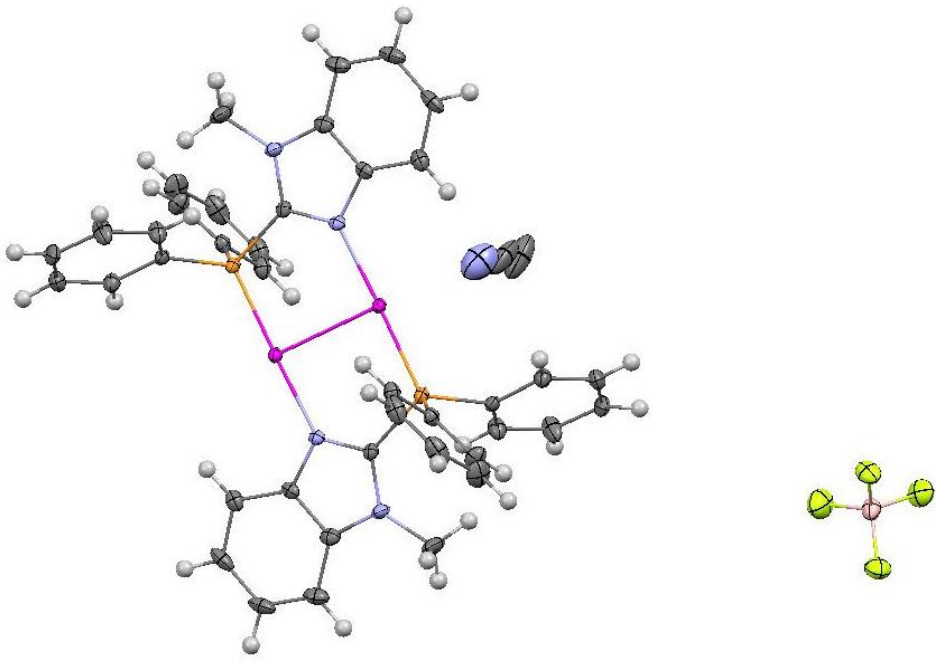

Figure 4.1. The X-ray crystallographic structure of **3**.

The complex, **3**, features an eight-membered ring system consisting of two metals, two phosphorus, two nitrogen, and two carbons. Atoms in the ring system are arranged in a head-to-tail and tail-to-head, P-Au-N and N-Au-P manner. Also, the solvent (CH_3CN) is seen trapped uncoordinated within the crystal as well as BF_4^- counterion stabilizing the charge of **3**.

Figure 4.2 shows the packing diagram of **3** looking down the a-axis. The unit cell view shows an arrangement of the dimers forming a channel filled with the counterion, BF_4^-. The **3** crystallizes in a monoclinic, $P2_1/n$, space group featuring symmetry operators, identity, screw axis, inversion center, and glide plane. The X-ray crystallographic details are given in Table 4.1. The complete X-ray crystallography details can be found in Appendix C.

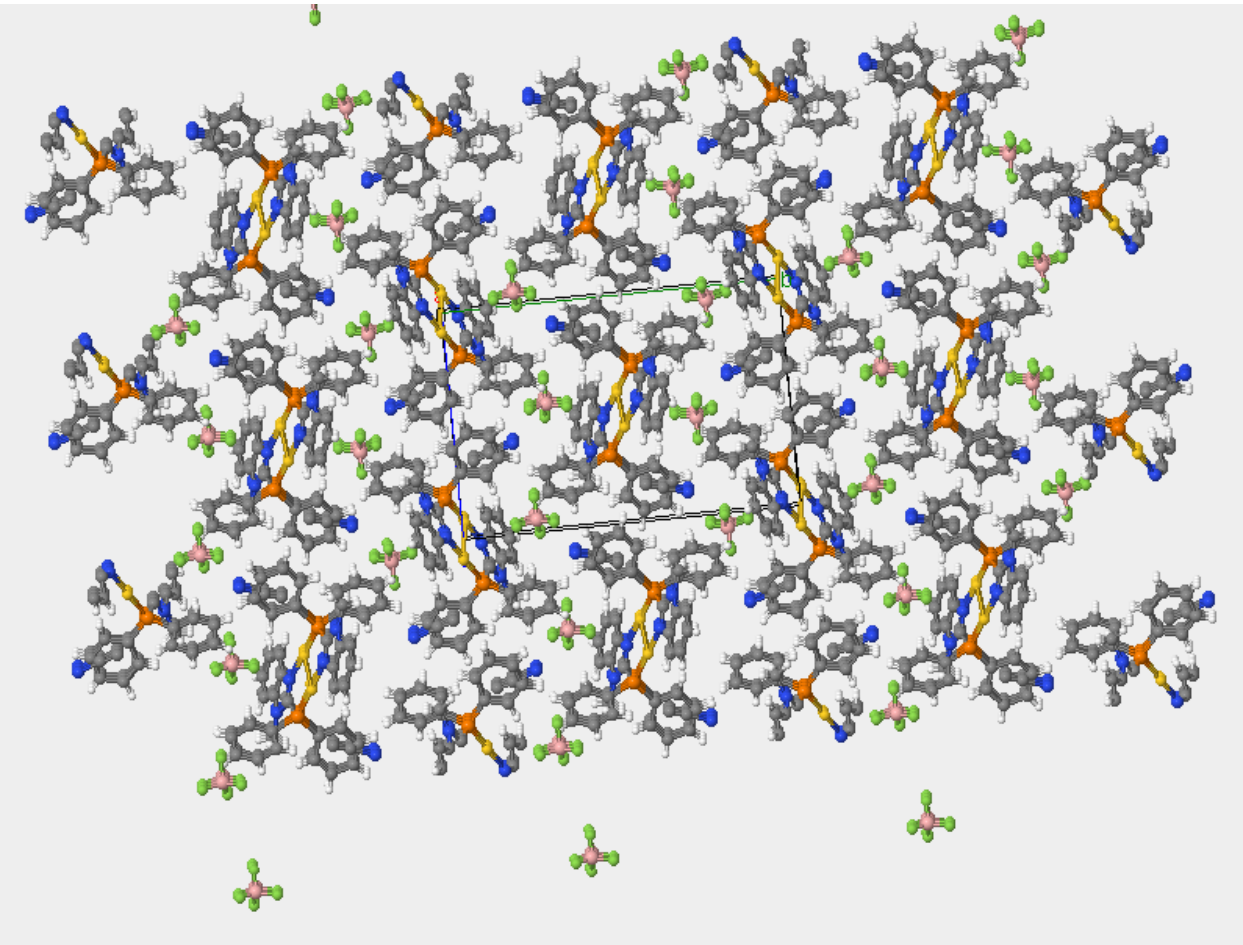

Figure 4.2. Packing diagram of **3**.

Table 4.1

*X-ray Crystallographic Details for **3***

Formula weight	643.17	
Temperature	200(2) K	
Wavelength	0.71073 Å	
Crystal size	0.200 x 0.500 x 0.600 mm	
Crystal habit	colorless needle	
Crystal system	monoclinic	
Space group	P 1 21/n 1	
Unit cell dimensions	a = 8.9993(8) Å	α = 90°
	b = 19.6166(18) Å	β = 100.966(2)°
	c = 13.4484(12) Å	γ = 90°
Volume	2330.8(4) $Å^3$	
Z	4	
Density (calculated)	1.833 Mg/cm^3	
Absorption coefficient	6.427 mm^{-1}	
F(000)	1240	
Theta range for data collection	2.08 to 25.04°	
Index ranges	-10<=h<=10, -23<=k<=23, -16<=l<=16	
Reflections collected	20345	
Independent reflections	4076 [R(int) = 0.0548]	
Coverage of independent reflections	98.80%	
Max. and min. transmission	0.3597 and 0.1134	
Structure solution technique	direct methods	
Structure solution program	SHELXS-97 (Sheldrick, 2008)	
Refinement method	Full-matrix least-squares on F^2	
Refinement program	SHELXL-97 (Sheldrick, 2008)	
Function minimized	$\Sigma w(F_o^2 - F_c^2)^2$	
Data / restraints / parameters	4076 / 0 / 291	
Goodness-of-fit on F^2	0.981	
Δ/σ_{max}	6.827	
Final R indices	3376 data; I>2σ(I)	R1 = 0.0264, wR2 = 0.0635
	all data	R1 = 0.0356, wR2 = 0.0699
Weighting scheme	w=1/[$\sigma^2(F_o^2)$+(0.0299P)2+4.7568P]	
	where P=(F_o^2+2F_c^2)/3	
Largest diff. peak and hole	1.225 and -0.808 $eÅ^{-3}$	
R.M.S. deviation from mean	0.146 $eÅ^{-3}$	

Table 4.2 provides selected bond angles and lengths for complex **3**. The geometry surrounding the gold appears to be near trigonal planar with an average bond angle of 119.08 º when examining the three bonds consisting of Au-N, Au-P, and Au-Au. However, the bond between the two gold atoms is not a "real" bond. It is an aurophilic interaction, because the distance is shorter than the sum of the van der Waals radii. The short Au-Au distance is 2.80 Å. Catalano [42] showed the Au-Au distance in his work to be similar at 2.82 Å. The actual geometry around the gold (I) is assigned as linear with P-Au-N bond angle of 178. 3 º. The bond lengths in angstroms corresponding for the Au-P and Au-N are 2.228 and 2.074, respectively. The bond angles for the P-Au-Au and N-Au-Au are 91.85 º and 87.1 º (respectively).

Table 4.2

*Selected bond lengths and angles for **3***

Bond Length (Å)	
Au1-Au2	2.808(4)
Au1-P1	2.228(3)
Au1-N2	2.074(4)
P1-C1	1.805(5)
P1-C15	1.836(5)
P1-C9	1.814(5)
Bond Angle (Å)	
N2-Au1-P1	178.31(11)
N2-Au1-Au2	87.08(11)
P1-Au1-Au2	91.86(3)
C15-P1-Au1	114.81(17)
C9-P1-Au1	112.46(18)
C1-P1-Au1	108.70(17)
C6-N2-Au1	122.80(3)
C1-N2-Au1	130.10(3)

4.1.2. Material characterization and PL studies. The complex **3** was characterized by NMR, IR, UV-Vis, and photoluminescence. The **3** crystals were observed not to be soluble in the standard deuterated solvent, $CDCl_3$. Instead the spectra had to be collected using deuterated solvents CD_3CN or DCM. The ^1H NMR spectrum has a similar profile with the ligand. The major difference here was the CH_3CN peak was present at 2.18 ppm as well as the residual solvent peak at 1.94 ppm. This confirms the assignment of the solvent in the X-ray crystal structure. The ^{31}P NMR revealed a single peak at 27.9 ppm. This is significantly different than the ligand, **1**, and the AuCl complex, **2**. The ^{31}P NMR is ~ 53.5 ppm down field from **1** and ~ 13.3 ppm from **2**.

The absorbance spectrum of **3** is shown in Figure 4.3. The spectrum is different from that of **1**. An overlap is found in Figure 4.4 of the ligand and **3** with only two major peaks at 198 and 279 nm. The peak at 198 nm is similar to **1**. However the peak at 279 nm is a broad hump masking the two well resolved peaks found in the spectrum of **1**. There is a shoulder at 226 nm similar to the peak found in the **2** complex. The molar extinction coefficient for the 198 nm peak was calculated to be 141000 M^{-1} cm^{-1} similar to that of **1**. The 224 nm shoulder has a molar extinction coefficient of 70700 M^{-1} cm^{-1}. The last peak seen at 279 nm has molar extinction coefficient 49400 M^{-1} cm^{-1}, respectively. Because of these molar extinction coefficient values (> 10^3 M^{-1} cm^{-1}), assignment to the spin allowed $\pi \rightarrow \pi^*$ is tolerable. This transition has been assigned to **1**, **2**, and **3** thus far.

The crystals were initially excited using a handheld UV lamp, excited by short and long wavelengths. They appear white in color. The photoluminescence steady-state excitation and emission of **3** were collected at liquid nitrogen temperature. The excitation spectrum for **3**, while monitoring the emission at 454 nm, is similar in profile to the free ligand ranging from 280 to

420 nm. The excitation maximizes at 331 nm with a several vibronic components with average spacing of ~1352. The emission profile for the ligand is also broad with several vibronic components seen while monitoring the emission range from 360 to 634 nm with excitation at 340 nm. Also with this complex some vibronic components found with the free ligand are no longer present. The vibronic components, 380, 420, 452, 474, 512, and 556 have an averaging space of ~1426 cm^{-1}. In Figure 4.5 can be seen the overlap of the excitation and emission spectra for **3**.

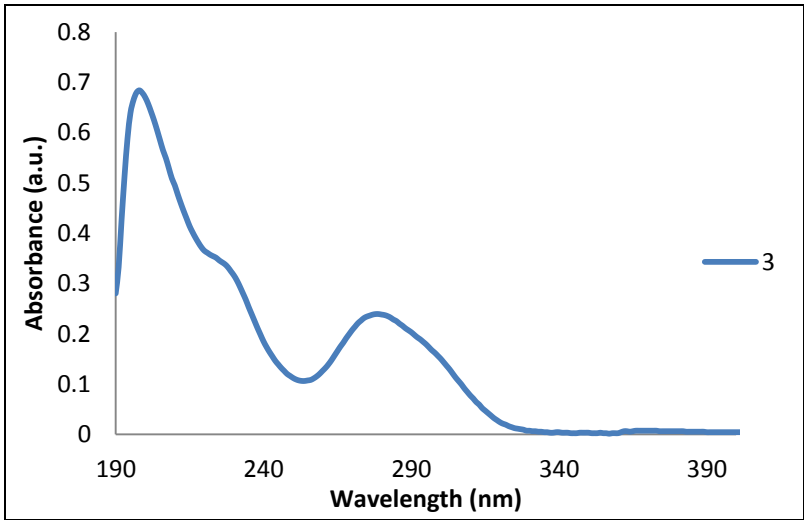

Figure 4.3. The absorbance spectra of **3**.

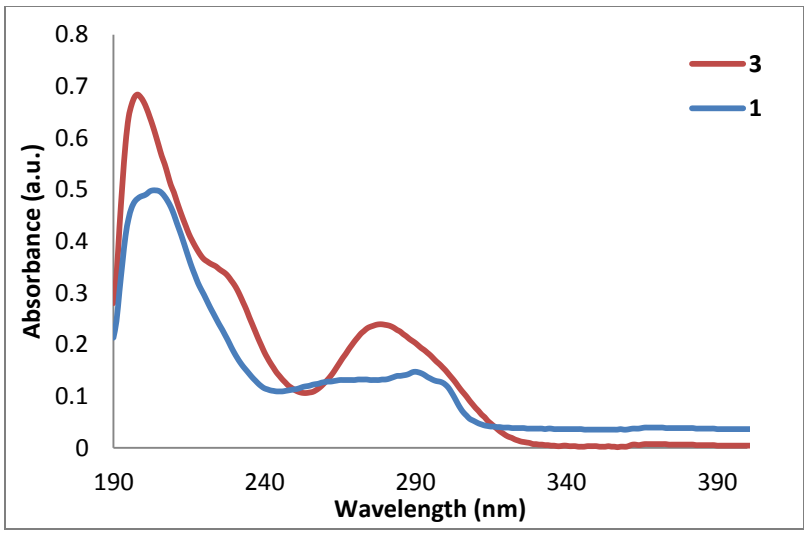

Figure 4.4. The absorbance overlap of **3** and the ligand.

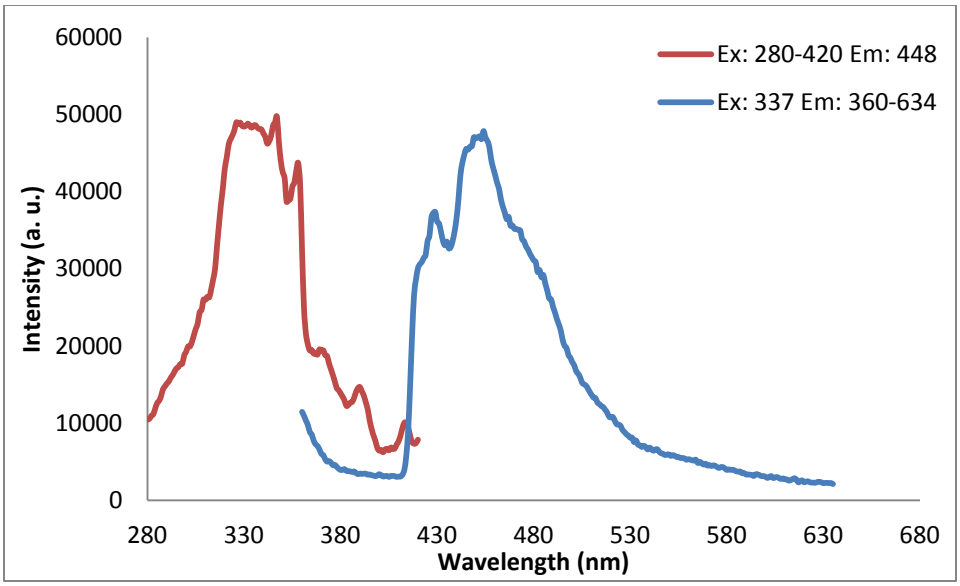

Figure 4.5. Overlap of the excitation and emission spectra of **3**.

4.1.3. Solvent effects on compound 3. Compound **3** was prepared in CH_3CN and crystallized with an CH_3CN molecule trapped in the crystal lattice. Several attempts were taken to remove CH_3CN from the lattice including recrystallization using a different solvent, gentle heating, and lattice perturbation. These studies were aimed at understanding the solvent effect in crystal modulation and the nature of luminescence changes induced due to the presence of the solvent in the lattice.

Gentle heating at 80 ºC for seven days did not effectively remove CH_3CN from the crystals. Noticeable changes that occurred were the degradation of the crystals from the pinkish color to dark purple/black. The dark color is an indication of decomposition in gold compounds. Each day for one week a single crystal was removed from a watch glass that was placed in an oven. The crystal was analyzed using IR as it requires very little sample. The C-N stretching peak was present on each IR spectrum. After seven days of heating the experiment had to cease as the crystals started to turn dark.

Following the synthesis of **3**, crystallization methods were used to obtain crystals using standard organic solvents other than CH_3CN, namely, THF layered with Et_2O, THF layered with hexanes, DCM layered with Et_2O and DCM layered with hexanes. All attempts yielded a white solid powder. NMR, IR, and photoluminescence spectra were collected for the powder with attempted recrystallization using THF/Et_2O.

Solvent dependent behaviors were evident in these studies. The ^1H NMR for the powder was collected using deuterated $CHCl_3$. As previously stated the crystals of **3** were not soluble in $CHCl_3$ as well as hexanes, nor Et_2O. However, the crystals of **3** were found to be very soluble in MeOH, CH_3CN, acetone, and soluble in THF and DCM. To further verify this observation, powder samples from all recrystallization steps, THF layered with Et_2O, THF layered with hexanes, DCM layered with Et_2O and DCM layered with hexanes, were dissolved in $CHCl_3$. The likely cause of this occurrence is result of a potentially large surface area of the crystal. Considering the crystal dissolves in the polar organic solvents THF and DCM, there should not be any hesitation towards dissolution in $CHCl_3$. Disruption of the crystal lattice caused an increase in surface area. This resulted in an increase in solubility in $CHCl_3$.

It was also observed that the crystals had unique tints to them that appeared removable when placed in oil. The same loss of tint is seen in Figure 4.6 (a) showing pictures of the crystals, amplified by microscopy, which did not dissolve in $CHCl_3$. The crystals appeared white in color and shattered. Balch presented polymorphs of linear Au (I) complexes with different physical properties. The description of the complex, $(C_6H_{11}NC)_2Au\ (I)](PF_6)$, polymorphs were present in two forms, colorless or pale yellow crystals. Owing to the fact that they both were obtained from the same solution, some association existed between the two forms.

While X-ray crystallography data of the pinkish crystals of complex **3** was produced, the proper conditions are not readily available to produce the same results from the powder form when using solvents other than acetonitrile for. From this observation, some intermolecular forces must exist between the dimer and CH_eCN that encourages crystallization. Further support for this observation comes from attempts to complete the synthesis of the dimer in DCM. While using the handheld UV lamp, the crystals luminesced bright blue in color as can be seen in Figure 4.6 (b). Photoluminescence details of these materials are given later.

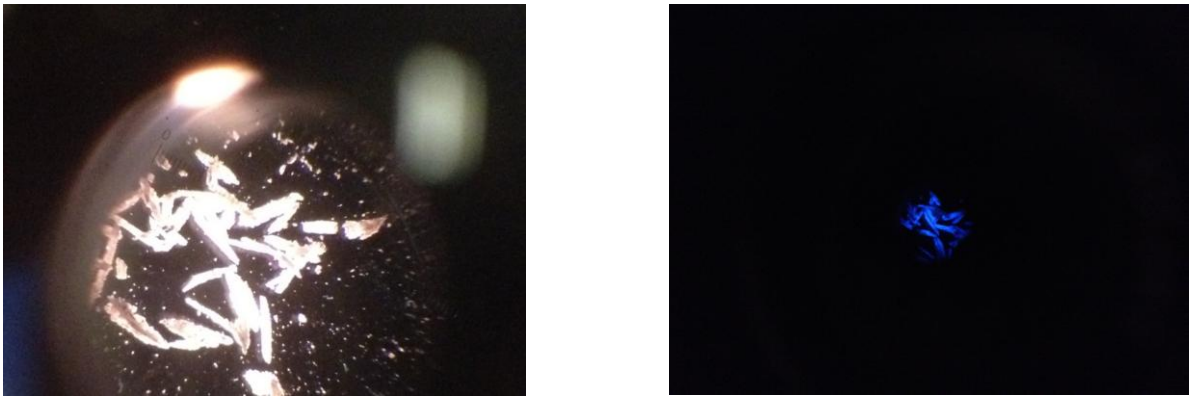

(a) (b)

Figure 4.6. (a) View of crystals after exposure to the solvent, $CDCl_3$, and (b) View of (a) under UV exposure.

In Figure 4.7, the ^1H NMR shows the acetonitrile peak at 1.99 ppm. When considering the concentration of the CH_3CN to the solvent $CDCl_3$, it is severly diminished, Figure 4.8 provides a comparison of the **3** ^1H NMR spectrum collected in CD_3CN. A note should be made about the $CDCl_3$, it is clearly hydrated with an H_2O peak at 1.53 ppm and the internal reference TMS is seen at 0.00 ppm. The ^{31}P NMR showed a small chang in position. The crystal, **3**, has a peak at 24.1 ppm whereas the the powder has a peak at 27.9 ppm.

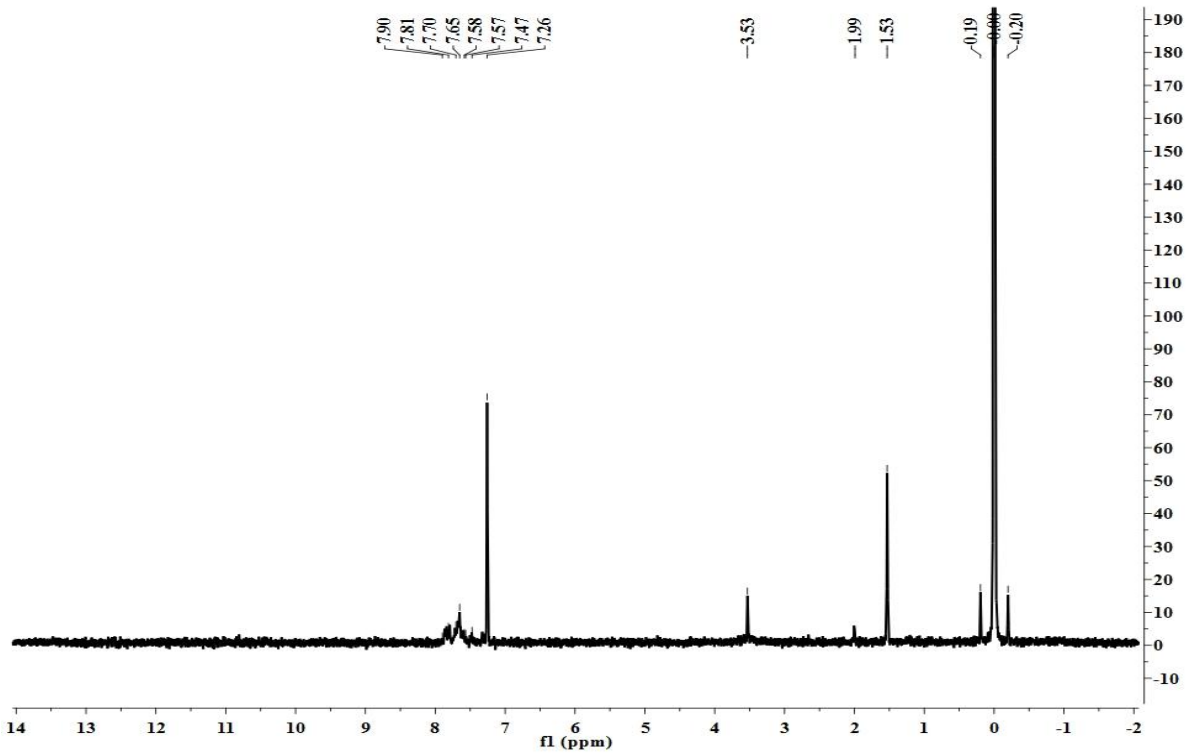

Figure 4.7. The ^{1}H NMR spectrum of **3**, the powder after recrystallization steps $CDCl_3$.

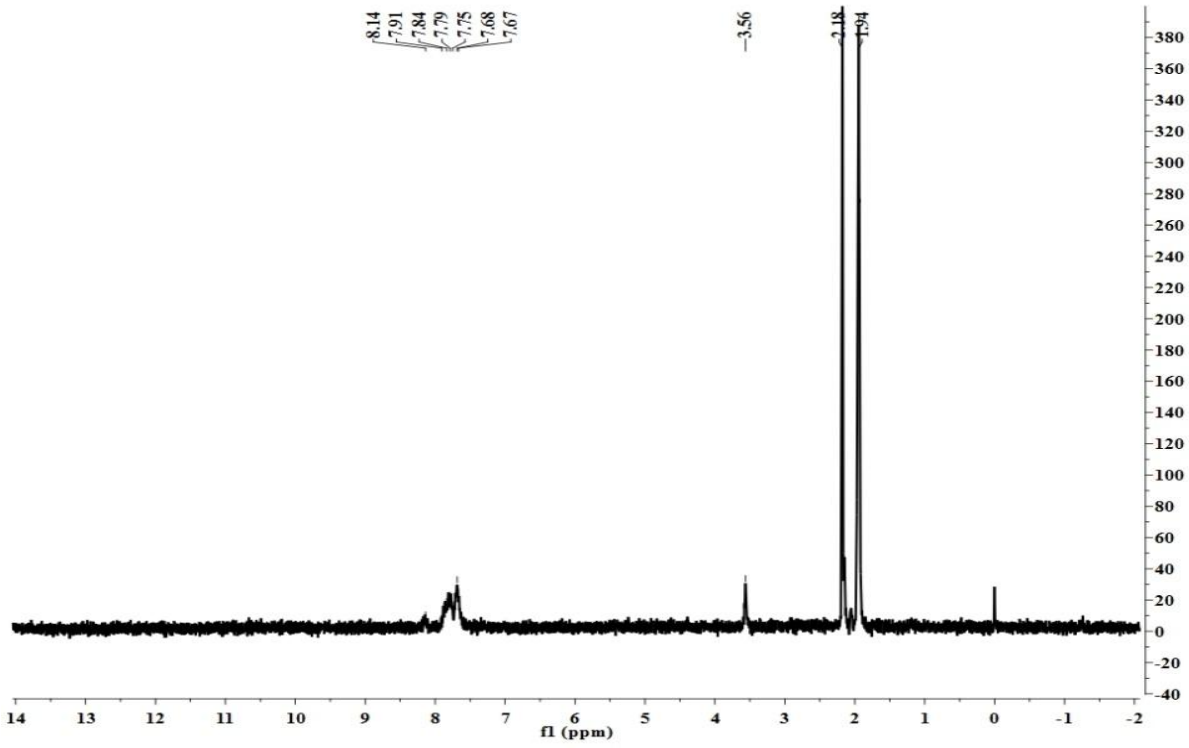

Figure 4.8. The ^{1}H NMR spectrum of **3** crystals in CD_3CN.

Corroboration of the NMR findings, IR spectra was acquired. The IR spectrum of **3** (Figure 4.9) revealed $\upsilon_{C\text{-}N}$ symmetric stretching of the CH_3CN is observed at 2250 cm^{-1}. Contrary to the positive identification of CH_3CN in Figure 4.9, the IR spectrum of the powder sample of **3** seen in Figure 4.10 does not contain the C-N stretching mode. Further verification was conducted by preparing a blank KBr pellet and spraying with CH_3CN not to saturate the pellet. The results are seen in the IR spectrum in Figure 4.11, where there is an obvious C-N stretching peak at 2250 cm^{-1}. These results show that the removal of CH_3CN is possible.

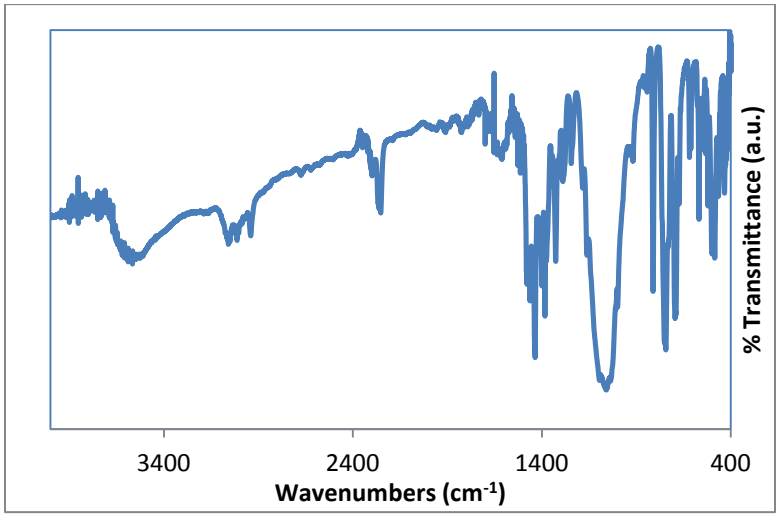

*Figure 4.*9. IR spectrum of X-ray quality crystals of **3**.

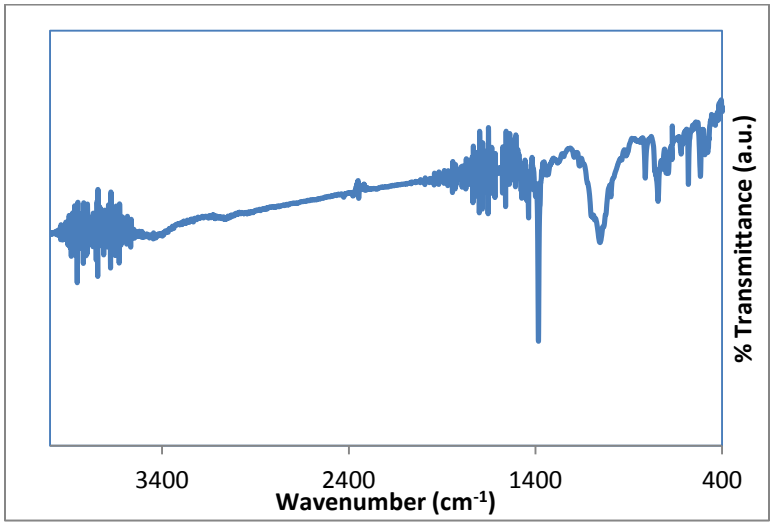

Figure 4.10. IR spectrum of the recrystallization powder of **3**.

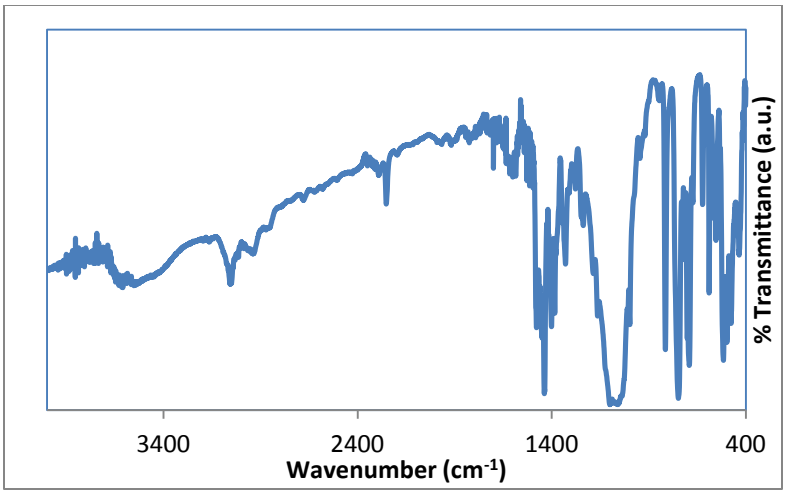

Figure 4.11. IR spectrum of the powder with CH_3CN spray.

The evaluation of vapor interaction using various solvents such as DCM, $CHCl_3$, and CH_3CN was conducted. In Figure 4.12 is a picture of the experimental apparatus used for vapor diffusion. Crystals were place inside the bottom of a vial. The end of a glass pipette was fire-sealed and placed inside the same vial with the crystals. The sealed tube was then filled with either DCM or $CHCl_3$. The vials were fitted with a cap and carefully wrapped with parafilm. The crystals were placed in a refrigerator or left on the benchtop overnight. Although exposure varies depending on the camera, altering color rendering, the luminescence of the crystalline material is shown to be brighter in the vial exposed to DCM or CH_3Cl.

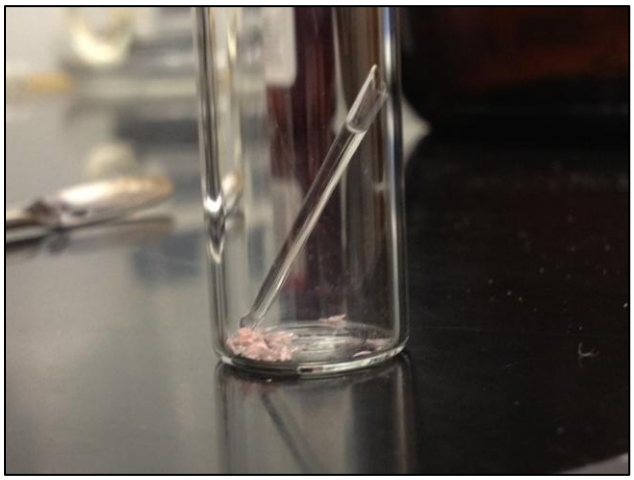

Figure 4.12. The set-up used for DCM vapor diffusion interactions with **3**.

There was a color change observed with the crystals. The apparent loss of the pinkish hue was seen without submersion in the solvent (photograph not shown here). Figure 4.13 represents the visual changes seen under the handheld UV light and using long-wavelength (360 nm) excitation. With the vial to the right crystals of **3** and the vial to the left has **3** exposed to DCM vapors.

Figure 4.13. Examination of the crystals of **3** and the vapor diffused crystals under a handheld UV light source.

The CH_3CN vapors were reintroduced to the crystals in the same manner as the DCM. The vial was capped and placed inside the refrigerator. The vial appeared to have droplets forming along the inside of the vial. After a week all of the crystals had dissolved. The process was repeated with the vial being placed in the back of a hood and left undisturbed for one week.

It should be noted that as cap of the vial was loosened and the solvent slowly evaporated leaving crystals of **3** verified by ^{31}P NMR. The dissolution of the crystals and subsequent crystallization further supports the conclusion there is sensitivity to CH_3CN with this system.

Continuation of the study regarding CH_3CN was completed by monitoring the photoluminescence profiles of **3** along with the vapor exposed crystals and powder samples. Comparison of collected the photoluminescence spectrum of **3** is presented in Figure 4.5, with that of the spectra of the powder sample, as well as the spectra of the DCM vapor exposed sample. The steady-state excitation and emission spectra of the previously described powder is presented in Figure 4.14. The profile is similar to **3**, although there is a shift in relative intensity. This could be due to disruption of the crystal lattice or placement of the sample in the instrument. The inference here is that the powder and crystal luminescence is the same and that presence of CH_3CN has no effect on the photoluminescence behavior of the complex.

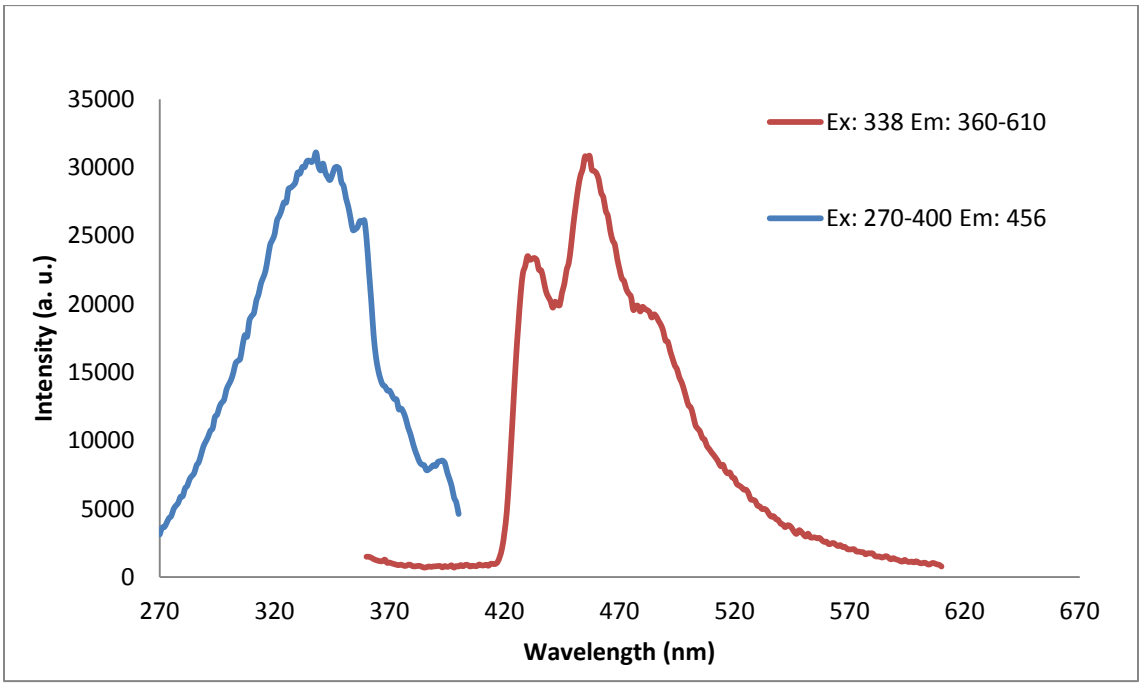

Figure 4.14. Excitation (blue) and emission (red) overlap spectra of the powder collected after the attempted recrystallization steps.

The photoluminescence profile for the DCM vapor exposed crystals is shown in Figure 4.15. The spectra were collected while using an excitation filter. The spectral profiles are different from that of the complex **3** and also the powder. The excitation maxima (λ_{exc}) shifts to 374 nm. Albeit, the shape of the profile was maintained, broad and containing several vibronic components with an average spacing of ~1402 cm^{-1}, the λ_{exc} red shifted by ~36 nm. The emission maxima (λ_{em}) blue shifted to 425 nm while having vibronic components with an average spacing of ~974 cm^{-1} is comparable to the profile of **3**. The Stokes shift for the **3** was calculated to be ~117 nm while the DCM vapor exposed crystals had a Stokes shift of approximately one half of that value, ~ 59 nm. The fluorescence behavior of the complex **3**, the powder, and the vapor exposed crystals all follow the trend found in $\pi \rightarrow \pi^*$, intraligand centered electronic transitions.

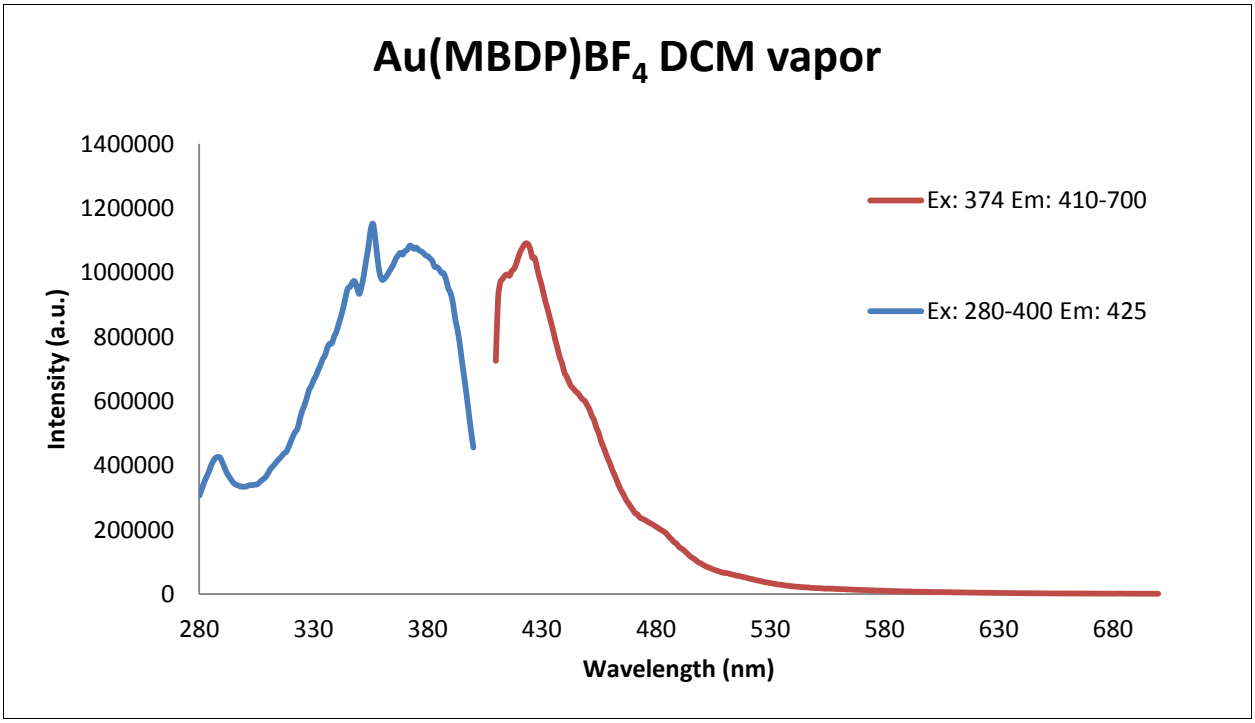

Figure 4.15. The overlap of excitation (blue) and emission (red) spectra of the DCM vapor diffused crystals.

To conclude this section, the IR spectrum seen in Figure 4.16 provided details showing a lack of CH_3CN in the DCM vapor exposed crystals. The removal of CH_3CN by DCM vapors was successful and subsequent reintroduction of CH_3CN was also successful. Finally, the pink color seen with these crystals have an unknown origin that does not affect the contents of the crystal lattice or is not seen in any of the spectroscopic techniques used in this investigation.

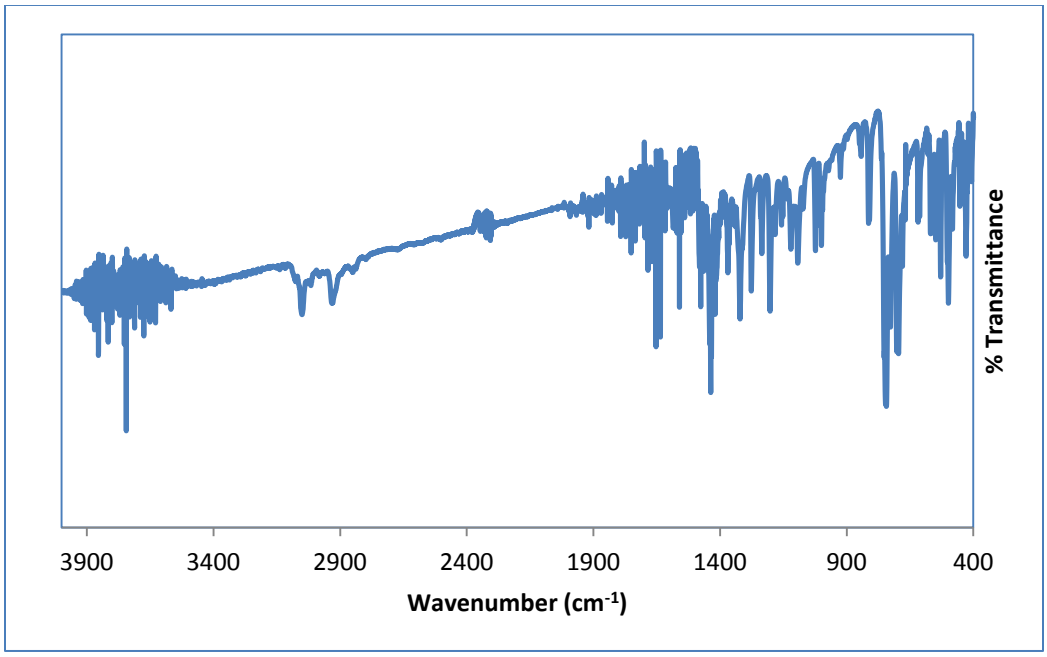

Figure 4.16. IR spectrum of the DCM vapor diffused crystals.

4.2. Structural and PL Studies of Dinuclear Silver (I) Complex with MBDP Ligand (4)

4.2.1. Structural analysis. The silver (I) tetrafluoroborate complex with the MBDP ligand (1:1 molar ratio) was prepared in CH_3CN at room temperature in an aluminum foil covered vessel and stirred for 3 hours in a darkened room. Partial removal of solvent followed by layering with Et_2O yielded colorless crystals after 4 days. The thermal ellipsoid view of the X-ray crystal structure of **4** is shown in Figure 4.17. Figure 4.18 is the packing diagram of **4** looking down the a-axis showing the dimers arrangement within the unit cell and the counterions, BF_4^-, similar to the packing found in **2**. It features the characteristic ring system of

the dinuclear metal and bidentate attribute of the P,N ligand, described in the introduction. The ring system consists of two silver (I) atoms bound in a head-to-tail and tail-to-head (P-Ag-N and N-Ag-P, respectively) manner to phosphorus and nitrogen atoms of two ligand molecules. The X-ray crystallographic details for **4** are given in Table 4.3. Complete X-ray crystallographic details are found in Appendix D.

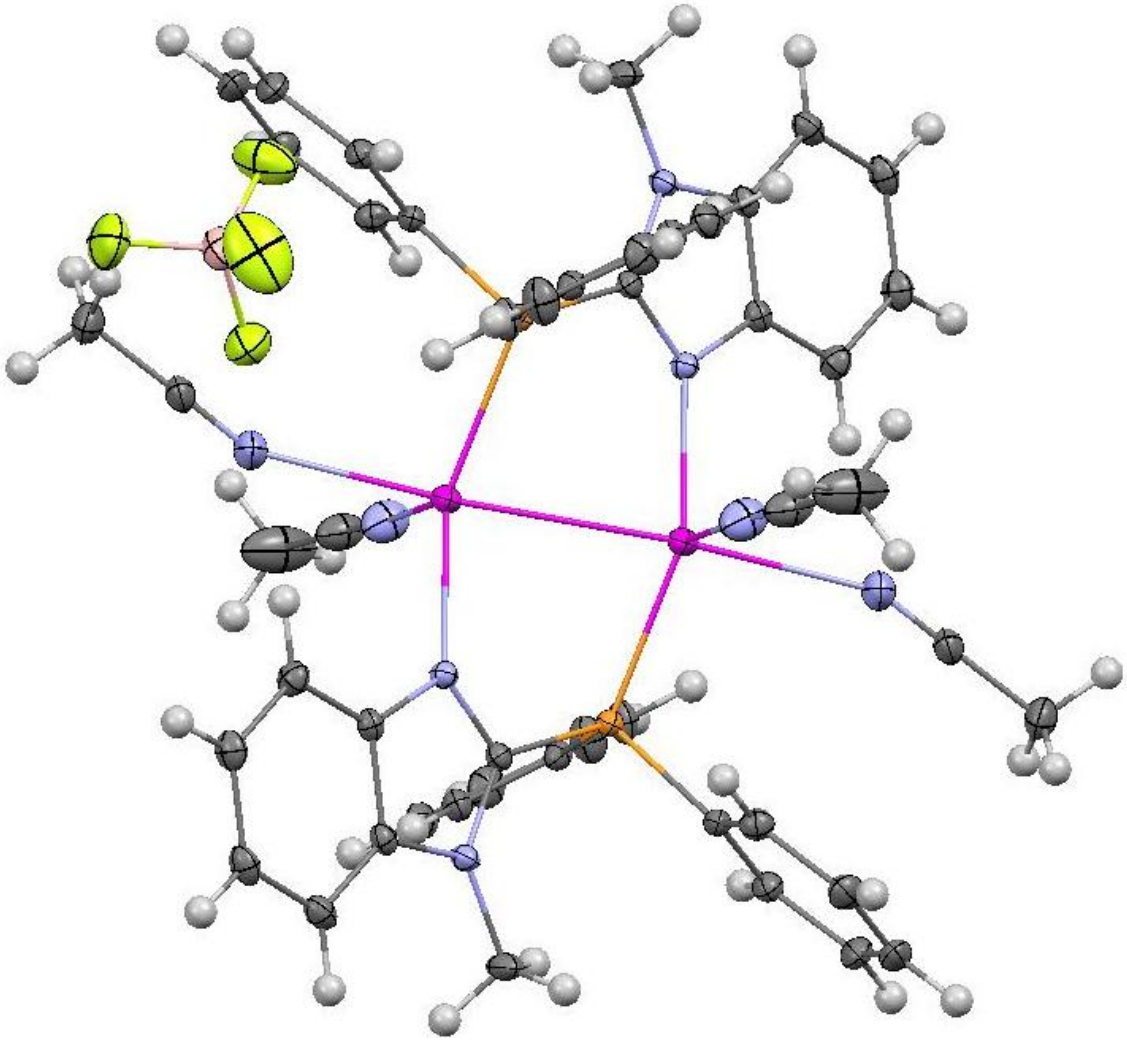

Figure 4.17. Thermal ellipsoid view of **4**.

There are two CH_3CN molecules attached to each of the silver atoms. This is typical of silver (I) complexes due to the preference of a tetrahedral geometry over linear. The dinuclear complex crystallizes in the triclinic space group P-1 having one molecule in the unit cell.

Table 4.3

X-ray structural data for 4

Chemical formula	$C_{48}H_{48}Ag_2B_2F_8N_8P_2$	
Formula weight	1188.24	
Temperature	200(2) K	
Wavelength	0.71073 Å	
Crystal size	0.200 x 0.400 x 0.600 mm	
Crystal habit	colorless needle	
Crystal system	triclinic	
Space group	P -1	
Unit cell dimensions	a = 10.5423(10) Å	α = 88.592(3)°
	b = 10.7638(10) Å	β = 73.097(3)°
	c = 12.3530(12) Å	γ = 84.422(3)°
Volume	1334.8(2) $Å^3$	
Z	1	
Density (calculated)	1.478 Mg/cm^3	
Absorption coefficient	0.862 mm^{-1}	
F(000)	598	
Theta range for data collection	1.72 to 25.09°	
Index ranges	-12<=h<=12, -12<=k<=12, -14<=l<=14	
Reflections collected	12591	
Independent reflections	4657 [R(int) = 0.0421]	
Coverage of independent reflections	97.80%	
Absorption correction	multi-scan	
Max. and min. transmission	0.8465 and 0.6259	
Structure solution technique	direct methods	
Structure solution program	SHELXS-97 (Sheldrick, 2008)	
Refinement method	Full-matrix least-squares on F^2	
Refinement program	SHELXL-97 (Sheldrick, 2008)	
Function minimized	$\Sigma w(F_o^2 - F_c^2)^2$	
Data / restraints / parameters	4657 / 0 / 320	
Goodness-of-fit on F^2	1.114	
Δ/σmax	0.013	
Final R indices	4096 data; I>2σ(I) R1 = 0.0337, wR2 = 0.0929	
	all data R1 = 0.0402, wR2 = 0.1040	
Weighting scheme	$w=1/[\sigma^2(F_o^2)+(0.0575P)^2+0.1523P]$	
	where $P=(F_o^2+2F_c^2)/3$	
Absolute structure parameter	0.0(1)	
Extinction coefficient	0.0027(10)	
Largest diff. peak and hole	0.874 and -0.425 $eÅ^{-3}$	
R.M.S. deviation from mean	0.097 $eÅ^{-3}$	

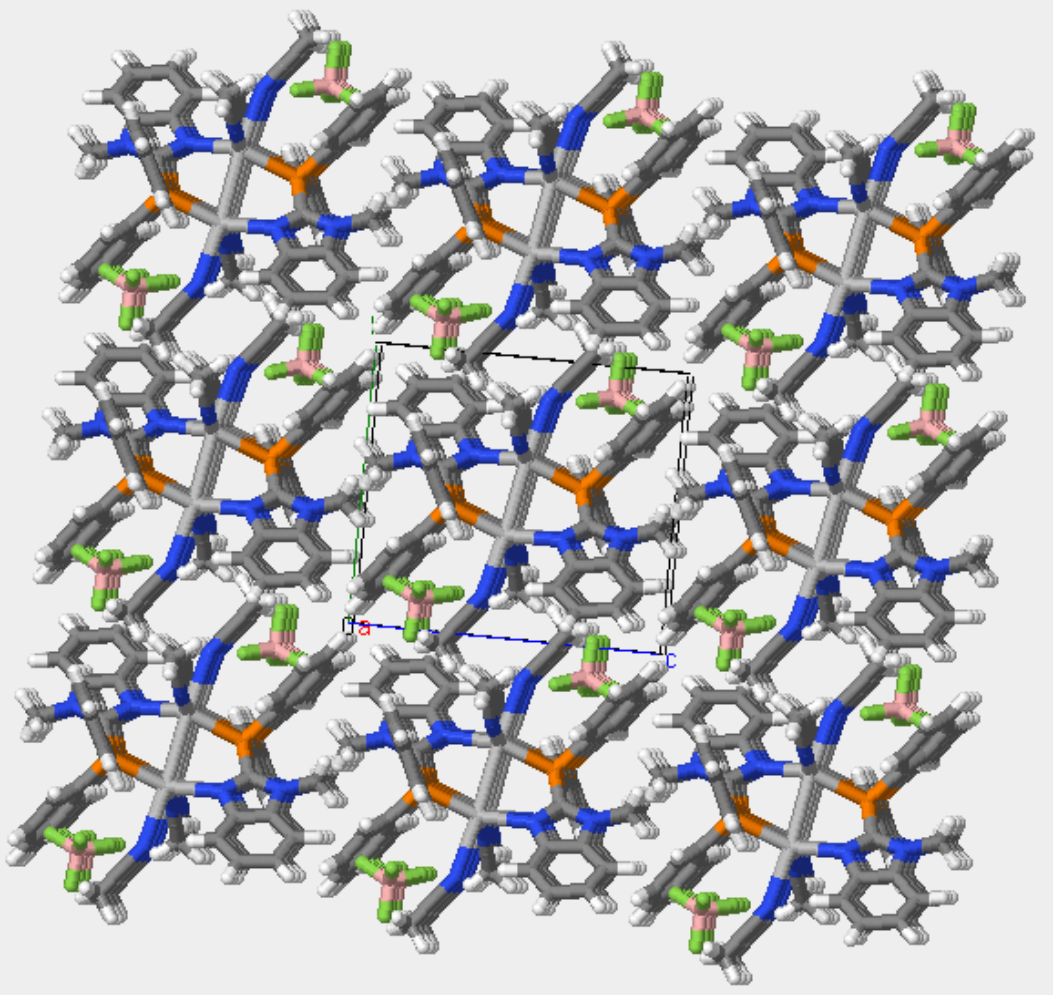

Figure 4.18. The packing diagram of **4**.

Table 4.4 provides selected bond angles and lengths for complex **4**. The geometry surrounding the silver appears to be trigonal bipyramidal considering the five bond types of three Ag-N, one Ag-P, and one Ag-Ag. The bond between the two Ag atoms, it is argentophilic. The same criteria used for determining aurophilic interactions with gold atoms having shorter distances than their van der Waals radii is also extended to silver. The actual geometry around the silver (I) is assigned as pseudo-tetrahedral with an average bond angle of 106.4 º. The short Ag-Ag bond distance is 3.017 Å. The bond lengths in angstroms corresponding to the Ag-P, Ag-N1, Ag-N3, and Ag-N4 are 2.883, 2.226, 2.502, and 2.429 (respectively). The bond angles for the P1-Ag1-N1, P1-Ag1-N3, P1-Ag1-N4, are 147.4 º, 96.0 º, and 109.9 º (respectively).

Table 4.4

*Selected bond lengths and bond angles for **4***

Bond Length (Å)	
Ag1-Ag2	3.017
Ag1-P1	2.388
Ag1-N1	2.226
Ag1-N3	2.502
Ag1-N4	2.429
Bond Angle (˚)	
N1-Ag1-P1	147.39(6)
N1-Ag1-N4	99.82(11)
P1-Ag1-N4	109.91(10)
N1-Ag1-N3	98.85(10)
P1-Ag1-N3	96.03(8)
N4-Ag1-N3	86.61(13)
N1-Ag1-Ag2	85.63(6)
P1-Ag1-Ag2	80.72(2)
N4-Ag1-Ag2	91.33(9)
N3-Ag1-Ag2	175.33(8)

Abdul Jalil [41] and Catalano [42] studied similar silver (I) complexes with a N,P imidazole-type ligand. The major difference in their studies was the choice of the anion, NO_3^- (Abdul Jalil) and ClO_4^- (Catalano). The Ag-Ag, Ag-P and Ag-N1, bond distances reported by Abdul Jalil were 2.92, 2.39, and 2.21 Å; whereas Catalano reported Ag-Ag, Ag-P, and Ag-N are 2.99, 2.38, and 2.20 Å. When comparing those Ag-Ag distances to complex **4**, there is a small variation of less than 0.1 Å . Albeit, there are differences in the reported geometries surrounding the Ag than with **4**, the variant distortions have no significant role with the Ag-Ag interaction. As for the Ag-P bond, complex **4** had a greater length on average of approximately 0.498 Å. Although the anion varied, the behavior of the Catalano complex is similar to **4** with CH_3CN bound to the Ag atom. However, comparably the Ag-N1 bond length (N of the imidazole ring), it is roughly estimated to be the same measuring 2.2 Å. The notable difference between **4** and the reported structures is the Ag-P relationship. Catalano reports P-Ag-N angles of 157.54, 86.75,

and 115.38 º whereas **4** have values of 147.39, 109.91, and 96.03 º. Moreover, the Ag-P bond distance is greatest in the **4** complex when compared to the mono- and dinuclear gold complexes, **2** (2.225 Å) and **3** (2.227 Å). The differences in these lengths are a result of the geometry surrounding the metal.

4.2.2. Material characterization and PL studies. The silver (I) complex, **4**, was characterized using ^{31}P and ^{1}H NMR in $CDCl_3$ at room temperature. The ^{31}P NMR data collected provided a single broad peak at -1.66 ppm, while using the standard phosphoric acid. Previous reports [31, 34, 47] of ^{31}P NMR data for silver phosphorus complexes have broad peaks as seen for complex **4**. The ^{1}H NMR was in good range with the ligand and other than small shifts and the appearance of CH_3CN, a sharp peak at 2.15 ppm as well as the CD_3CN peak at 1.96 ppm.

The photoluminescence steady-state excitation and emission of **4** were collected at liquid nitrogen temperature. The excitation spectrum for **4**, while monitoring the emission at 451 nm, is similar in profile to the free ligand ranging from 280 to 430 nm. The excitation maximizes at 322 nm with a second, smaller broad band at 358 with a slight red shift in the profile when compared to the ligand. The emission profile for the ligand is also broad with several vibronic components seen while monitoring the emission range from 350 to 620 nm with excitation at 322 nm. Also with this complex some vibronic components found with the free ligand are no longer present. The vibronic components, 380, 425, 452, 474, 512, and 556 have an averaging space of ~1639. cm^{-1}. Figure 4.19 shows the overlap of the excitation and emission spectra for **4**.

The absorbance bands seen at 200, 262, and 291 nm in the absorption spectra of Figure 4.20 corresponds to a HOMO – LUMO gap of ~ 50000 cm^{-1}. The molar extinction coefficients for each band were calculated to be 168000, 38000, and 41900 M^{-1} cm^{-1} (respectively) similar to the other complexes and ligand. More importantly, other than a slight difference in peak picking,

this absorbance spectrum looks very similar to the ligand and is shown in Figure 4.21. This is significant assigning the $\pi \rightarrow \pi^*$ transition.

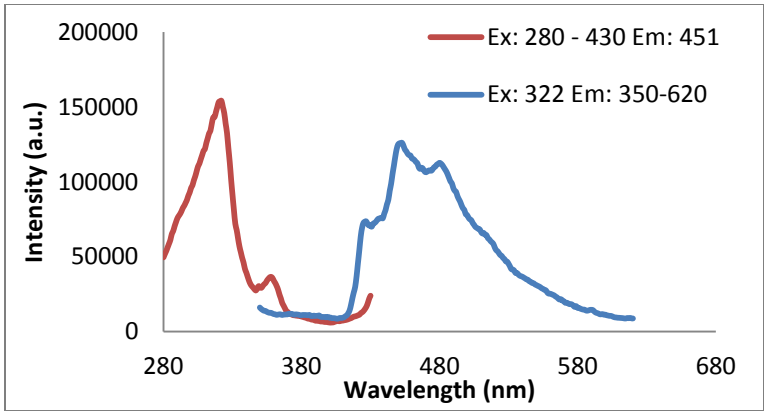

Figure 4.19. Overlap of Excitation (red) and Emission (blue) Spectra of the silver complex, **4**.

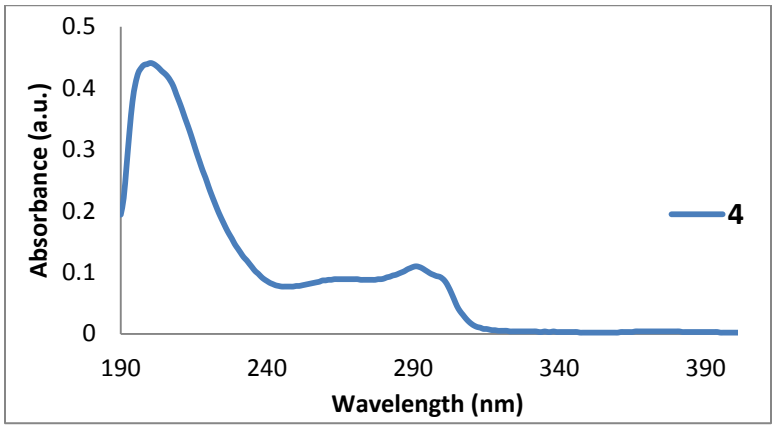

Figure 4.20. Absorption spectrum of **4**.

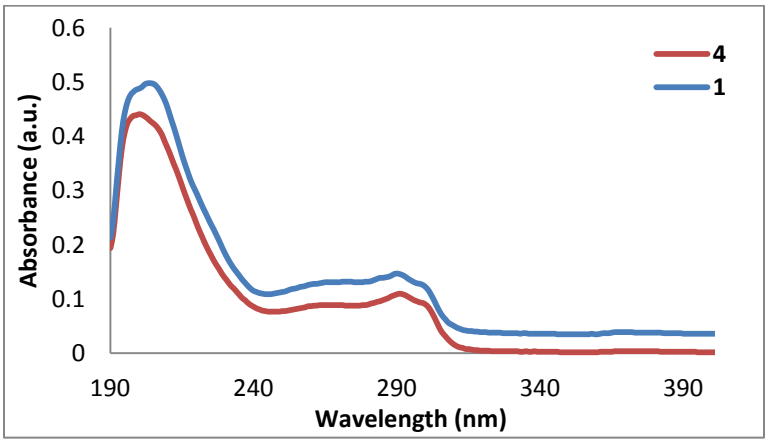

Figure 4.21. Absorption overlap of the **1** and **4**.

4.3. Structural and PL Studies of Tetranuclear Silver (I) Complex with MBDP Ligand (5)

4.3.1. Structural analysis. The silver (I) trifluoromethanesulfonate complex with the MBDP ligand (1:1 molar ratio) was prepared in CH_3CN at room temperature in an aluminum foil covered vessel and stirred for 3 hours in a dark room. Removal of solvent yielded an off-white solid. Dissolving the solid in CH_2Cl_2 followed by layering with Et_2O yielded colorless crystals after 4 days. The X-ray crystallographic details for **5** are given in Table 4.5. The complete X-ray

crystallographic details are found in Appendix E. For simplification purposes, the hydrogen atoms have been hidden in the thermal ellipsoid view of the X-ray crystal structure of **5** is shown in Figure 4.22. This extraordinary structure features four Ag atoms with short metal-metal distances. There are two ligands bridging two silver atoms together. The weakly coordinated triflate anion also formed a bond with to Ag ion through an O. Finally, the unexpected bridging of the diphenylphosphonic acid, a byproduct of the ligand synthesis, with bonding through the O, bringing the two silver dimers together to form a tetranuclear macrocycle. Shown in Figure 4.23 is a simplified structure of **5** showing the four Ag atoms are represented by the color silver, the O are shown in red, and the P are highlighted in orange.

The silver (I) complexes with weakly coordinating anions such as NO_3^- [47] and ClO_4^- [48], usually result with entrapment in the coordination sphere of the complex. However, the **5** complex has two triflate molecules coordinated to the silver (I) metal ion through oxygen bonds. Silver (I) prefers the tetrahedral geometry, binding with anions, $CF_3SO_3^-$, ClO_4^-, or NO_3^-, or solvents such as CH_3CN does occur to obtain the higher geometry. The structure of the **5** complex forms a rectangular shape with the silver atoms only. A prismic-type hollow develops with silver and oxygen atoms as the endpoints. The macrocycle is non-polymeric as individual molecules align as seen in the packing diagram (Figure 4.24).

Table 4.5

*X-ray structural data for **5***

Chemical formula	$C_{70}H_{54}Ag_4F_6N_4O_{10}P_4S_2$	
Formula weight	1844.65	
Temperature	200(2) K	
Wavelength	0.71073 Å	
Crystal size	0.200 x 0.300 x 0.400 mm	
Crystal system	monoclinic	
Space group	P 1 21/n 1	
Unit cell dimensions	a = 20.973(2) Å	α = 90°
	b = 14.8853(13) Å	β = 106.566(3)°
	c = 24.206(3) Å	γ = 90°
Volume	7243.2(12) $Å^3$	
Z	4	
Density (calculated)	1.692 Mg/cm^3	
Absorption coefficient	1.286 mm^{-1}	
F(000)	3664	
Theta range for data collection	1.14 to 26.02°	
Index ranges	-25<=h<=25, -17<=k<=17, -29<=l<=29	
Reflections collected	132869	
Independent reflections	14158 [R(int) = 0.1601]	
Max. and min. transmission	0.7829 and 0.6272	
Structure solution technique	direct methods	
Structure solution program	SHELXS-97 (Sheldrick, 2008)	
Refinement method	Full-matrix least-squares on F^2	
Refinement program	SHELXL-97 (Sheldrick, 2008)	
Function minimized	$\Sigma\, w(F_o^2 - F_c^2)^2$	
Data / restraints / parameters	14158 / 0 / 868	
Goodness-of-fit on F^2	1.277	
Δ/σmax	0.026	
Final R indices	9076 data; I>2σ(I)	R1 = 0.0763, wR2 = 0.2054
	all data	R1 = 0.1252, wR2 = 0.2469
Weighting scheme	w=1/[σ2(Fo^2)+(0.0768P)2+22.4554P]	
	where P=(Fo^2+2Fc^2)/3	
Extinction coefficient	0.0032(2)	
Largest diff. peak and hole	3.142 and -1.560 e$Å^{-3}$	
R.M.S. deviation from mean	0.401 e$Å^{-3}$	

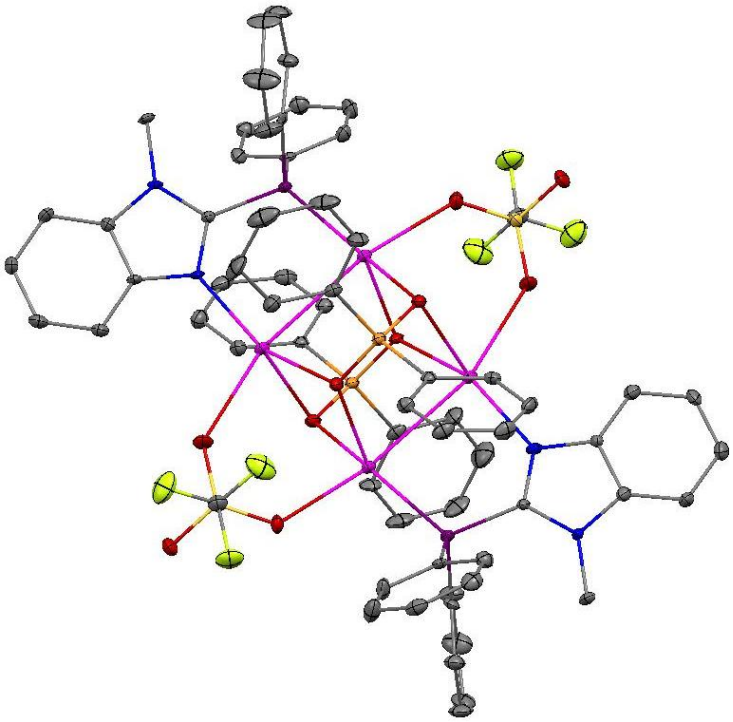

Figure 4.22. The thermal ellipsoid view of the tetranuclear silver (I) complex, **5**, X-ray crystal structure.

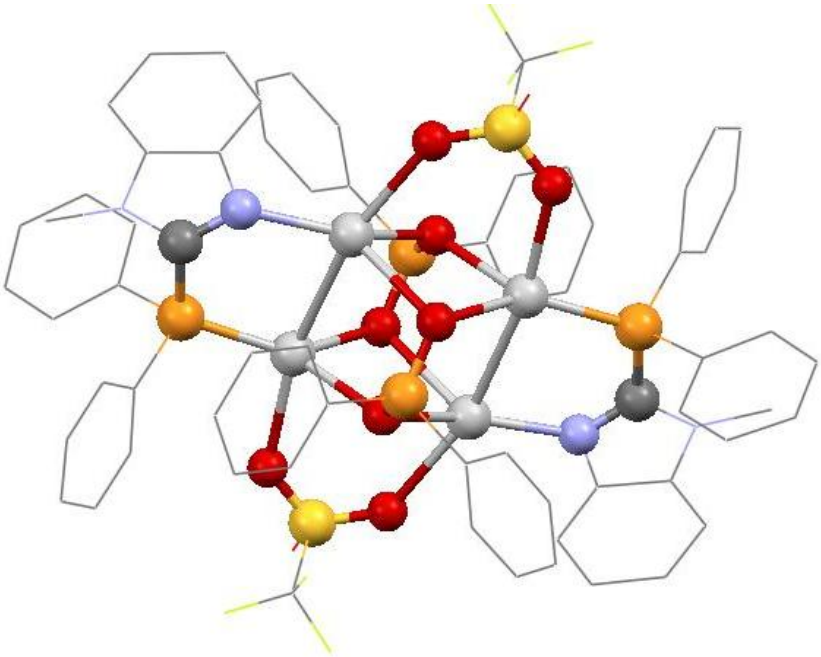

Figure 4.23. X-ray crystal structure of **5** highlighting the MBDP and DPPO bridging four silver atoms to form the macrocycle.

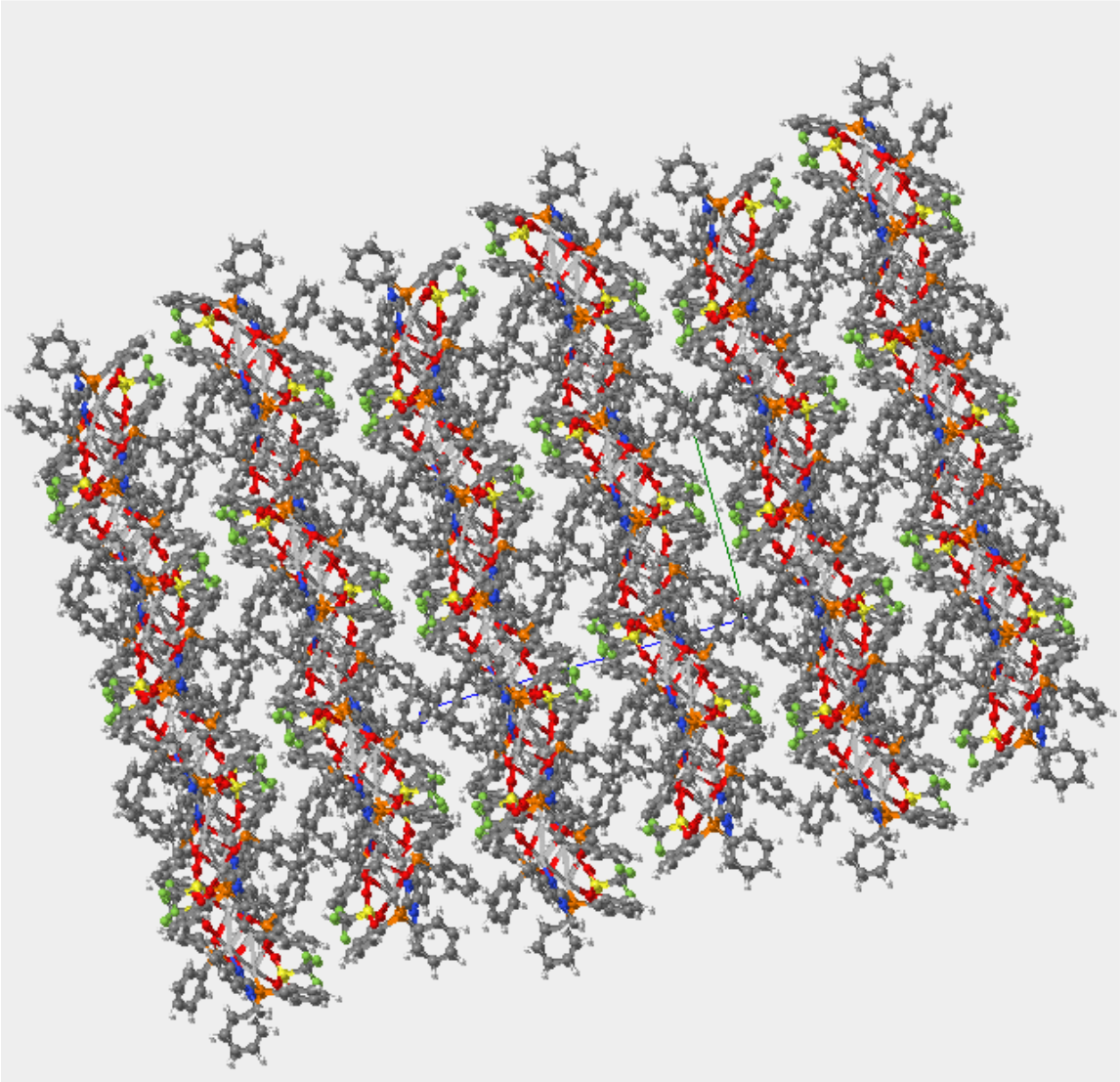

Figure 4.24. The packing diagram of the silver complex, **5**, along the *c*-axis displaying a layering of silver clusters forming a channel that is interrupted by phenyl rings.

The two silver atoms coordinated through one ligand at the P and N sites, have short argentophilic distances of 3.05 Å on average. Whereas the two Ag atoms bridged together through the O bonds of the diphenylphosphonic acid, have a slightly longer distance of nearly 3.52 Å, thus forming the rectangular shape of the four silver atoms. Tables 4.6 and 4.7 provide selected bond lengths and angles for **5**.

Table 4.6

*Selected bond lengths for **5***

Atom1	Atom2	Length
Ag1	Ag2	3.046(9)
Ag1	N3	2.192(8)
Ag1	O3	2.550(8)
Ag1	O8	2.602(6)
Ag1	O10	2.264(7)
Ag2	P3	2.354(3)
Ag2	O6	2.465(6)
Ag2	O7	2.352(6)
Ag2	O9	2.305(7)
Ag3	Ag4	3.076(9)
Ag3	P1	2.341(2)
Ag3	O1	2.484(6)
Ag3	O8	2.280(7)
Ag3	O10	2.364(6)
Ag4	N1	2.188(8)
Ag4	O4	2.551(8)
Ag4	O7	2.295(7)
Ag4	O9	2.502(6)
P1	C1	1.819(8)
P1	C9	1.840(1)
P1	C14	1.820(1)
P2	C52	1.810(1)
P2	C58	1.810(1)
P2	O9	1.529(6)
P2	O10	1.514(7)
P3	C34	1.810(1)
P3	C39	1.84(1)
P3	C44	1.81(8)
P4	C20	1.79(1)
P4	C27	1.81(1)
P4	O7	1.50(7)
P4	O8	1.52(6)

Table 4.7

*Selected bond angles for **5***

Atom1	Atom2	Atom3	Angle
Ag2	Ag1	N3	87.0(2)
Ag2	Ag1	O3	163.0(2)
Ag2	Ag1	O8	88.0(1)
Ag2	Ag1	O10	81.2(2)
N3	Ag1	O3	109.8(3)
N3	Ag1	O8	124.3(2)
N3	Ag1	O10	152.2(3)
O3	Ag1	O8	84.8(2)
O3	Ag1	O10	82.4(3)
O8	Ag1	O10	80.5(2)
Ag1	Ag2	P3	85.8(6)
Ag1	Ag2	O6	169.6(2)
Ag1	Ag2	O7	80.4(2)
Ag1	Ag2	O9	86.9(2)
P3	Ag2	O6	102.1(2)
P3	Ag2	O7	126.0(2)
P3	Ag2	O9	146.6(2)
O6	Ag2	O7	89.4(2)
O6	Ag2	O9	89.9(2)
O7	Ag2	O9	84.6(2)
Ag4	Ag3	P1	85.06(7)
Ag4	Ag3	O1	166.0(2)
Ag4	Ag3	O8	88.0(2)
Ag4	Ag3	O10	79.2(2)
P1	Ag3	O1	103.6(2)
P1	Ag3	O8	143.3(2)
P1	Ag3	O10	127.9(2)
O1	Ag3	O8	91.3(2)
O1	Ag3	O10	86.7(2)
O8	Ag3	O10	85.6(2)
Ag3	Ag4	N1	87.5(2)
Ag3	Ag4	O4	163.1(2)
Ag3	Ag4	O7	79.3(2)
Ag3	Ag4	O9	88.9(2)
N1	Ag4	O4	108.5(3)

Garrison and coworkers[49] reported a tetranuclear Ag (I) system with the hexafluorophosphate. They reported Ag-Ag distances less that 3.0 Å, Ag-N distances of 2.3 Å and Ag-O distances of 2.4 Å. Complex **5** has on average Ag-Ag distances slightly longer at 3.07 Å, Ag-N bonds measuring ~2.2 Å, and Ag-O bond distances with averages of ~2.2 Å. Comparison of the Ag-P bond for complex **5** with distances reported by references Catalano[42], Abdul Jalil[41], and Camalli[47] are 2.38, 2.39, and 2.4 Å, respectively. The Ag-P bond of **5** has an average distance of 2.35 Å, just slightly shorter than those reports. The geometry for **5** is similar to the silver complex **4** with an average bond angle of 106.435 º. The complex **5** has a near tetrahedral geometry also with bond angle averages of ~ 106 ˚.

4.3.2. Material characterization and PL studies. NMR spectroscopy of complex **5** is detailed with the ^{31}P NMR showing a sharp peak ~ 24.2 ppm. The ^{1}HMR is not very well ordered but shows the following peaks: 3.5 (s), 7.3-7.6 (m), 8.0 (m). This coincides very well with the ligand and complexes **2**, **3**, and **4**.

The photoluminescence of **5** was examined in the solid state at room temperature. As shown in Figure 4.25, **5** exhibit emission with a λ_{max} of 558 nm when excited at 420 nm. Comparing the luminescence profile to the ligand, 1-methylbenzimidazole diphenylphosphine (**1**), room temperature profile (Figure 4.26), the overall shape of the emission band is similar. However, when excited at 315 nm the emission λ_{max} is 398 nm. That is red shifting of approximately 160 nm suggesting the 4d-5s orbitals of the silver participates in the metal centered transitions mixed with some ligand to metal charge transfer. [50-52]

Lowering the temperature to 77 K generates an increase of the emission intensity of **5**. Figure 4.27 shows the emission profile of **5** at 77 K with the overlap of the room temperature profile. The emission band maximizes at 654 nm when excited at 476 nm. The metal centered

transition is more pronounced here with a red shift of ~96 nm. This shift is seen in a number of Ag (I) clusters coordinated with various aromatic ancillary ligands. [35, 50, 52-54]

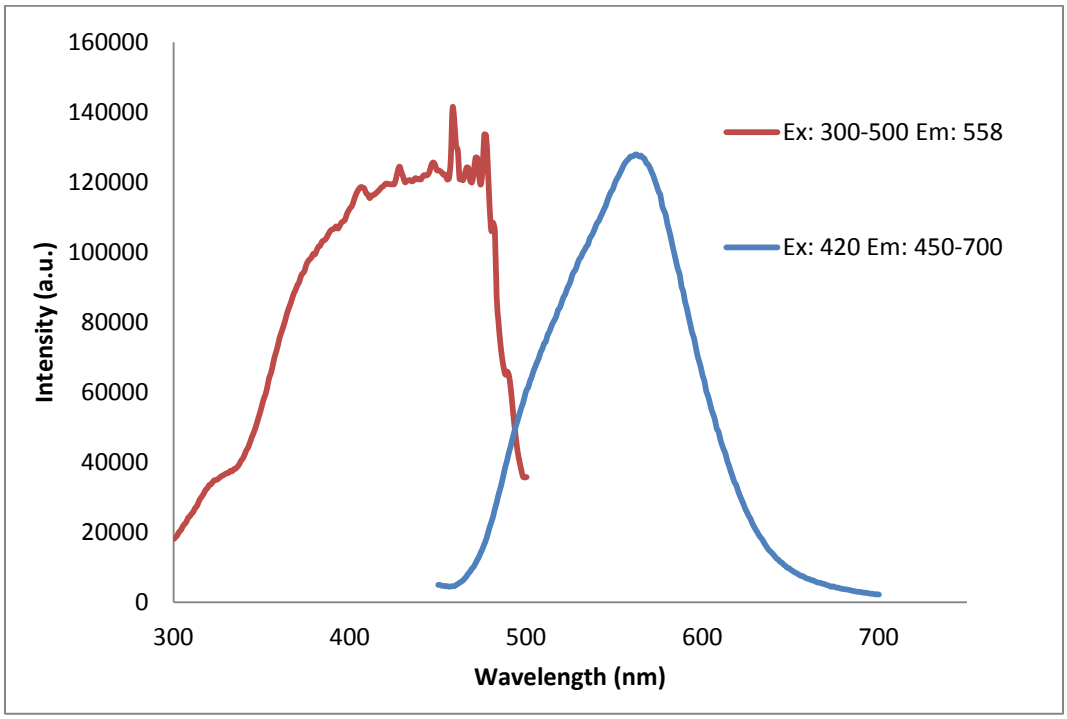

Figure 4.25. Room temperature excitation (red) and emission (blue) of complex **5**.

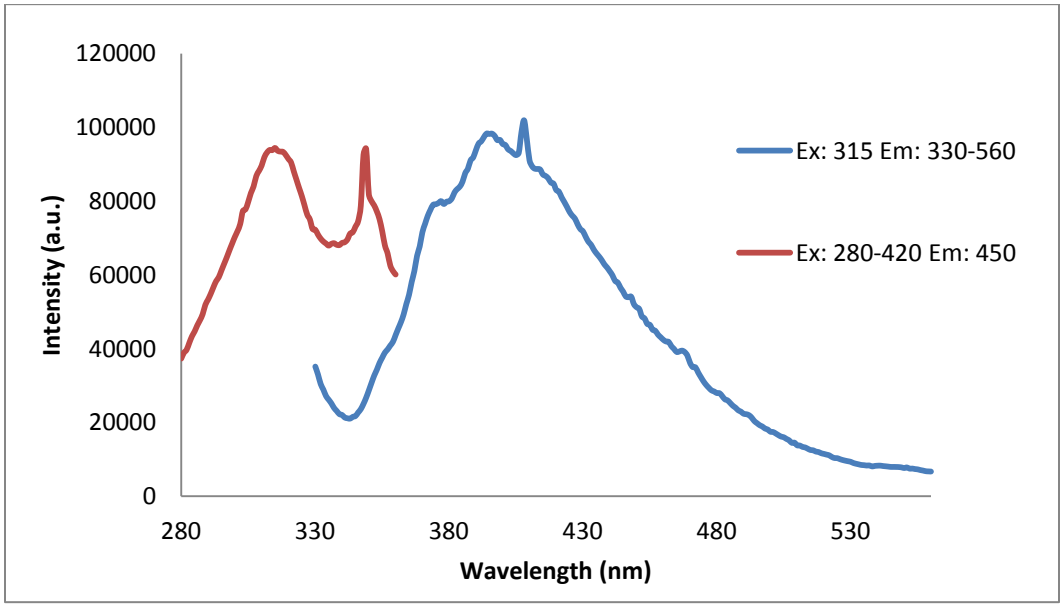

Figure 4.26. Room temperature excitation (red) and emission (blue) of the ligand, **1**.

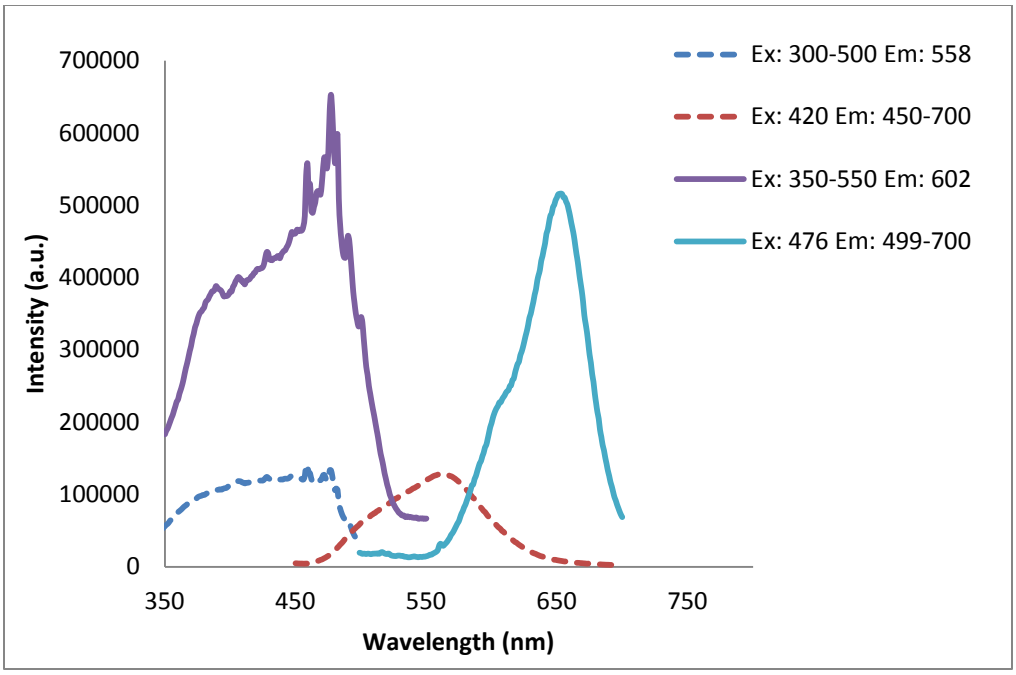

Figure 4.27. Photoluminescence profile of the room temperature excitation (blue dashed) and emission (red dashed) overlapped with the 77 K temperature excitation (violet solid) and emission (blue solid) of the tetranuclear silver complex, **5**.

4.4. Structural Analysis of Mixed Metal Au-Ag Bimetallic Complex with MBDP Ligand (6)

4.4.1. Structural analysis. Au (I) and Ag (I) compounds in the form of thtAuCl, $AgBF_4$, respectively were mixed with the ligand, **1**, in a 1:2:3 ratios using CH_3CN as the solvent. The synthesis was conducted in a dark room with very little exposure to ambient light. After stirring for one hour the white solid AgCl was collected while the filtrate was allowed to continue stirring for two additional hours. The volume of solvent was reduced by high pressure vacuum removal and layered with Et_2O and placed in the refrigerator overnight. A white solid was collected.

4.4.2. Material characterization and PL studies. The interest in photoluminescent materials offered a unique opportunity to engage in exploration of short metal-metal interactions. Thus far, the interactions of Ag (I) and Au (I) and the ligand, 1-methylimidazole

diphenylphosphine have been investigated individually. The solid was characterized using NMR, IR, and photoluminescence. With a limited number of examples of structurally characterized Au – Ag bimetallic complexes, the Catalano[42] work will be used for comparison purposes.

The bimetallic complex, **6**, was characterized using ^{31}P and ^{1}H NMR in $CDCl_3$ at room temperature. The ^{31}P NMR data provided a single broad peak at 1.46 ppm, while using the standard phosphoric acid as an external reference. The previously reported ^{31}P NMR data by Catalano was a sharp peak at 17.5 ppm, regardless of any equilibrium studies conducted in reference to a two- or three-ligand system. The ^{1}H NMR was similar to the ligand with the following peaks: 3.29 (s), 7.39-7.51 (m), and 7.93 (m). The NMR data shows that there is a similarity in the chemical environment when compared with that of the other metal complexes; however these results are not definitive of the desired mixed binuclear complex.

The complex, **6** under the handheld UV lamp the solid appears to have green emission. The steady-state photoluminescence spectra of **6** were collected at liquid nitrogen temperature. The luminescence profile for this complex was found to be different from complexes of **2**, **3**, or **4** however somewhat similar to complex **5**. The excitation spectrum for **6**, is shown as an overlap in Figure 4.28 (a). While monitoring the emission at 444, 507, and 526 nm very different excitation profiles emerged. The excitation spectrum with λ_{max} is 322 nm is very similar to the free ligand and metal complexes, **2**, **3**, and **4** spanning across 280 to 410 nm. Whilst the excitation profile where λ_{max} is 374 and 412 nm is similar to **5**. The emission profiles that were collected while maintaining fixed excitations are shown in an overlap in Figure 4.28 (b). The largest peak at 324 nm corresponds to ligand centered emission as seen throughout this work. The lower energy bands arise as a result of metal-metal interactions.

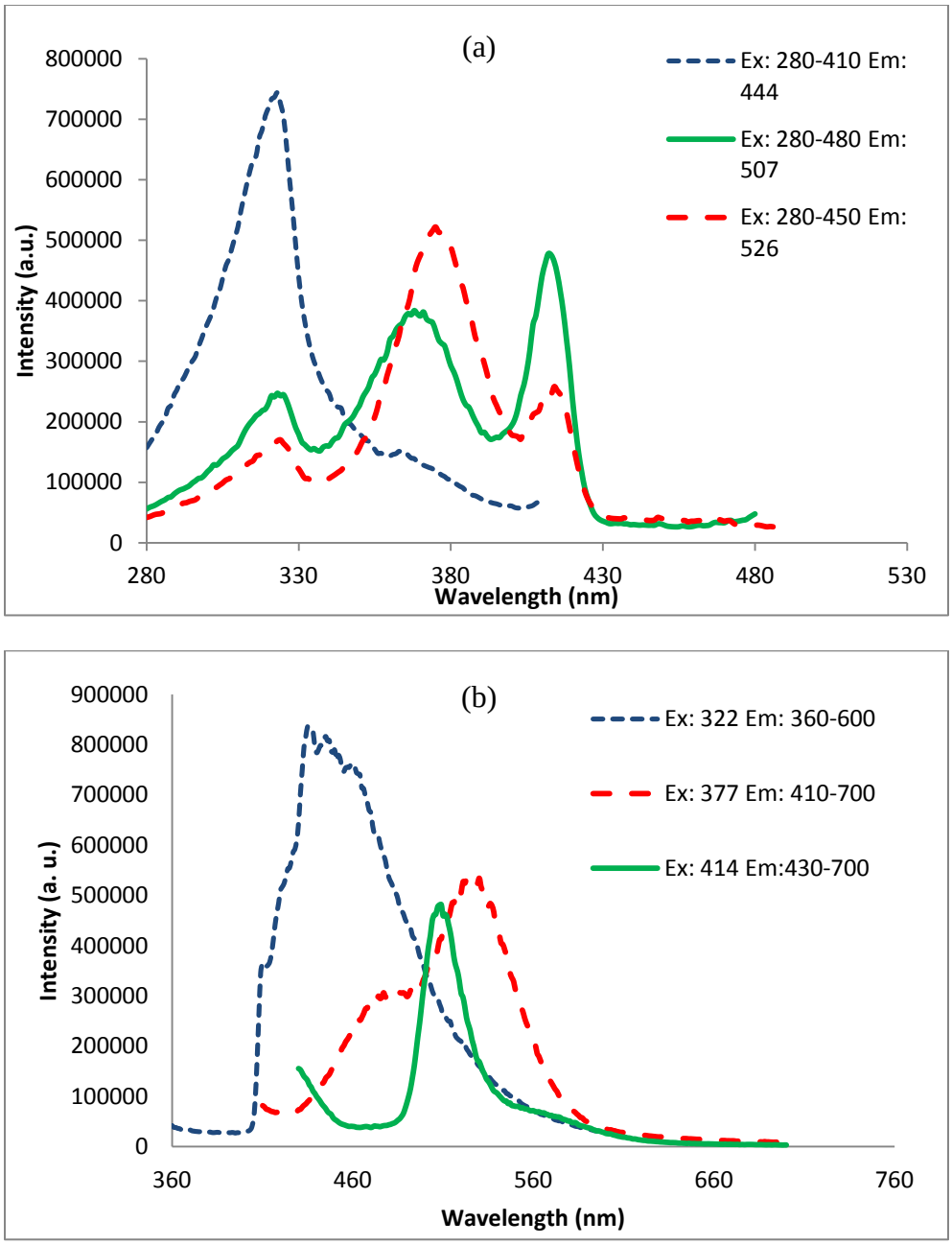

Figure 4.28. (a) Overlap of excitation spectra while monitoring emission at 444 (blue) nm, 507 (green) nm, and 526 (red) nm; and (b) Overlap of emission spectra while monitoring fixed excitation at 322 (blue), 377 (green), and 377 (red) nm.

While monitoring the emission maxima of 437 nm, the excitation bands generated are 322 and a smaller 367nm, as seen by the blue dashed line in Figure 4.28 (a) and (b). This is very

similar to the ligand excitation and emission profile. However the second profile, represented by the red dashed lines, has an emission profile with two peaks around 470 and 520 nm when the excitation maxima of 377 nm is explored. Finally, the emission profile for the green solid line shows a single peak near 503 nm corresponding to the excitation maxima of 417 nm. The three emission profiles all arise while monitoring different excitation wavelengths. The red shift in emission is indicative of a low energy charge transfer generated by metal 4d – 5s orbitals for silver or 6d – 5s orbitals for gold.

Albeit the structure is not known, the longer wavelength peaks are suggestive of metal – metal interactions. Although Catalano[42] shows a single broad excitation and emission profile, the author notes that under UV light the bimetallic system appears yellow while complexes of single metallic systems appeared blue. He concluded that the source is due to the ligand centered intra-ligand charge transfer.

However in this case, the same conclusion cannot be drawn. The representative emission is arising from two different sources, a blue and yellow emission band upon excitation at the respective wavelengths, hence the green color. The most likely reason is excitation of the ligand results in emission. Meanwhile excitation at longer wavelengths excites the metal, inciting metal – metal charge transfer with some possibility of ligand contribution. Lifetime measurements will need to be conducted for proper assignment of this emission profile.

CHAPTER 5

Conclusion

In conclusion, we have successful synthesized the ligand, 1-methylbenzimidazole diphenylphosphine and have shown the X-ray crystallographic structure. Further characterizations as well as DFT theoretical calculations show the electronic properties to be governed by a $\pi \rightarrow \pi^*$ transition.

We used this ligand to coordinate to gold (I) and silver (I) metal. The X-ray crystal structure for 1-methylbenzimidazole diphenylphosphine gold (I) chloride displayed the P-Au-Cl bond was in good range with other known phosphino-gold (I) chloride complexes. We have correlated the experimentally obtained characterizations with the theoretical calculations including structure and electronic properties. We were able to coordinate the 1-methylbenzimidazole diphenylphosphine to silver (I) tetrafluoroborate and gold (I) tetrafluoroborate in order to get two metal ions in close proximity to each other. The existence of the short metal – metal interactions did not form continuous intermolecular chains, yet individual dimers of two ligands and two metals. We characterized the dimers and completed solid steady-state photoluminescence studies. We assigned the electronic properties as ligand centered $\pi \rightarrow \pi^*$ transitions considering the large molar absorptivity extinction coefficients.

Sensitivity of the gold (I) tetrafluoroborate dimers to acetonitrile was observed. It was shown that without the presence of acetonitrile crystallization did not occur. The complex when introduced to solvent vapors such as dichloromethane or chloroform, the photoluminescence intensity increases. Finally, when reintroduced to acetonitrile vapor dissolution occurs followed crystallization.

The X-ray crystal structure of a new tetranuclear silver (I) triflate complex with a

capsule-like shape was described. The photoluminescent shift from intraligand $\pi \rightarrow \pi^*$ transition to metal centered emission was characterized. Finally, the synthesis of a binuclear complex that exhibited a complicated luminescent profile was discussed. Future works for these complexes include solution photoluminescence studies, lifetime and quantum efficiency measurements.

References

1. Farhadi, K., Forough, M., Molaei, R., Hajizadeh, S., and Rafipour, A., *Highly selective Hg^{2+} colorimetric sensor using green synthesized and unmodified silver nanoparticles.* Sensors and Actuators B: Chemical, 2012. **161**(1): p. 880-885.
2. Kang, N.K., Jun, T.S., La, D.-D., Oh, J.H., Cho, Y.W., and Kim, Y.S., *Evaluation of the limit-of-detection capability of carbon black-polymer composite sensors for volatile breath biomarkers.* Sensors and Actuators B: Chemical, 2010. **147**(1): p. 55-60.
3. Moragues, M.E., Esteban, J., Ros-Lis, J.V., Martínez-Máñez, R., Marcos, M.D., Martínez, M., Soto, J., and Sancenón, F., *Sensitive and Selective Chromogenic Sensing of Carbon Monoxide via Reversible Axial CO Coordination in Binuclear Rhodium Complexes.* Journal of the American Chemical Society, 2011. **133**(39): p. 15762-15772.
4. Roberts, J.M., Veres, P.R., Cochran, A.K., Warneke, C., Burling, I.R., Yokelson, R.J., Lerner, B., Gilman, J.B., Kuster, W.C., Fall, R., and de Gouw, J., *Isocyanic acid in the atmosphere and its possible link to smoke-related health effects.* Proceedings of the National Academy of Sciences, 2011. **108**(22): p. 8966-8971.
5. Mizaikoff, B., Göbel, R., Krska, R., Taga, K., Kellner, R., Tacke, M., and Katzir, A., *Infrared fiber-optical chemical sensors with reactive surface coatings.* Sensors and Actuators B: Chemical, 1995. **29**(1–3): p. 58-63.
6. Liao, Y.-H. and Chou, J.-C., *Preparation and characteristics of ruthenium dioxide for pH array sensors with real-time measurement system.* Sensors and Actuators B: Chemical, 2008. **128**(2): p. 603-612.

7. Liu, Y., Dong, H., Zhang, W., Ye, Z., Wang, G., and Yuan, J., *Preparation of a novel colorimetric luminescence sensor strip for the detection of indole-3-acetic acid.* Biosensors and Bioelectronics, 2010. **25**(10): p. 2375-2378.

8. Pingwu, D., *A highly selective vapochromic methanol sensor based on one step synthesis of a simple platinum terpyridine complex.* Inorganica Chimica Acta, 2010. **363**(7): p. 1355-1358.

9. Kato, M., Omura, A., Toshikawa, A., Kishi, S., and Sugimoto, Y., *Vapor-Induced Luminescence Switching in Crystals of the Syn Isomer of a Dinuclear (Bipyridine)platinum (II) Complex Bridged with Pyridine-2-Thiolate Ions.* Angewandte Chemie International Edition, 2002. **41**(17): p. 3183-3185.

10. Wadas, T.J., Wang, Q.-M., Kim, Y.-j., Flaschenreim, C., Blanton, T.N., and Eisenberg, R., *Vapochromism and Its Structural Basis in a Luminescent Pt (II) Terpyridine−Nicotinamide Complex.* Journal of the American Chemical Society, 2004. **126**(51): p. 16841-16849.

11. Ni, J., Wu, Y.-H., Zhang, X., Li, B., Zhang, L.-Y., and Chen, Z.-N., *Luminescence Vapochromism of a Platinum (II) Complex for Detection of Low Molecular Weight Halohydrocarbon.* Inorganic Chemistry, 2009. **48**(21): p. 10202-10210.

12. Abe, T. and Shinozaki, K., *Tuning of Luminescence Spectra of Neutral Ruthenium (II) Complexes by Crystal Waters.* Inorganic Chemistry, 2005. **44**(4): p. 849-851.

13. Abe, T., Suzuki, T., and Shinozaki, K., *Luminescence Change by the Solvent of Crystallization, Solvent Reorganization, and Vapochromism of Neutral Dicyanoruthenium (II) Complex in the Solid State.* Inorganic Chemistry, 2010. **49**(4): p. 1794-1800.

14. Das, S. and Bharadwaj, P.K., *Self-Assembly of a Luminescent Zinc (II) Complex: a Supramolecular Host−Guest Fluorescence Signaling System for Selective Nitrobenzene Inclusion.* Inorganic Chemistry, 2006. **45**(14): p. 5257-5259.

15. Liu, Z., Bian, Z., Bian, J., Li, Z., Nie, D., and Huang, C., *Acetonitrile-Vapor-Induced Color and Luminescence Changes in a Cyclometalated Heteroleptic Iridium Complex.* Inorganic Chemistry, 2008. **47**(18): p. 8025-8030.

16. Fernández, E.J., López-de-Luzuriaga, J.M., Monge, M., Montiel, M., Olmos, M.E., Pérez, J., Laguna, A., Mendizabal, F., Mohamed, A.A., and Fackler, J.P., *A Detailed Study of the Vapochromic Behavior of {Tl[Au(C_6Cl_5)$_2$]}n.* Inorganic Chemistry, 2004. **43**(12): p. 3573-3581.

17. Fernández, E.J., López-de-Luzuriaga, J.M., Monge, M., Olmos, M.E., Pérez, J., Laguna, A., Mohamed, A.A., and Fackler, J.P., *{Tl[Au(C_6Cl_5)$_2$]}n: A Vapochromic Complex.* Journal of the American Chemical Society, 2003. **125**(8): p. 2022-2023.

18. Forward, J.M., Bohmann, D., Fackler, J.P., and Staples, R.J., *Luminescence Studies of Gold (I) Thiolate Complexes.* Inorganic Chemistry, 1995. **34**(25): p. 6330-6336.

19. Assefa, Z., McBurnett, B.G., Staples, R.J., Fackler, J.P., Assmann, B., Angermaier, K., and Schmidbaur, H., *Syntheses, Structures, and Spectroscopic Properties of Gold (I) Complexes of 1,3,5-Triaza-7-phosphaadamantane (TPA). Correlation of the Supramolecular Au ••• Au Interaction and Photoluminescence for the Species (TPA)AuCl and [(TPA-HCl)AuCl].* Inorganic Chemistry, 1995. **34**(1): p. 75-83.

20. Mansour, M.A., Connick, W.B., Lachicotte, R.J., Gysling, H.J., and Eisenberg, R., *Linear Chain Au (I) Dimer Compounds as Environmental Sensors: A Luminescent Switch for the*

Detection of Volatile Organic Compounds. Journal of the American Chemical Society, 1998. **120**(6): p. 1329-1330.

21. Balch, A., *Remarkable Luminescence Behaviors and Structural Variations of Two-Coordinate Gold (I) Complexes*, in *Photofunctional Transition Metal Complexes*, V. Yam, Editor. 2007, Springer Berlin / Heidelberg. p. 1-40.
22. Balch, A.L., Olmstead, M.M., and Vickery, J.C., *Gold (I) Compounds without Significant Aurophilic Intermolecular Interactions: Synthesis, Structure, and Electronic Properties of $Ph_3PAuC(O)NHMe$ and $Au_3(PhCH_2NCOMe)_3$: Comparative Monomeric and Trimeric Analogues of the Solvoluminescent Trimer, $Au_3(MeNCOMe)_3$.* Inorganic Chemistry, 1999. **38**(15): p. 3494-3499.
23. King, C., Khan, M.N.I., Staples, R.J., and Fackler, J.P., *Luminescent mononuclear gold (I) phosphines.* Inorganic Chemistry, 1992. **31**(15): p. 3236-3238.
24. King, C., Wang, J.C., Khan, M.N.I., and Fackler, J.P., *Luminescence and metal-metal interactions in binuclear gold (I) compounds.* Inorganic Chemistry, 1989. **28**(11): p. 2145-2149.
25. Assefa, Z., Omary, M.A., McBurnett, B.G., Mohamed, A.A., Patterson, H.H., Staples, R.J., and Fackler, J.P., *Syntheses, Structure, and Photoluminescence Properties of the 1-Dimensional Chain Compounds $[(TPA)_2Au][Au(CN)_2]$ and (TPA)AuCl (TPA = 1,3,5-Triaza-7-phosphaadamantane).* Inorganic Chemistry, 2002. **41**(24): p. 6274-6280.
26. Forward, J.M., Assefa, Z., and Fackler, J.P., *Photoluminescence of gold (I) phosphine complexes in aqueous solution.* Journal of the American Chemical Society, 1995. **117**(35): p. 9103-9104.

27. Schmidbaur, H., Cronje, S., Djordjevic, B., and Schuster, O., *Understanding gold chemistry through relativity.* Chemical Physics, 2005. **311**(1–2): p. 151-161.

28. Schmidbaur, H., *The aurophilicity phenomenon: A decade of experimental findings, theoretical concepts and emerging applications.* Gold Bulletin, 2000. **33**(1): p. 3-10.

29. Arvapally, R.K., Sinha, P., Hettiarachchi, S.R., Coker, N.L., Bedel, C.E., Patterson, H.H., Elder, R.C., Wilson, A.K., and Omary, M.A., *Photophysics of Bis(thiocyanato)gold (I) Complexes: Intriguing Structure - Luminescence Relationships.* The Journal of Physical Chemistry C, 2007. **111**(28): p. 10689-10699.

30. Shakirova, J.R., Grachova, E.V., Gurzhiy, V.V., Koshevoy, I.O., Melnikov, A.S., Sizova, O.V., Tunik, S.P., and Laguna, A., *Luminescent heterometallic gold-copper alkynyl complexes stabilized by tridentate phosphine.* Dalton Transactions, 2012. **41**(10).

31. Bachechi, F., Burini, A., Fontani, M., Galassi, R., Macchioni, A., Pietroni, B.R., Zanello, P., and Zuccaccia, C., *Solid state and solution investigations of derivatives of Group 11 metal ions with 1-benzyl-2-imidazolyldiphenylphosphine (L). Electrochemical behavior of* $[M_2L_3]^{2+}$ *(M=CuI; AgI) and* $[AuL_2]^{+}$ *complexes.* Inorganica Chimica Acta, 2001. **323**(1-2): p. 45-54.

32. Burini, A., Fackler, J.P., Galassi, R., Grant, T.A., Omary, M.A., Rawashdeh-Omary, M.A., Pietroni, B.R., and Staples, R.J., *Supramolecular Chain Assemblies Formed by Interaction of a π-Molecular Acid Complex of Mercury with π-Base Trinuclear Gold Complexes.* Journal of the American Chemical Society, 2000. **122**(45): p. 11264-11265.

33. Burini, A., Galassi, R., Ricci, S., Bachechi, F., Mohamed, A.A., and Fackler, J.P., *Mono and Tetranuclear Gold (I) Complexes of Tris(1-benzylimidazole-2-yl)phosphine.* Inorganic Chemistry, 2009. **49**(2): p. 513-518.

34. Burini, A., Pietroni, B.R., Galassi, R., Valle, G., and Calogero, S., *Dinuclear gold (I) and silver (I) derivatives with bridging phosphines containing an imidazole ring; X-ray crystal structure of (1-benzyl-2-imidazolyl)diphenylphosphinegold (I) chloride.* Inorganica Chimica Acta, 1995. **229**(1-2): p. 299-305.

35. Catalano, V.J. and Moore, A.L., *Mono-, Di-, and Trinuclear Luminescent Silver (I) and Gold (I) N-Heterocyclic Carbene Complexes Derived from the Picolyl-Substituted Methylimidazolium Salt: 1-Methyl-3-(2-pyridinylmethyl)-1H-imidazolium Tetrafluoroborate.* Inorganic Chemistry, 2005. **44**(19): p. 6558-6566.

36. Boehme, C. and Frenking, G., *N-Heterocyclic Carbene, Silylene, and Germylene Complexes of MCl (M = Cu, Ag, Au). A Theoretical Study*[1]. Organometallics, 1998. **17**(26): p. 5801-5809.

37. A.Herrmann, W., Weskamp, T., and Bohm, V.P.W., *Metal complexes of stable carbenes,* in *Advances in Organometallic Chemistry*. 2001, Academic Press. p. 1-69.

38. Lee, M.-T. and Hu, C.-H., *Density Functional Study of N-Heterocyclic and Diamino Carbene Complexes: Comparison with Phosphines.* Organometallics, 2004. **23**(5): p. 976-983.

39. Rawashdeh-Omary, M.A., Omary, M.A., Fackler, J.P., Galassi, R., Pietroni, B.R., and Burini, A., *Chemistry and Optoelectronic Properties of Stacked Supramolecular Entities of Trinuclear Gold (I) Complexes Sandwiching Small Organic Acids.* Journal of the American Chemical Society, 2001. **123**(39): p. 9689-9691.

40. Bachechi, F., Burini, A., Galassi, R., Macchioni, A., Rosa Pietroni, B., Ziarelli, F., and Zuccaccia, C., *Solid state and solution structural studies of silver(I) cyclic complexes*

bearing the (Bzim)Ph_2P ligand. Journal of Organometallic Chemistry, 2000. **593–594**(0): p. 392-402.

41. Abdul Jalil, M., Yamada, T., Fujinami, S., Honjo, T., and Nishikawa, H., *An imidazole-based P-N bridging ligand and its binuclear copper (I), silver (I) and palladium (I) complexes: synthesis, characterizations and X-ray structures.* Polyhedron, 2001. **20**(7-8): p. 627-633.
42. Catalano, V.J. and Horner, S.J., *Luminescent Gold (I) and Silver (I) Complexes of 2-(Diphenylphosphino)-1-methylimidazole (dpim): Characterization of a Three-Coordinate Au (I)−Ag (I) Dimer with a Short Metal−Metal Separation.* Inorganic Chemistry, 2003. **42**(25): p. 8430-8438.
43. Peruzzo, V., Pretzsch, C., Tisato, F., Porchia, M., Refosco, F., Marzano, C., Gandin, V., Schiller, E., Walther, M., and Pietzsch, H.-J., *Synthesis and characterization of novel tetrahedral copper (I) complexes comprising tridentate PNP-aminodiphosphines and tetradentate PN(X)P-substituted aminodiphosphines (X=O, S).* Inorganica Chimica Acta, 2012. **387**(0): p. 163-172.
44. Uson, R., Laguna, A., Laguna, M., Briggs, D.A., Murray, H.H., and Fackler, J.P., *(Tetrahydrothiophene)Gold (I) or Gold (III) Complexes*, in *Inorganic Syntheses*. 2007, John Wiley & Sons, Inc. p. 85-91.
45. Gaussian 09, R.A., M. J. Frisch, G. W. Trucks, H. B. Schlegel, G. E. Scuseria, M. A. Robb, J. R. Cheeseman, G. Scalmani, V. Barone, B. Mennucci, G. A. Petersson, H. Nakatsuji, M. Caricato, X. Li, H. P. Hratchian, A. F. Izmaylov, J. Bloino, G. Zheng, J. L. Sonnenberg, M. Hada, M. Ehara, K. Toyota, R. Fukuda, J. Hasegawa, M. Ishida, T. Nakajima, Y. Honda, O. Kitao, H. Nakai, T. Vreven, J. A. Montgomery, Jr., J. E. Peralta,

F. Ogliaro, M. Bearpark, J. J. Heyd, E. Brothers, K. N. Kudin, V. N. Staroverov, R. Kobayashi, J. Normand, K. Raghavachari, A. Rendell, J. C. Burant, S. S. Iyengar, J. Tomasi, M. Cossi, N. Rega, J. M. Millam, M. Klene, J. E. Knox, J. B. Cross, V. Bakken, C. Adamo, J. Jaramillo, R. Gomperts, R. E. Stratmann, O. Yazyev, A. J. Austin, R. Cammi, C. Pomelli, J. W. Ochterski, R. L. Martin, K. Morokuma, V. G. Zakrzewski, G. A. Voth, P. Salvador, J. J. Dannenberg, S. Dapprich, A. D. Daniels, Ö. Farkas, J. B. Foresman, J. V. Ortiz, J. Cioslowski, and D. J. Fox, Gaussian, Inc., Wallingford CT, 2009., *Gaussian W09*. 2009.

46. Moore, S.S. and Whitesides, G.M., *Synthesis and coordinating properties of heterocyclic-substituted tertiary phosphines.* The Journal of Organic Chemistry, 1982. **47**(8): p. 1489-1493.

47. Camalli, M. and Caruso, F., *Crystal and molecular structure of bis(tricyclohexylphosphine)silver (I) nitrate and bis(tricyclohexylphosphine)silver (I) perchlorate; correlation of the structures with the silver-phosphorus coupling constants.* Inorganica Chimica Acta, 1988. **144**(2): p. 205-211.

48. Liu, C.W., Pan, H., Fackler, J.P., Wu, G., Wasylishen, R.E., and Shang, M., *Studies of $[Ag(PPh_3)_2]NO_3$, $[Ag\{P(CH_2CH_2CN)_3\}_2]NO_3$ and $[Ag\{P(C_6H_4Me\text{-}m)_3\}_2]NO_3$ by X-ray diffraction and solid-state nuclear magnetic resonance.* Journal of the Chemical Society, Dalton Transactions, 1995(22): p. 3691-3697.

49. Garrison, J.C., Simons, R.S., Kofron, W.G., Tessier, C.A., and Youngs, W.J., *Synthesis and structural characterization of a silver complex of a mixed-donor N-heterocyclic carbene linked cyclophane.* Chemical Communications, 2001(18): p. 1780-1781.

50. Vogler, A. and Kunkely, H., *Photoluminescence of tetrameric silver (I) complexes.* Chemical Physics Letters, 1989. **158**(1–2): p. 74-76.

51. Becke, A., *Density-functional thermochemistry. III. The role of exact exchange.* The Journal of Chemical Physics, 1993. **98**(7): p. 5648-5652.

52. Çolak, A.T., Pamuk, G., Yeşilel, O.Z., and Yılmaz, F., *A photoluminescent dinuclear silver (I) complex exhibits CH···Ag close interactions and a new coordination mode of the pyridine-2,3-dicarboxylate.* Inorganic Chemistry Communications, 2011. **14**(10): p. 1591-1595.

53. Chih-Fan, W., Shie-Ming, P., Chi-Keung, C., and Chi-Ming, C., *Luminescent silver (I) cluster. Synthesis, spectroscopic properties and x-ray crystal structure of* $[Ag_3(C;CPh)_2(dppm)_3Cl \cdot 4Et_2O \cdot H_2O$ *{dppm = bis(diphenylphosphino)methane}.* Polyhedron, 1996. **15**(11): p. 1853-1858.

54. Ren, C.-X., Ye, B.-H., Zhu, H.-L., Shi, J.-X., and Chen, X.-M., *Syntheses, structures and photoluminescent properties of silver (I) complexes with in situ generated hexahydropyrimidine derivatives.* Inorganica Chimica Acta, 2004. **357**(2): p. 443-450.

Appendix A

X-ray Crystallography Data of MBDP

Table 1

Data collection and structure refinement for MBDP.

Formula weight	316.33	
Temperature	200(2) K	
Wavelength	0.71073 Å	
Crystal size	0.050 x 0.500 x 0.600 mm	
Crystal habit	colorless plate	
Crystal system	Triclinic	
Space group	P -1	
Unit cell dimensions	a = 9.5496(10) Å	α = 74.271(3)°
	b = 9.8705(12) Å	β = 67.185(3)°
	c = 10.5033(12) Å	γ = 70.111(3)°
Volume	847.01(17) $Å^3$	
Z	2	
Density (calculated)	1.240 Mg/cm^3	
Absorption coefficient	0.163 mm^{-1}	
F(000)	332	
Theta range for data collection	2.13 to 25.05°	
Index ranges	-11<=h<=11, -11<=k<=11, -12<=l<=12	
Reflections collected	8019	
Independent reflections	2956 [R(int) = 0.0382]	
Coverage of independent reflections	98.10%	
Max. and min. transmission	0.9919 and 0.9086	
Structure solution technique	direct methods	
Structure solution program	SHELXS-97 (Sheldrick, 2008)	
Refinement method	Full-matrix least-squares on F^2	
Refinement program	SHELXL-97 (Sheldrick, 2008)	
Function minimized	$\Sigma\ w(Fo^2 - Fc^2)^2$	
Data / restraints / parameters	2956 / 0 / 210	
Goodness-of-fit on F2	2.676	
Δ/σ_{max}	0.008	
Final R indices	2597 data; I>2σ(I) R1 = 0.0743, wR2 = 0.2507 all data R1 = 0.0803, wR2 = 0.2563	
Weighting scheme	$w=1/[\sigma^2(Fo^2)+(0.0675P)^2+0.0000P]$ where $P=(Fo^2+2Fc^2)/3$	
Extinction coefficient	0.0060(90)	
Largest diff. peak and hole	2.307 and -0.277 $eÅ^{-3}$	
R.M.S. deviation from mean	0.075 $eÅ^{-3}$	

Table 2

Atomic coordinates and equivalent isotropic atomic displacement parameters (Å2) for MBDP.

	x/a	**y/b**	**z/c**	**U(eq)***
P1	0.71431(9)	0.21908(9)	0.82914(10)	0.0370(4)
N2	0.7974(3)	0.4676(3)	0.8204(3)	0.0348(7)
C8	0.7311(5)	0.4140(5)	0.5205(4)	0.0600(11)
C12	0.7221(5)	0.1574(4)	0.2777(5)	0.0617(11)
C13	0.8609(5)	0.1416(4)	0.1626(4)	0.0540(10)
C14	0.8530(4)	0.1617(4)	0.0310(4)	0.0439(9)
C9	0.7093(3)	0.2013(3)	0.0075(3)	0.0368(8)
C1	0.7603(3)	0.3958(3)	0.7553(3)	0.0347(8)
N1	0.7676(3)	0.4620(3)	0.6209(3)	0.0404(7)
C7	0.8114(3)	0.5876(4)	0.5988(3)	0.0382(8)
C6	0.8348(4)	0.6982(4)	0.4840(4)	0.0525(10)
C5	0.8731(4)	0.8151(4)	0.5003(4)	0.0562(11)
C4	0.8844(5)	0.8216(4)	0.6262(4)	0.0565(10)
C2	0.8271(3)	0.5912(3)	0.7247(3)	0.0356(8)
C15	0.5065(4)	0.2687(3)	0.8433(3)	0.0373(8)
C16	0.4051(4)	0.4056(4)	0.8641(3)	0.0410(9)
C17	0.2484(4)	0.4353(4)	0.8734(3)	0.0401(8)
C18	0.1931(4)	0.3291(4)	0.8616(3)	0.0400(8)
C19	0.2931(4)	0.1932(4)	0.8419(4)	0.0470(9)
C20	0.4484(4)	0.1625(3)	0.8297(4)	0.0442(9)
C11	0.5785(5)	0.1941(4)	0.2552(4)	0.0569(11)
C10	0.5723(4)	0.2159(4)	0.1230(4)	0.0451(9)
C3	0.8644(4)	0.7088(4)	0.7399(4)	0.0460(9)

* U(eq) is defined as one third of the trace of the orthogonalized Uij tensor.

Table 3

Bond lengths (Å) for MBDP.

P1-C9	1.817(4)	P1-C15	1.830(3)
P1-C1	1.833(3)	N2-C1	1.311(4)
N2-C2	1.388(4)	C8-N1	1.458(4)
C8-H8A	0.98	C8-H8B	0.98
C8-H8C	0.98	C12-C11	1.391(6)
C12-C13	1.401(6)	C12-H1	0.95
C13-C14	1.370(5)	C13-H2	0.95
C14-C9	1.394(5)	C14-H3	0.95
C9-C10	1.392(4)	C1-N1	1.371(4)
N1-C7	1.374(4)	C7-C6	1.393(5)
C7-C2	1.398(5)	C6-C5	1.392(6)
C6-H8	0.95	C5-C4	1.388(6)
C5-H9	0.95	C4-C3	1.396(5)
C4-H10	0.95	C2-C3	1.388(5)
C15-C16	1.385(4)	C15-C20	1.402(4)
C16-C17	1.392(5)	C16-H13	0.95
C17-C18	1.375(5)	C17-H14	0.95
C18-C19	1.371(5)	C18-H15	0.95
C19-C20	1.370(5)	C19-H16	0.95
C20-H17	0.95	C11-C10	1.368(5)
C11-H18	0.95	C10-H19	0.95
C3-H21	0.95		

Table 4

Bond angles (°) for MBDP.

C9-P1-C15	103.98(14)	C9-P1-C1	100.03(14)
C15-P1-C1	101.13(14)	C1-N2-C2	104.8(3)
N1-C8-H8A	109.5	N1-C8-H8B	109.5
H8A-C8-H8B	109.5	N1-C8-H8C	109.5
H8A-C8-H8C	109.5	H8B-C8-H8C	109.5
C11-C12-C13	118.8(4)	C11-C12-H1	120.6
C13-C12-H1	120.6	C14-C13-C12	119.8(4)
C14-C13-H2	120.1	C12-C13-H2	120.1
C13-C14-C9	121.6(3)	C13-C14-H3	119.2
C9-C14-H3	119.2	C10-C9-C14	118.0(3)
C10-C9-P1	124.4(3)	C14-C9-P1	117.5(2)
N2-C1-N1	113.1(3)	N2-C1-P1	124.6(3)
N1-C1-P1	122.2(2)	C1-N1-C7	106.6(3)
C1-N1-C8	127.7(3)	C7-N1-C8	125.7(3)
N1-C7-C6	132.2(3)	N1-C7-C2	105.4(3)
C6-C7-C2	122.3(3)	C5-C6-C7	116.8(3)
C5-C6-H8	121.6	C7-C6-H8	121.6
C6-C5-C4	121.2(3)	C6-C5-H9	119.4
C4-C5-H9	119.4	C5-C4-C3	121.6(4)
C5-C4-H10	119.2	C3-C4-H10	119.2
C3-C2-N2	129.7(3)	C3-C2-C7	120.3(3)
N2-C2-C7	110.0(3)	C16-C15-C20	118.5(3)
C16-C15-P1	123.6(2)	C20-C15-P1	117.8(2)
C17-C16-C15	120.3(3)	C17-C16-H13	119.8
C15-C16-H13	119.8	C18-C17-C16	120.3(3)
C18-C17-H14	119.9	C16-C17-H14	119.8
C17-C18-C19	119.5(3)	C17-C18-H15	120.2
C19-C18-H15	120.2	C18-C19-C20	121.1(3)
C18-C19-H16	119.4	C20-C19-H16	119.4
C19-C20-C15	120.2(3)	C19-C20-H17	119.9
C15-C20-H17	119.9	C10-C11-C12	120.8(4)
C10-C11-H18	119.6	C12-C11-H18	119.6
C11-C10-C9	121.0(3)	C11-C10-H19	119.5
C9-C10-H19	119.5	C4-C3-C2	117.6(4)
C4-C3-H21	121.2	C2-C3-H21	121.2

Table 5

Anisotropic atomic displacement parameters (Å2) for MBDP.

	U11	**U22**	**U33**	**U23**	**U13**	**U12**
P1	0.0288(6)	0.0344(6)	0.0536(7)	-0.0148(4)	-0.0146(4)	-0.0079(4)
N2	0.0330(14)	0.0397(15)	0.0355(14)	-0.0079(11)	-0.0091(11)	-0.0152(12)
C8	0.059(2)	0.083(3)	0.047(2)	-0.029(2)	-0.0179(18)	-0.015(2)
C12	0.081(3)	0.040(2)	0.069(3)	-0.0122(18)	-0.040(2)	-0.0008(19)
C13	0.059(2)	0.040(2)	0.076(3)	-0.0018(18)	-0.040(2)	-0.0140(18)
C14	0.0340(18)	0.0372(18)	0.063(2)	-0.0040(16)	-0.0193(16)	-0.0116(14)
C9	0.0303(17)	0.0250(15)	0.055(2)	-0.0067(13)	-0.0134(15)	-0.0078(12)
C1	0.0233(15)	0.0420(18)	0.0390(17)	-0.0147(14)	-0.0066(13)	-0.0066(13)
N1	0.0329(15)	0.0566(18)	0.0355(14)	-0.0180(13)	-0.0111(11)	-0.0083(13)
C7	0.0276(16)	0.0423(18)	0.0382(17)	-0.0109(14)	-0.0088(13)	-0.0001(14)
C6	0.039(2)	0.066(2)	0.0364(18)	-0.0035(17)	-0.0106(15)	-0.0002(18)
C5	0.049(2)	0.047(2)	0.053(2)	0.0053(17)	-0.0102(18)	-0.0067(17)
C4	0.055(2)	0.043(2)	0.063(2)	0.0009(18)	-0.0135(19)	-0.0166(17)
C2	0.0310(17)	0.0354(16)	0.0348(16)	-0.0030(13)	-0.0091(13)	-0.0062(13)
C15	0.0392(18)	0.0349(17)	0.0444(18)	-0.0112(14)	-0.0161(14)	-0.0114(14)
C16	0.0368(18)	0.0388(18)	0.055(2)	-0.0179(15)	-0.0146(15)	-0.0120(14)
C17	0.0412(19)	0.0358(17)	0.0464(19)	-0.0130(14)	-0.0172(15)	-0.0058(14)
C18	0.0365(18)	0.0469(19)	0.0413(18)	-0.0024(15)	-0.0170(14)	-0.0155(15)
C19	0.046(2)	0.045(2)	0.064(2)	-0.0093(17)	-0.0251(17)	-0.0213(16)
C20	0.0414(19)	0.0338(17)	0.065(2)	-0.0131(16)	-0.0215(17)	-0.0097(15)
C11	0.054(2)	0.046(2)	0.056(2)	-0.0112(17)	-0.0154(19)	0.0040(17)
C10	0.0346(18)	0.0393(18)	0.057(2)	-0.0103(15)	-0.0154(16)	-0.0027(14)
C3	0.048(2)	0.047(2)	0.0470(19)	-0.0055(15)	-0.0140(16)	-0.0212(16)

Note. The anisotropic atomic displacement factor exponent takes the form: -2π2[h2 a*2 U11 + ... + 2 hka* b* U12]

Table 6

Hydrogen atomic coordinates and isotropic atomic displacement parameters (Å2) for MBDP.

	x/a	**y/b**	**z/c**	**U(eq)***
H8A	0.7468	0.4833	0.4328	0.09
H8B	0.6212	0.4093	0.5587	0.09
H8C	0.8008	0.3171	0.5027	0.09
H1	0.726	0.1434	1.3695	0.074
H2	0.9601	0.117	1.1757	0.065
H3	0.9479	0.1484	0.9538	0.053
H8	0.825	0.6941	0.3986	0.063
H9	0.8919	0.8919	0.4238	0.067
H10	0.9062	0.9048	0.6353	0.068
H13	0.4425	0.4796	0.8721	0.049
H14	0.1794	0.5294	0.8879	0.048
H15	0.0864	0.3498	0.8672	0.048
H16	0.2539	0.1191	0.8365	0.056
H17	0.517	0.069	0.8119	0.053
H18	0.4836	0.2041	1.3325	0.068
H19	0.473	0.2414	1.1097	0.054
H21	0.876	0.7124	0.8247	0.055

* U(eq) is defined as one third of the trace of the orthogonalized Uij tensor.

Appendix B

*X-ray Crystallography Data of Complex **2***

Table 1

*Data collection and structure refinement for **2***

Chemical formula	$C_{20}H_{17}AuClN_2P$	
Formula weight	548.74	
Temperature	200(2) K	
Wavelength	0.71073 Å	
Crystal size	0.050 x 0.050 x 1.000 mm	
Crystal system	monoclinic	
Space group	P 2_1/c	
Unit cell dimensions	a = 15.650(3) Å	α = 90°
	b = 7.4736(12) Å	β = 113.462(5)°
	c = 17.493(3) Å	γ = 90°
Volume	1876.9(6) $Å^3$	
Z	4	
Density (calculated)	1.942 Mg/cm^3	
Absorption coefficient	8.070 mm^{-1}	
F(000)	1048	
Theta range for data collection	1.42 to 25.07°	
Index ranges	-18<=h<=18, -8<=k<=8, -20<=l<=20	
Reflections collected	14408	
Independent reflections	3323 [R(int) = 0.1081]	
Absorption correction	multi-scan	
Max. and min. transmission	0.6884 and 0.0456	
Structure solution technique	direct methods	
Structure solution program	SHELXS-97 (Sheldrick, 2008)	
Refinement method	Full-matrix least-squares on F^2	
Refinement program	SHELXL-97 (Sheldrick, 2008)	
Function minimized	$\Sigma\ w(Fo^2 - Fc^2)^2$	
Data / restraints / parameters	3323 / 0 / 228	
Goodness-of-fit on F2	1.11	
Final R indices	2552 data; I>2σ(I)	R1 = 0.0820, wR2 = 0.2230
	all data	R1 = 0.0989, wR2 = 0.2335
Weighting scheme	$w=1/[\sigma^2(Fo^2)+(0.0947P)^2+95.0646P]$	
	where $P=(Fo^2+2Fc^2)/3$	
Extinction coefficient	0.0003(3)	
Largest diff. peak and hole	5.790 and -2.966 $eÅ^{-3}$	
R.M.S. deviation from mean	0.325 $eÅ^{-3}$	

Table 2

*Atomic coordinates and equivalent isotropic atomic displacement parameters (Å2) for **2**.*

	x/a	**y/b**	**z/c**	**U(eq)***
Au1	0.26316(5)	0.41265(11)	0.35061(5)	0.0299(4)
Cl1	0.2806(4)	0.5964(8)	0.2539(3)	0.0404(12)
P1	0.2360(3)	0.2409(7)	0.4424(3)	0.0274(11)
N1	0.4211(11)	0.146(2)	0.5479(10)	0.026(4)
N2	0.3102(12)	0.945(2)	0.5322(11)	0.036(4)
C1	0.4680(13)	0.307(3)	0.5371(13)	0.033(5)
C2	0.3285(14)	0.100(3)	0.5093(12)	0.029(4)
C3	0.3973(13)	0.880(3)	0.5913(12)	0.033(5)
C4	0.4194(15)	0.723(3)	0.6380(13)	0.037(5)
C5	0.5119(15)	0.704(3)	0.6924(13)	0.040(5)
C6	0.5787(15)	0.831(4)	0.7014(14)	0.050(7)
C7	0.5596(15)	0.987(3)	0.6549(14)	0.041(5)
C8	0.4669(13)	0.009(3)	0.5998(12)	0.030(4)
C9	0.2030(13)	0.367(3)	0.5143(12)	0.030(5)
C10	0.1718(17)	0.546(3)	0.4947(14)	0.041(6)
C11	0.144(2)	0.640(4)	0.5468(17)	0.058(7)
C12	0.1478(19)	0.570(3)	0.6203(17)	0.052(7)
C13	0.1742(15)	0.394(4)	0.6386(14)	0.044(6)
C14	0.2038(13)	0.296(3)	0.5860(12)	0.032(5)
C15	0.0601(13)	0.092(3)	0.4007(14)	0.037(5)
C16	0.1445(13)	0.081(3)	0.3929(11)	0.026(4)
C17	0.9899(15)	0.971(3)	0.3590(14)	0.043(6)
C18	0.0026(16)	0.838(3)	0.3097(14)	0.044(6)
C19	0.0870(15)	0.827(3)	0.3027(13)	0.037(5)
C20	0.1567(13)	0.950(3)	0.3451(11)	0.028(4)

* U(eq) is defined as one third of the trace of the orthogonalized Uij tensor.

Table 3

*Bond lengths (Å) for **2**.*

Au1-P1	2.225(5)	Au1-Cl1	2.279(5)
P1-C2	1.79(2)	P1-C16	1.80(2)
P1-C9	1.804(19)	N1-C8	1.37(3)
N1-C2	1.38(2)	N1-C1	1.46(2)
N2-C2	1.30(3)	N2-C3	1.43(3)
C1-H2	0.98	C1-H3	0.98
C1-H1	0.98	C3-C4	1.40(3)
C3-C8	1.42(3)	C4-C5	1.39(3)
C4-H7	0.95	C5-C6	1.37(3)
C5-H6	0.95	C6-C7	1.39(4)
C6-H5	0.95	C7-C8	1.40(3)
C7-H4	0.95	C9-C14	1.36(3)
C9-C10	1.42(3)	C10-C11	1.35(3)
C10-H12	0.95	C11-C12	1.37(4)
C11-H11	0.95	C12-C13	1.38(3)
C12-H10	0.95	C13-C14	1.39(3)
C13-H9	0.95	C14-H8	0.95
C15-C16	1.38(3)	C15-C17	1.39(3)
C15-H13	0.95	C16-C20	1.35(3)
C17-C18	1.38(3)	C17-H14	0.95
C18-C19	1.38(3)	C18-H15	0.95
C19-C20	1.39(3)	C19-H16	0.95
C20-H17	0.95		

Table 4

*Bond angles (°) for **2**.*

P1-Au1-Cl1	175.96(19)	C2-P1-C16	101.9(9)
C2-P1-C9	103.4(9)	C16-P1-C9	106.8(9)
C2-P1-Au1	118.2(7)	C16-P1-Au1	112.3(6)
C9-P1-Au1	113.1(7)	C8-N1-C2	108.1(16)
C8-N1-C1	123.2(16)	C2-N1-C1	128.8(16)
C2-N2-C3	105.2(17)	N1-C1-H2	109.5
N1-C1-H3	109.5	H2-C1-H3	109.5
N1-C1-H1	109.5	H2-C1-H1	109.5
H3-C1-H1	109.5	N2-C2-N1	113.0(17)
N2-C2-P1	120.4(15)	N1-C2-P1	126.4(14)
C4-C3-C8	120.7(19)	C4-C3-N2	131.(2)
C8-C3-N2	108.5(19)	C5-C4-C3	116.(2)
C5-C4-H7	122.2	C3-C4-H7	122.2
C6-C5-C4	123.(2)	C6-C5-H6	118.3
C4-C5-H6	118.3	C5-C6-C7	123.(2)
C5-C6-H5	118.7	C7-C6-H5	118.7
C6-C7-C8	115.(2)	C6-C7-H4	122.4
C8-C7-H4	122.4	N1-C8-C7	132.(2)
N1-C8-C3	105.2(17)	C7-C8-C3	122.(2)
C14-C9-C10	117.9(19)	C14-C9-P1	122.7(17)
C10-C9-P1	119.4(16)	C11-C10-C9	120.(2)
C11-C10-H12	120.1	C9-C10-H12	120.1
C10-C11-C12	122.(2)	C10-C11-H11	118.8
C12-C11-H11	118.8	C11-C12-C13	118.(2)
C11-C12-H10	120.8	C13-C12-H10	120.8
C12-C13-C14	120.(2)	C12-C13-H9	120.1
C14-C13-H9	120.1	C9-C14-C13	122.(2)
C9-C14-H8	119.2	C13-C14-H8	119.2
C16-C15-C17	120.(2)	C16-C15-H13	120.1
C17-C15-H13	120.1	C20-C16-C15	118.7(18)
C20-C16-P1	119.9(15)	C15-C16-P1	121.4(15)
C18-C17-C15	121.(2)	C18-C17-H14	119.4
C15-C17-H14	119.4	C19-C18-C17	118.(2)
C19-C18-H15	120.8	C17-C18-H15	120.8
C18-C19-C20	119.(2)	C18-C19-H16	120.3
C20-C19-H16	120.3	C16-C20-C19	122.3(19)
C16-C20-H17	118.8	C19-C20-H17	118.8

Table 5

*Anisotropic atomic displacement parameters (Å2) for **2**.*

	U11	**U22**	**U33**	**U23**	**U13**	**U12**
Au1	0.0297(5)	0.0293(5)	0.0262(5)	0.0053(3)	0.0062(3)	-0.0001(3)
Cl1	0.046(3)	0.035(3)	0.040(3)	0.015(2)	0.017(2)	0.005(2)
P1	0.024(2)	0.030(3)	0.022(2)	0.004(2)	0.003(2)	0.001(2)
N1	0.030(9)	0.013(8)	0.026(8)	0.003(7)	0.001(7)	-0.002(7)
N2	0.033(10)	0.032(11)	0.031(9)	0.005(8)	0.000(8)	-0.003(8)
C1	0.021(10)	0.028(12)	0.040(12)	-0.007(9)	0.001(9)	-0.006(8)
C2	0.031(10)	0.022(10)	0.028(10)	0.001(9)	0.007(8)	-0.003(8)
C3	0.022(10)	0.052(14)	0.020(9)	-0.004(9)	0.003(8)	0.004(9)
C4	0.033(11)	0.034(13)	0.036(11)	0.015(10)	0.007(9)	0.011(10)
C5	0.040(13)	0.031(13)	0.035(11)	0.014(10)	0.000(10)	0.010(10)
C6	0.022(11)	0.070(18)	0.037(12)	0.003(12)	-0.010(9)	0.022(11)
C7	0.028(11)	0.038(14)	0.045(13)	-0.008(11)	0.004(10)	0.007(10)
C8	0.029(10)	0.032(12)	0.031(10)	-0.008(9)	0.016(9)	-0.002(9)
C9	0.019(9)	0.036(12)	0.028(10)	-0.016(9)	0.002(8)	-0.005(8)
C10	0.057(14)	0.026(12)	0.042(12)	0.018(10)	0.022(11)	0.022(10)
C11	0.08(2)	0.035(15)	0.061(17)	-0.004(13)	0.032(16)	0.013(13)
C12	0.075(18)	0.031(14)	0.069(17)	-0.007(12)	0.050(15)	0.007(12)
C13	0.030(11)	0.072(18)	0.031(11)	-0.006(12)	0.012(10)	-0.008(11)
C14	0.029(10)	0.029(12)	0.034(11)	0.005(9)	0.009(9)	0.002(9)
C15	0.017(9)	0.043(13)	0.043(12)	-0.018(11)	0.004(9)	-0.004(9)
C16	0.029(10)	0.017(10)	0.022(9)	0.008(8)	-0.002(8)	0.005(8)
C17	0.024(11)	0.052(15)	0.040(12)	0.000(11)	0.001(10)	-0.001(10)
C18	0.032(12)	0.045(14)	0.039(12)	-0.007(11)	-0.002(10)	-0.009(10)
C19	0.037(12)	0.032(12)	0.026(10)	-0.004(9)	-0.005(9)	-0.004(10)
C20	0.024(10)	0.034(12)	0.017(9)	0.001(8)	-0.002(8)	-0.002(8)

Note. The anisotropic atomic displacement factor exponent takes the form: -2π2[h2 a*2 U11 + ... + 2 hka* b* U12]

Table 6

*Hydrogen atomic coordinates and isotropic atomic displacement parameters (Å2) for **2**.*

	x/a	**y/b**	**z/c**	**U(eq)***
H2	0.5271	0.3225	0.5854	0.05
H3	0.4282	0.4117	0.5322	0.05
H1	0.48	0.2961	0.4865	0.05
H7	0.374	-0.3661	0.6329	0.044
H6	0.5299	-0.4016	0.725	0.048
H5	0.6404	-0.1891	0.7411	0.06
H4	0.6063	0.0731	0.6602	0.049
H12	0.1703	0.5997	0.4449	0.05
H11	0.1218	0.7579	0.532	0.07
H10	0.1324	0.6418	0.6579	0.062
H9	0.1722	0.3393	0.6869	0.053
H8	0.225	0.1768	0.6005	0.038
H13	0.0503	0.1825	0.4345	0.045
H14	-0.0681	-0.0202	0.3643	0.051
H15	-0.0458	-0.2452	0.2814	0.052
H16	0.0976	-0.2629	0.2693	0.045
H17	0.2148	-0.0581	0.3401	0.034

* U(eq) is defined as one third of the trace of the orthogonalized Uij tensor.

Appendix C

*X-ray Crystallography Data of Complex **3***

Table 1

*X-ray Crystallographic Details for **3**.*

Chemical formula	$C_{22}H_{22}AuBF_4N_3P$	
Formula weight	643.17	
Temperature	200(2) K	
Wavelength	0.71073 Å	
Crystal size	0.200 x 0.500 x 0.600 mm	
Crystal habit	colorless needle	
Crystal system	monoclinic	
Space group	P 2_1/n	
Unit cell dimensions	a = 8.9993(8) Å	α = 90°
	b = 19.6166(18) Å	β = 100.966(2)°
	c = 13.4484(12) Å	γ = 90°
Volume	2330.8(4) $Å^3$	
Z	4	
Density (calculated)	1.833 Mg/cm^3	
Absorption coefficient	6.427 mm^{-1}	
F(000)	1240	
Theta range for data collection	2.08 to 25.04°	
Index ranges	-10<=h<=10, -23<=k<=23, -16<=l<=16	
Reflections collected	20345	
Independent reflections	4076 [R(int) = 0.0548]	
Coverage of independent reflections	98.80%	
Max. and min. transmission	0.3597 and 0.1134	
Structure solution technique	direct methods	
Structure solution program	SHELXS-97 (Sheldrick, 2008)	
Refinement method	Full-matrix least-squares on F^2	
Refinement program	SHELXL-97 (Sheldrick, 2008)	
Function minimized	$\Sigma\, w(F_o^2 - F_c^2)^2$	
Data / restraints / parameters	4076 / 0 / 291	
Goodness-of-fit on F^2	0.981	
Δ/σ_{max}	6.827	
Final R indices	3376 data; I>2σ(I)	R1 = 0.0264, wR2 = 0.0635
	all data	R1 = 0.0356, wR2 = 0.0699
Weighting scheme	$w=1/[\sigma^2(F_o^2)+(0.0299P)2+4.7568P]$	
	where $P=(F_o^2+2F_c^2)/3$	
Largest diff. peak and hole	1.225 and -0.808 $eÅ^{-3}$	
R.M.S. deviation from mean	0.146 $eÅ^{-3}$	

Table 2

*Atomic coordinates and equivalent isotropic atomic displacement parameters (Å2) for **3**.*

	x/a	**y/b**	**z/c**	**U(eq)***
Au1	0.91236(2)	0.994397(8)	0.075544(14)	0.02896(9)
P1	0.09227(15)	0.04320(6)	0.19010(10)	0.0301(3)
F1	0.9540(5)	0.26976(19)	0.9564(4)	0.0843(13)
F2	0.0616(6)	0.2199(3)	0.8369(3)	0.1048(16)
F3	0.9901(4)	0.15670(16)	0.9588(3)	0.0704(11)
F4	0.1919(5)	0.2267(2)	0.9978(3)	0.0778(12)
N3	0.8387(13)	0.8259(6)	0.3905(8)	0.163(4)
C22	0.739(2)	0.9463(6)	0.3324(9)	0.152(6)
N2	0.7496(4)	0.94697(18)	0.9678(3)	0.0297(9)
C1	0.2498(6)	0.0674(2)	0.1284(4)	0.0307(11)
N1	0.3794(5)	0.0995(2)	0.1716(3)	0.0394(11)
C25	0.4271(8)	0.1237(4)	0.2764(5)	0.068(2)
C2	0.4670(7)	0.1060(3)	0.0987(5)	0.0422(13)
C6	0.6141(6)	0.9231(2)	0.9889(4)	0.0329(12)
C7	0.5576(6)	0.9244(2)	0.0792(5)	0.0432(14)
C23	0.4166(7)	0.8951(3)	0.0739(6)	0.0557(19)
C5	0.6644(7)	0.1340(3)	0.0137(6)	0.0596(18)
C4	0.6105(7)	0.1351(3)	0.1019(5)	0.0566(17)
C9	0.1734(6)	0.9850(3)	0.2908(4)	0.0369(12)
C14	0.1698(7)	0.9162(3)	0.2670(5)	0.0454(14)
C13	0.2373(8)	0.8695(3)	0.3397(6)	0.065(2)
C12	0.3084(8)	0.8910(4)	0.4329(6)	0.072(2)
C11	0.3076(8)	0.9594(4)	0.4584(5)	0.071(2)
C10	0.2413(8)	0.0065(3)	0.3878(5)	0.0540(17)
C15	0.0341(6)	0.1195(2)	0.2473(4)	0.0319(11)
C16	0.9460(6)	0.1121(3)	0.3209(4)	0.0439(14)
C17	0.8902(7)	0.1694(3)	0.3613(5)	0.0504(15)
C18	0.9206(7)	0.2338(3)	0.3292(5)	0.0546(17)
C19	0.0025(8)	0.2403(3)	0.2545(6)	0.069(2)
C20	0.0600(7)	0.1837(3)	0.2131(5)	0.0520(16)
B1	0.0487(10)	0.2188(4)	0.9360(6)	0.055(2)
C27	0.7762(17)	0.8961(7)	0.3572(8)	0.133(5)

* U(eq) is defined as one third of the trace of the orthogonalized Uij tensor.

Table 3

*Bond lengths (Å) for **3**.*

Au1-N2	2.074(4)	Au1-P1	2.2277(13)
Au1-Au1#1	2.8079(4)	P1-C15	1.805(5)
P1-C9	1.814(5)	P1-C1	1.836(5)
F1-B1	1.374(8)	F2-B1	1.360(8)
F3-B1	1.385(7)	F4-B1	1.402(9)
N3-C27	1.522(16)	C22-C27	1.073(16)
N2-C1#1	1.325(6)	N2-C6	1.385(6)
C1-N2#1	1.325(6)	C1-N1	1.356(6)
N1-C2	1.376(7)	N1-C25	1.471(7)
C25-H4A	0.98	C25-H4B	0.98
C25-H4C	0.98	C2-C6#1	1.385(8)
C2-C4	1.405(8)	C6-C2#1	1.385(8)
C6-C7	1.403(7)	C7-C23	1.382(8)
C7-H7	0.95	C23-C5#1	1.385(9)
C23-H8	0.95	C5-C4	1.365(9)
C5-C23#1	1.385(9)	C5-H9	0.95
C4-H10	0.95	C9-C14	1.387(7)
C9-C10	1.397(8)	C14-C13	1.393(8)
C14-H12	0.95	C13-C12	1.362(10)
C13-H13	0.95	C12-C11	1.386(10)
C12-H14	0.95	C11-C10	1.377(8)
C11-H15	0.95	C10-H16	0.95
C15-C20	1.376(7)	C15-C16	1.388(7)
C16-C17	1.384(7)	C16-H18	0.95
C17-C18	1.379(8)	C17-H19	0.95
C18-C19	1.360(8)	C18-H20	0.95
C19-C20	1.385(8)	C19-H21	0.95
C20-H22	0.95		

Table 4

*Bond angles (°) for **3**.*

N2-Au1-P1	178.31(11)	N2-Au1-Au1#1	87.08(11)
P1-Au1-Au1#1	91.86(3)	C15-P1-C9	108.1(2)
C15-P1-C1	106.8(2)	C9-P1-C1	105.3(2)
C15-P1-Au1	114.81(17)	C9-P1-Au1	112.46(18)
C1-P1-Au1	108.70(17)	C1#1-N2-C6	107.2(4)
C1#1-N2-Au1	130.1(3)	C6-N2-Au1	122.8(3)
N2#1-C1-N1	110.8(4)	N2#1-C1-P1	122.2(4)
N1-C1-P1	127.0(4)	C1-N1-C2	107.5(4)
C1-N1-C25	129.1(5)	C2-N1-C25	123.4(5)
N1-C25-H4A	109.5	N1-C25-H4B	109.5
H4A-C25-H4B	109.5	N1-C25-H4C	109.5
H4A-C25-H4C	109.5	H4B-C25-H4C	109.5
N1-C2-C6#1	106.7(5)	N1-C2-C4	131.6(6)
C6#1-C2-C4	121.7(6)	N2-C6-C2#1	107.9(4)
N2-C6-C7	130.5(5)	C2#1-C6-C7	121.6(5)
C23-C7-C6	115.4(6)	C23-C7-H7	122.3
C6-C7-H7	122.3	C7-C23-C5#1	123.0(6)
C7-C23-H8	118.5	C5#1-C23-H8	118.5
C4-C5-C23#1	122.0(6)	C4-C5-H9	119
C23#1-C5-H9	119	C5-C4-C2	116.3(6)
C5-C4-H10	121.8	C2-C4-H10	121.8
C14-C9-C10	119.8(5)	C14-C9-P1	116.9(4)
C10-C9-P1	123.4(4)	C9-C14-C13	119.4(6)
C9-C14-H12	120.3	C13-C14-H12	120.3
C12-C13-C14	120.6(6)	C12-C13-H13	119.7
C14-C13-H13	119.7	C13-C12-C11	120.3(6)
C13-C12-H14	119.9	C11-C12-H14	119.9
C10-C11-C12	120.1(7)	C10-C11-H15	120
C12-C11-H15	120	C11-C10-C9	119.8(6)
C11-C10-H16	120.1	C9-C10-H16	120.1
C20-C15-C16	119.3(5)	C20-C15-P1	122.3(4)
C16-C15-P1	118.0(4)	C17-C16-C15	119.7(5)
C17-C16-H18	120.2	C15-C16-H18	120.2
C18-C17-C16	120.8(5)	C18-C17-H19	119.6
C16-C17-H19	119.6	C19-C18-C17	119.0(5)
C19-C18-H20	120.5	C17-C18-H20	120.5
C18-C19-C20	121.2(5)	C18-C19-H21	119.4
C20-C19-H21	119.4	C15-C20-C19	119.9(5)
C15-C20-H22	120	C19-C20-H22	120
F2-B1-F1	110.8(7)	F2-B1-F3	109.7(6)
F1-B1-F3	108.6(6)	F2-B1-F4	109.8(6)
F1-B1-F4	109.7(6)	F3-B1-F4	108.1(6)
C22-C27-N3	176.5(18)		

Table 5

*Anisotropic atomic displacement parameters (Å2) for **3**.*

	U11	**U22**	**U33**	**U23**	**U13**	**U12**
Au1	0.03346(16)	0.03006(12)	0.02492(13)	-0.00409(7)	0.00950(9)	-0.00526(8)
P1	0.0374(8)	0.0276(6)	0.0256(7)	-0.0031(5)	0.0071(6)	-0.0030(5)
F1	0.091(3)	0.052(2)	0.107(3)	-0.005(2)	0.011(3)	0.013(2)
F2	0.125(4)	0.127(4)	0.070(3)	-0.001(3)	0.038(3)	-0.027(3)
F3	0.070(3)	0.0380(18)	0.110(3)	-0.0003(19)	0.034(2)	-0.0107(16)
F4	0.066(3)	0.078(3)	0.092(3)	0.000(2)	0.022(2)	-0.018(2)
N3	0.203(11)	0.148(9)	0.128(9)	-0.001(7)	0.008(8)	-0.023(8)
C22	0.299(18)	0.084(7)	0.076(7)	-0.016(6)	0.041(9)	-0.030(10)
N2	0.029(2)	0.0231(18)	0.037(2)	-0.0004(17)	0.0057(19)	-0.0018(16)
C1	0.037(3)	0.026(2)	0.030(3)	0.000(2)	0.009(2)	-0.001(2)
N1	0.035(3)	0.043(2)	0.037(3)	-0.007(2)	-0.001(2)	-0.010(2)
C25	0.062(5)	0.084(5)	0.051(4)	-0.020(4)	-0.004(4)	-0.028(4)
C2	0.042(4)	0.033(3)	0.051(4)	0.003(2)	0.008(3)	-0.003(2)
C6	0.030(3)	0.022(2)	0.048(3)	0.006(2)	0.011(3)	0.004(2)
C7	0.051(4)	0.033(3)	0.051(4)	0.007(2)	0.022(3)	0.005(2)
C23	0.041(4)	0.048(3)	0.087(5)	0.025(3)	0.036(4)	0.012(3)
C5	0.029(4)	0.054(4)	0.095(6)	0.015(4)	0.011(4)	-0.004(3)
C4	0.040(4)	0.051(3)	0.077(5)	0.008(3)	0.006(4)	-0.011(3)
C9	0.038(3)	0.043(3)	0.031(3)	0.005(2)	0.010(3)	0.004(2)
C14	0.056(4)	0.038(3)	0.046(3)	0.002(3)	0.019(3)	0.005(3)
C13	0.084(5)	0.046(3)	0.076(5)	0.019(3)	0.044(5)	0.018(3)
C12	0.074(5)	0.079(5)	0.069(5)	0.040(4)	0.032(4)	0.033(4)
C11	0.085(6)	0.087(5)	0.035(4)	0.019(4)	0.000(4)	0.018(4)
C10	0.064(5)	0.054(4)	0.039(4)	0.005(3)	-0.003(3)	0.005(3)
C15	0.035(3)	0.033(2)	0.027(3)	-0.005(2)	0.004(2)	-0.003(2)
C16	0.052(4)	0.041(3)	0.042(3)	-0.004(2)	0.017(3)	-0.004(3)
C17	0.048(4)	0.061(4)	0.047(4)	-0.009(3)	0.021(3)	-0.001(3)
C18	0.055(4)	0.046(3)	0.067(4)	-0.024(3)	0.022(4)	-0.002(3)
C19	0.085(5)	0.032(3)	0.105(6)	-0.007(3)	0.056(5)	-0.006(3)
C20	0.067(4)	0.036(3)	0.061(4)	-0.002(3)	0.034(4)	-0.005(3)
B1	0.071(6)	0.044(4)	0.057(5)	-0.007(3)	0.028(4)	-0.011(4)
C27	0.222(15)	0.121(9)	0.056(6)	-0.030(7)	0.030(8)	-0.076(11)

Table 6

*Hydrogen atomic coordinates and isotropic atomic displacement parameters (Å2) for **3**.*

	x/a	**y/b**	**z/c**	**U(eq)***
H4A	0.3375	0.1346	0.3049	0.102
H4B	0.4897	0.1646	0.2769	0.102
H4C	0.4858	0.088	0.3172	0.102
H7	-0.3876	-0.056	0.1397	0.052
H8	-0.6267	-0.1052	0.1331	0.067
H9	0.7604	0.1538	0.0123	0.071
H10	0.6669	0.1545	0.1622	0.068
H12	0.1217	-0.099	0.2017	0.054
H13	0.2337	-0.1778	0.3241	0.078
H14	0.3587	-0.1411	0.4807	0.086
H15	0.353	-0.0261	0.5247	0.085
H16	0.2417	0.0535	0.4051	0.065
H18	-0.076	0.068	0.3433	0.053
H19	-0.1698	0.1643	0.4118	0.06
H20	-0.1151	0.273	0.3588	0.066
H21	0.0207	0.2844	0.2304	0.083
H22	0.1171	0.1892	0.1611	0.062

* U(eq) is defined as one third of the trace of the orthogonalized Uij tensor.

Appendix D

*X-ray Crystallography Data of Complex **4***

Table 1

*X-ray structural data for **4**.*

Chemical formula	$C_{48}H_{48}Ag_2B_2F_8N_8P_2$	
Formula weight	1188.24	
Temperature	200(2) K	
Wavelength	0.71073 Å	
Crystal size	0.200 x 0.400 x 0.600 mm	
Crystal habit	colorless needle	
Crystal system	triclinic	
Space group	P -1	
Unit cell dimensions	a = 10.5423(10) Å	α = 88.592(3)°
	b = 10.7638(10) Å	β = 73.097(3)°
	c = 12.3530(12) Å	γ = 84.422(3)°
Volume	1334.8(2) $Å^3$	
Z	1	
Density (calculated)	1.478 Mg/cm^3	
Absorption coefficient	0.862 mm^{-1}	
F(000)	598	
Theta range for data collection	1.72 to 25.09°	
Index ranges	-12<=h<=12, -12<=k<=12, -14<=l<=14	
Reflections collected	12591	
Independent reflections	4657 [R(int) = 0.0421]	
Coverage of independent reflections	97.80%	
Absorption correction	multi-scan	
Max. and min. transmission	0.8465 and 0.6259	
Structure solution technique	direct methods	
Structure solution program	SHELXS-97 (Sheldrick, 2008)	
Refinement method	Full-matrix least-squares on F^2	
Refinement program	SHELXL-97 (Sheldrick, 2008)	
Function minimized	$\Sigma w(F_o^2 - F_c^2)^2$	
Data / restraints / parameters	4657 / 0 / 320	
Goodness-of-fit on F^2	1.114	
Δ/σmax	0.013	
Final R indices	4096 data; I>2σ(I) R1 = 0.0337, wR2 = 0.0929	
	all data R1 = 0.0402, wR2 = 0.1040	
Weighting scheme	$w=1/[\sigma^2(F_o^2)+(0.0575P)^2+0.1523P]$	
	where $P=(F_o^2+2F_c^2)/3$	
Absolute structure parameter	0.0(1)	
Extinction coefficient	0.0027(10)	
Largest diff. peak and hole	0.874 and -0.425 $eÅ^{-3}$	
R.M.S. deviation from mean	0.097 $eÅ^{-3}$	

Table 2

*Atomic coordinates and equivalent isotropic atomic displacement parameters (Å2) for **4**.*

	x/a	**y/b**	**z/c**	**U(eq)***
Ag1	0.48353(2)	0.36607(2)	0.478193(18)	0.03671(13)
P1	0.50839(8)	0.44807(7)	0.29252(6)	0.0280(2)
F1	0.2556(3)	0.1598(3)	0.1322(3)	0.1122(12)
F2	0.1934(3)	0.1414(3)	0.3191(2)	0.0832(8)
F3	0.0422(3)	0.1520(4)	0.2258(4)	0.1551(18)
F4	0.1805(4)	0.9831(3)	0.2143(3)	0.1059(11)
N1	0.3601(2)	0.3646(2)	0.6581(2)	0.0287(5)
N2	0.6910(2)	0.6108(2)	0.1543(2)	0.0313(6)
N3	0.4720(4)	0.1445(3)	0.4279(3)	0.0646(10)
N4	0.7006(4)	0.2974(4)	0.5009(3)	0.0694(10)
C1	0.6182(3)	0.5729(3)	0.2583(2)	0.0287(6)
C2	0.3571(3)	0.5064(3)	0.2592(3)	0.0322(7)
C3	0.3390(3)	0.6198(3)	0.2082(3)	0.0369(7)
C4	0.2166(4)	0.6600(3)	0.1930(3)	0.0451(9)
C5	0.1133(4)	0.5872(4)	0.2266(3)	0.0531(10)
C6	0.1296(4)	0.4724(4)	0.2754(4)	0.0590(11)
C7	0.2510(3)	0.4332(3)	0.2938(3)	0.0468(9)
C8	0.5923(3)	0.3259(3)	0.1905(2)	0.0296(7)
C9	0.7209(3)	0.2812(3)	0.1886(3)	0.0401(8)
C10	0.7851(4)	0.1801(3)	0.1193(3)	0.0507(9)
C11	0.7219(4)	0.1239(3)	0.0546(3)	0.0508(10)
C12	0.5943(4)	0.1678(3)	0.0568(3)	0.0482(9)
C13	0.5287(3)	0.2682(3)	0.1246(3)	0.0378(7)
C14	0.6962(4)	0.5650(4)	0.0429(3)	0.0515(10)
C15	0.7655(3)	0.7030(3)	0.1735(3)	0.0316(7)
C16	0.2678(3)	0.2818(3)	0.7095(3)	0.0305(7)
C17	0.2102(3)	0.1940(3)	0.6621(3)	0.0399(8)
C18	0.1208(3)	0.1241(3)	0.7357(3)	0.0450(8)
C19	0.9118(3)	0.8597(3)	0.1466(3)	0.0437(8)
C20	0.8562(3)	0.7742(3)	0.0985(3)	0.0417(8)
C21	0.4745(4)	0.0650(3)	0.3707(3)	0.0483(9)
C22	0.4785(4)	0.9602(3)	0.2976(4)	0.0606(11)
C23	0.7919(4)	0.2467(5)	0.5118(3)	0.0654(12)
C24	0.9098(6)	0.1768(7)	0.5296(5)	0.129(3)
B1	0.1663(5)	0.1095(4)	0.2215(4)	0.0559(12)

* U(eq) is defined as one third of the trace of the orthogonalized Uij tensor.

Table 3

*Bond lengths (Å) for **4**.*

Ag1-N1	2.226(2)	Ag1-P1	2.3883(8)
Ag1-N4	2.429(3)	Ag1-N3	2.502(4)
Ag1-Ag1#1	3.0171(5)	P1-C2	1.812(3)
P1-C8	1.818(3)	P1-C1	1.821(3)
F1-B1	1.364(6)	F2-B1	1.376(5)
F3-B1	1.329(6)	F4-B1	1.356(5)
N1-C1#1	1.332(4)	N1-C16	1.387(4)
N2-C1	1.366(4)	N2-C15	1.388(4)
N2-C14	1.458(4)	N3-C21	1.117(5)
N4-C23	1.101(5)	C1-N1#1	1.331(4)
C2-C3	1.382(4)	C2-C7	1.390(5)
C3-C4	1.385(5)	C3-H3	0.95
C4-C5	1.363(5)	C4-H4	0.95
C5-C6	1.379(5)	C5-H5	0.95
C6-C7	1.388(5)	C6-H6	0.95
C7-H7	0.95	C8-C13	1.386(4)
C8-C9	1.388(4)	C9-C10	1.393(5)
C9-H9	0.95	C10-C11	1.363(5)
C10-H10	0.95	C11-C12	1.374(5)
C11-H11	0.95	C12-C13	1.382(4)
C12-H12	0.95	C13-H13	0.95
C14-H14A	0.98	C14-H14B	0.98
C14-H14C	0.98	C15-C16#1	1.394(4)
C15-C20	1.397(4)	C16-C15#1	1.394(4)
C16-C17	1.397(4)	C17-C18	1.375(5)
C17-H17	0.95	C18-C19#1	1.404(5)
C18-H18	0.95	C19-C20	1.370(5)
C19-C18#1	1.404(5)	C19-H19	0.95
C20-H20	0.95	C21-C22	1.452(5)
C22-H22A	0.98	C22-H22B	0.98
C22-H22C	0.98	C23-C24	1.458(6)
C24-H24A	0.98	C24-H24B	0.98
C24-H24C	0.98		

Symmetry transformations used to generate equivalent atoms:

#1 -x+1, -y+1, -z+1

Table 4

*Bond angles (°) for **4**.*

N1-Ag1-P1	147.39(6)	N1-Ag1-N4	99.82(11)
P1-Ag1-N4	109.91(10)	N1-Ag1-N3	98.85(10)
P1-Ag1-N3	96.03(8)	N4-Ag1-N3	86.61(13)
N1-Ag1-Ag1#1	85.63(6)	P1-Ag1-Ag1#1	80.72(2)
N4-Ag1-Ag1#1	91.33(9)	N3-Ag1-Ag1#1	175.33(8)
C2-P1-C8	107.44(14)	C2-P1-C1	106.37(14)
C8-P1-C1	104.06(14)	C2-P1-Ag1	116.76(10)
C8-P1-Ag1	108.30(10)	C1-P1-Ag1	113.05(10)
C1#1-N1-C16	106.1(2)	C1#1-N1-Ag1	124.9(2)
C16-N1-Ag1	127.71(19)	C1-N2-C15	106.5(2)
C1-N2-C14	128.8(3)	C15-N2-C14	124.6(3)
C21-N3-Ag1	156.1(3)	C23-N4-Ag1	168.0(4)
N1#1-C1-N2	112.0(3)	N1#1-C1-P1	119.3(2)
N2-C1-P1	128.6(2)	C3-C2-C7	119.0(3)
C3-C2-P1	124.6(2)	C7-C2-P1	116.3(2)
C2-C3-C4	120.3(3)	C2-C3-H3	119.9
C4-C3-H3	119.9	C5-C4-C3	120.3(3)
C5-C4-H4	119.8	C3-C4-H4	119.8
C4-C5-C6	120.5(3)	C4-C5-H5	119.7
C6-C5-H5	119.7	C5-C6-C7	119.4(4)
C5-C6-H6	120.3	C7-C6-H6	120.3
C2-C7-C6	120.5(3)	C2-C7-H7	119.8
C6-C7-H7	119.8	C13-C8-C9	119.5(3)
C13-C8-P1	122.8(2)	C9-C8-P1	117.4(2)
C8-C9-C10	119.6(3)	C8-C9-H9	120.2
C10-C9-H9	120.2	C11-C10-C9	120.5(3)
C11-C10-H10	119.7	C9-C10-H10	119.7
C10-C11-C12	119.9(3)	C10-C11-H11	120
C12-C11-H11	120	C11-C12-C13	120.6(3)
C11-C12-H12	119.7	C13-C12-H12	119.7
C12-C13-C8	119.8(3)	C12-C13-H13	120.1
C8-C13-H13	120.1	N2-C14-H14A	109.5
N2-C14-H14B	109.5	H14A-C14-H14B	109.5
N2-C14-H14C	109.5	H14A-C14-H14C	109.5
H14B-C14-H14C	109.5	N2-C15-C16#1	106.4(3)
N2-C15-C20	131.3(3)	C16#1-C15-C20	122.2(3)
N1-C16-C15#1	108.9(3)	N1-C16-C17	130.3(3)
C15#1-C16-C17	120.8(3)	C18-C17-C16	117.0(3)
C18-C17-H17	121.5	C16-C17-H17	121.5

Table 4 *(cont.)*

C17-C18-C19#1	121.6(3)	C17-C18-H18	119.2
C19#1-C18-H18	119.2	C20-C19-C18#1	122.2(3)
C20-C19-H19	118.9	C18#1-C19-H19	118.9
C19-C20-C15	116.1(3)	C19-C20-H20	121.9
C15-C20-H20	121.9	N3-C21-C22	179.0(4)
C21-C22-H22A	109.5	C21-C22-H22B	109.5
H22A-C22-H22B	109.5	C21-C22-H22C	109.5
H22A-C22-H22C	109.5	H22B-C22-H22C	109.5
N4-C23-C24	177.8(6)	C23-C24-H24A	109.5
C23-C24-H24B	109.5	H24A-C24-H24B	109.5
C23-C24-H24C	109.5	H24A-C24-H24C	109.5
H24B-C24-H24C	109.5	F3-B1-F4	109.8(4)
F3-B1-F1	110.9(4)	F4-B1-F1	110.6(4)
F3-B1-F2	109.9(5)	F4-B1-F2	107.5(4)
F1-B1-F2	108.0(4)		

Symmetry transformations used to generate equivalent atoms:

#1 -x+1, -y+1, -z+1

Table 5

*Anisotropic atomic displacement parameters (Å2) for **4**.*

	U11	U22	U33	U23	U13	U12
Ag1	0.0493(2)	0.03406(18)	0.02626(17)	0.00298(10)	-0.00930(12)	-0.00747(12)
P1	0.0330(4)	0.0265(4)	0.0249(4)	0.0012(3)	-0.0084(3)	-0.0043(3)
F1	0.119(3)	0.152(3)	0.080(2)	0.030(2)	-0.0294(19)	-0.088(2)
F2	0.105(2)	0.0758(18)	0.0733(18)	-0.0101(14)	-0.0314(16)	-0.0077(15)
F3	0.079(2)	0.179(4)	0.236(5)	0.057(4)	-0.089(3)	-0.032(2)
F4	0.141(3)	0.0663(19)	0.113(3)	-0.0140(17)	-0.032(2)	-0.0335(18)
N1	0.0295(13)	0.0304(13)	0.0261(13)	0.0007(10)	-0.0073(10)	-0.0050(10)
N2	0.0358(14)	0.0330(14)	0.0251(13)	0.0049(10)	-0.0074(11)	-0.0080(11)
N3	0.093(3)	0.0405(19)	0.054(2)	-0.0004(16)	-0.0115(19)	-0.0087(18)
N4	0.058(2)	0.087(3)	0.066(2)	-0.012(2)	-0.0276(19)	0.014(2)
C1	0.0311(15)	0.0271(15)	0.0281(15)	0.0016(12)	-0.0100(12)	-0.0004(12)
C2	0.0343(16)	0.0318(16)	0.0311(16)	-0.0042(13)	-0.0105(13)	-0.0015(13)
C3	0.0409(18)	0.0322(17)	0.0364(17)	0.0023(14)	-0.0095(14)	-0.0032(14)
C4	0.048(2)	0.041(2)	0.044(2)	0.0065(15)	-0.0136(16)	0.0071(16)
C5	0.042(2)	0.054(2)	0.064(3)	-0.0030(19)	-0.0207(19)	0.0098(17)
C6	0.042(2)	0.052(2)	0.082(3)	0.009(2)	-0.016(2)	-0.0089(18)
C7	0.0387(19)	0.0361(19)	0.066(2)	0.0068(17)	-0.0153(18)	-0.0069(15)
C8	0.0369(16)	0.0263(15)	0.0244(15)	0.0007(12)	-0.0070(13)	-0.0033(13)
C9	0.0373(18)	0.044(2)	0.0384(18)	-0.0005(15)	-0.0096(15)	-0.0040(15)
C10	0.046(2)	0.047(2)	0.048(2)	-0.0008(17)	-0.0008(17)	0.0079(17)
C11	0.065(2)	0.037(2)	0.0386(19)	-0.0052(16)	0.0015(18)	0.0024(18)
C12	0.072(3)	0.0373(19)	0.0376(19)	-0.0051(15)	-0.0184(18)	-0.0085(18)
C13	0.0453(19)	0.0346(18)	0.0350(17)	-0.0011(14)	-0.0142(15)	-0.0029(14)
C14	0.073(3)	0.056(2)	0.0258(17)	0.0021(16)	-0.0109(17)	-0.018(2)
C15	0.0297(15)	0.0275(16)	0.0367(17)	0.0047(13)	-0.0091(13)	-0.0004(12)
C16	0.0270(15)	0.0273(16)	0.0371(17)	0.0037(13)	-0.0091(13)	-0.0032(12)
C17	0.0381(17)	0.0391(19)	0.0435(19)	-0.0033(15)	-0.0117(15)	-0.0084(15)
C18	0.0383(18)	0.0393(19)	0.059(2)	0.0035(17)	-0.0149(17)	-0.0116(15)
C19	0.0343(18)	0.0371(19)	0.057(2)	0.0128(16)	-0.0082(16)	-0.0100(15)
C20	0.0379(18)	0.0419(19)	0.0406(19)	0.0110(15)	-0.0046(15)	-0.0046(15)
C21	0.057(2)	0.0323(19)	0.050(2)	0.0065(17)	-0.0091(18)	-0.0026(16)
C22	0.076(3)	0.039(2)	0.066(3)	-0.0089(19)	-0.021(2)	0.0034(19)
C23	0.054(2)	0.092(3)	0.047(2)	-0.008(2)	-0.017(2)	0.019(2)
C24	0.084(4)	0.210(8)	0.076(4)	-0.007(4)	-0.023(3)	0.075(4)
B1	0.060(3)	0.051(3)	0.066(3)	0.004(2)	-0.030(2)	-0.019(2)

Note. The anisotropic atomic displacement factor exponent takes the form: -2π2[h2 a*2 U11 + ... + 2 hka* b* U12]

Table 6

*Hydrogen atomic coordinates and isotropic atomic displacement parameters (Å2) for **4**.*

	x/a	**y/b**	**z/c**	**U(eq)***
H3	0.4109	0.6705	0.1835	0.044
H4	0.2045	0.7386	0.1589	0.054
H5	0.0294	0.6158	0.2163	0.064
H6	0.0584	0.4206	0.2962	0.071
H7	0.2617	0.3558	0.3302	0.056
H9	0.765	0.3193	0.2342	0.048
H10	0.8736	0.1501	0.117	0.061
H11	0.766	0.0545	0.0081	0.061
H12	0.5508	0.1288	0.0113	0.058
H13	0.4403	0.2975	0.1261	0.045
H14A	0.7685	0.498	0.0193	0.077
H14B	0.7122	0.6334	-0.0118	0.077
H14C	0.6113	0.5328	0.0462	0.077
H17	0.2319	0.1832	0.5825	0.048
H18	0.0801	0.0632	0.7063	0.054
H19	0.9746	0.9097	0.0988	0.052
H20	0.8782	0.7639	0.0189	0.05
H22A	0.5684	-0.0557	0.2455	0.091
H22B	0.4148	-0.0204	0.2542	0.091
H22C	0.4551	-0.1141	0.3438	0.091
H24A	0.9719	0.2351	0.5385	0.194
H24B	0.9531	0.1223	0.4643	0.194
H24C	0.8835	0.126	0.598	0.194

* U(eq) is defined as one third of the trace of the orthogonalized Uij tensor.

Appendix E

*X-ray Crystallography Data of Complex **5***

Table 1

*X-ray structural data for **5**.*

Chemical formula	$C_{70}H_{54}Ag_4F_6N_4O_{10}P_4S_2$	
Formula weight	1844.65	
Temperature	200(2) K	
Wavelength	0.71073 Å	
Crystal size	0.200 x 0.300 x 0.400 mm	
Crystal system	monoclinic	
Space group	P 1 21/n 1	
Unit cell dimensions	a = 20.973(2) Å	α = 90°
	b = 14.8853(13) Å	β = 106.566(3)°
	c = 24.206(3) Å	γ = 90°
Volume	7243.2(12) $Å^3$	
Z	4	
Density (calculated)	1.692 Mg/cm^3	
Absorption coefficient	1.286 mm^{-1}	
F(000)	3664	
Theta range for data collection	1.14 to 26.02°	
Index ranges	-25<=h<=25, -17<=k<=17, -29<=l<=29	
Reflections collected	132869	
Independent reflections	14158 [R(int) = 0.1601]	
Max. and min. transmission	0.7829 and 0.6272	
Structure solution technique	direct methods	
Structure solution program	SHELXS-97 (Sheldrick, 2008)	
Refinement method	Full-matrix least-squares on F^2	
Refinement program	SHELXL-97 (Sheldrick, 2008)	
Function minimized	$\Sigma\, w(F_o^2 - F_c^2)^2$	
Data / restraints / parameters	14158 / 0 / 868	
Goodness-of-fit on F^2	1.277	
Δ/σmax	0.026	
Final R indices	9076 data; I>2σ(I)	R1 = 0.0763, wR2 = 0.2054
	all data	R1 = 0.1252, wR2 = 0.2469
Weighting scheme	w=1/[σ2(Fo^2)+(0.0768P)2+22.4554P]	
	where P=(Fo^2+2Fc^2)/3	
Extinction coefficient	0.0032(2)	
Largest diff. peak and hole	3.142 and -1.560 $eÅ^{-3}$	
R.M.S. deviation from mean	0.401 $eÅ^{-3}$	

Table 2

*Atomic coordinates and equivalent isotropic atomic displacement parameters (Å2) for **5**.*

	x/a	**y/b**	**z/c**	**U(eq)***
Ag1	0.61533(3)	0.35698(5)	0.29837(4)	0.0333(2)
Ag2	0.50470(3)	0.48996(5)	0.24442(3)	0.0299(2)
Ag3	0.49998(3)	0.17851(5)	0.26966(3)	0.0294(2)
Ag4	0.38839(3)	0.31501(5)	0.21942(4)	0.0329(2)
N1	0.3175(4)	0.2064(5)	0.2175(3)	0.0252(17)
N2	0.2718(4)	0.0736(5)	0.2244(4)	0.032(2)
N3	0.6855(4)	0.4627(5)	0.2917(3)	0.0276(18)
N4	0.7330(3)	0.5885(5)	0.2729(4)	0.0280(18)
P1	0.41328(11)	0.07721(16)	0.26520(11)	0.0246(5)
P2	0.48675(12)	0.36560(16)	0.34823(11)	0.0245(5)
P3	0.59075(11)	0.59109(16)	0.24367(11)	0.0259(5)
P4	0.51620(12)	0.30106(17)	0.16612(11)	0.0257(5)
C1	0.3296(4)	0.1213(6)	0.2353(4)	0.027(2)
C2	0.2624(5)	0.9763(6)	0.2310(5)	0.034(2)
C3	0.2201(4)	0.1326(7)	0.1998(4)	0.030(2)
C4	0.1525(5)	0.1185(7)	0.1835(5)	0.044(3)
C5	0.1147(5)	0.1928(8)	0.1589(6)	0.051(3)
C6	0.1440(6)	0.2750(8)	0.1519(6)	0.049(3)
C7	0.2115(5)	0.2879(7)	0.1702(5)	0.040(3)
C8	0.2490(4)	0.2136(6)	0.1944(4)	0.028(2)
C9	0.4101(4)	0.9788(7)	0.2184(5)	0.034(2)
C10	0.3955(7)	0.9934(9)	0.1612(6)	0.062(4)
C11	0.4169(6)	0.8908(7)	0.2408(6)	0.046(3)
C12	0.4063(7)	0.8191(8)	0.2026(7)	0.065(4)
C13	0.3909(9)	0.8321(10)	0.1449(7)	0.086(5)
C14	0.4164(4)	0.0332(6)	0.3362(4)	0.027(2)
C15	0.3628(5)	0.0312(7)	0.3589(4)	0.033(2)
C16	0.3705(5)	0.9928(7)	0.4124(5)	0.039(3)
C17	0.4290(6)	0.9567(8)	0.4427(5)	0.045(3)
C18	0.4842(5)	0.9617(8)	0.4199(5)	0.047(3)
C19	0.4774(5)	0.9987(7)	0.3676(5)	0.038(3)
C20	0.4661(5)	0.2294(7)	0.1116(4)	0.031(2)
C21	0.4930(6)	0.1546(8)	0.0925(5)	0.049(3)
C22	0.4566(9)	0.0997(9)	0.0490(6)	0.068(4)
C23	0.3901(10)	0.1217(11)	0.0247(6)	0.079(5)
C24	0.3604(7)	0.1948(11)	0.0422(6)	0.066(4)
C25	0.3995(5)	0.2488(8)	0.0851(5)	0.047(3)
C26	0.3399(6)	0.5430(8)	0.0865(5)	0.047(3)

Table 2 *(cont.)*

	x/a	y/b	z/c	U(eq)*
C27	0.5705(5)	0.3581(6)	0.1314(4)	0.026(2)
C28	0.5453(5)	0.3983(7)	0.0779(4)	0.033(2)
C29	0.5863(6)	0.4362(8)	0.0504(5)	0.045(3)
C30	0.6538(6)	0.4357(8)	0.0751(5)	0.047(3)
C31	0.6804(5)	0.3990(8)	0.1298(6)	0.046(3)
C32	0.6399(5)	0.3586(7)	0.1573(5)	0.034(2)
C33	0.5208(5)	0.6691(8)	0.1416(5)	0.047(3)
C34	0.5824(5)	0.6317(6)	0.1716(4)	0.029(2)
C35	0.5086(6)	0.7009(9)	0.0861(6)	0.058(4)
C36	0.5572(6)	0.6961(8)	0.0583(5)	0.046(3)
C37	0.6175(6)	0.6579(8)	0.0858(5)	0.049(3)
C38	0.6315(5)	0.6261(7)	0.1434(5)	0.039(3)
C39	0.5951(5)	0.6915(6)	0.2887(5)	0.031(2)
C40	0.5987(6)	0.7776(8)	0.2687(6)	0.047(3)
C41	0.6057(7)	0.8485(8)	0.3075(7)	0.059(4)
C42	0.6082(7)	0.8346(9)	0.3653(7)	0.063(4)
C43	0.6014(8)	0.7496(11)	0.3832(6)	0.073(4)
C44	0.6738(4)	0.5446(6)	0.2703(4)	0.025(2)
C45	0.7435(5)	0.6833(6)	0.2608(5)	0.036(2)
C46	0.7833(5)	0.5293(7)	0.2964(4)	0.029(2)
C47	0.8519(5)	0.5376(7)	0.3080(5)	0.038(3)
C48	0.8899(5)	0.4657(8)	0.3338(5)	0.046(3)
C49	0.8600(5)	0.3871(7)	0.3487(5)	0.041(3)
C50	0.7923(5)	0.3792(7)	0.3365(5)	0.036(2)
C51	0.6674(6)	0.1212(9)	0.4309(6)	0.052(3)
C52	0.4311(4)	0.3056(6)	0.3800(4)	0.025(2)
C53	0.3624(5)	0.3142(7)	0.3568(5)	0.037(2)
C54	0.4566(5)	0.2518(7)	0.4289(5)	0.037(2)
C55	0.4140(6)	0.2099(8)	0.4546(5)	0.045(3)
C56	0.3453(7)	0.2187(8)	0.4300(6)	0.056(4)
C57	0.3201(6)	0.2715(8)	0.3821(5)	0.047(3)
C58	0.5350(5)	0.4382(7)	0.4048(4)	0.035(2)
C59	0.5066(6)	0.5159(7)	0.4189(5)	0.042(3)
C60	0.5390(8)	0.5688(9)	0.4626(6)	0.063(4)
C61	0.6004(8)	0.5479(10)	0.4936(6)	0.067(4)
C62	0.6294(8)	0.4716(11)	0.4806(7)	0.079(5)
C63	0.5976(6)	0.4156(9)	0.4365(6)	0.055(3)
C64	0.3881(10)	0.9183(11)	0.1234(7)	0.097(6)
C65	0.7537(4)	0.4510(6)	0.3091(4)	0.026(2)
C0K	0.5953(6)	0.6766(8)	0.3454(5)	0.049(3)

Table 2 *(cont.)*

	x/a	**y/b**	**z/c**	**U(eq)***
F1	0.6591(4)	0.0374(5)	0.4467(3)	0.073(2)
F2	0.7285(5)	0.1459(6)	0.4648(4)	0.087(3)
F3	0.6241(5)	0.1722(6)	0.4437(4)	0.088(3)
F4	0.2815(4)	0.5200(7)	0.0512(4)	0.087(3)
F5	0.3530(4)	0.6249(5)	0.0690(3)	0.068(2)
F6	0.3868(5)	0.4893(6)	0.0783(4)	0.086(3)
O1	0.6003(3)	0.0977(5)	0.3279(3)	0.0418(19)
O2	0.7159(3)	0.0654(5)	0.3503(4)	0.051(2)
O3	0.6790(4)	0.2194(5)	0.3479(4)	0.049(2)
O4	0.3239(4)	0.4529(5)	0.1711(4)	0.047(2)
O5	0.2878(3)	0.6073(5)	0.1604(4)	0.046(2)
O6	0.4049(3)	0.5738(5)	0.1908(3)	0.0373(17)
O7	0.4698(3)	0.3677(4)	0.1815(3)	0.0308(15)
O8	0.5597(3)	0.2457(4)	0.2158(3)	0.0280(15)
O9	0.4440(3)	0.4216(4)	0.2984(3)	0.0297(15)
O10	0.5350(3)	0.3001(4)	0.3340(3)	0.0280(15)
S1	0.66578(12)	0.12639(18)	0.35569(13)	0.0354(6)
S2	0.33903(11)	0.54431(17)	0.16065(12)	0.0326(6)

* U(eq) is defined as one third of the trace of the orthogonalized Uij tensor.

Table 3

*Bond lengths (Å) for **5**.*

Ag1-N3	2.191(7)	Ag1-O10	2.264(6)
Ag1-O3	2.550(7)	Ag1-O8	2.602(6)
Ag1-Ag2	3.0461(11)	Ag2-O9	2.306(6)
Ag2-P3	2.354(2)	Ag2-O7	2.352(7)
Ag2-O6	2.464(6)	Ag3-O8	2.281(6)
Ag3-P1	2.341(2)	Ag3-O10	2.365(6)
Ag3-O1	2.484(7)	Ag3-Ag4	3.0760(10)
Ag4-N1	2.188(7)	Ag4-O7	2.295(6)
Ag4-O9	2.502(7)	Ag4-O4	2.552(7)
N1-C1	1.338(12)	N1-C8	1.390(11)
N2-C1	1.364(11)	N2-C3	1.389(12)
N2-C2	1.476(12)	N3-C44	1.320(12)
N3-C65	1.383(11)	N4-C46	1.368(12)
N4-C44	1.387(11)	N4-C45	1.471(12)
P1-C1	1.819(9)	P1-C14	1.824(10)
P1-C9	1.841(11)	P2-O10	1.514(6)
P2-O9	1.528(7)	P2-C58	1.809(10)
P2-C52	1.807(9)	P3-C44	1.814(9)
P3-C34	1.806(10)	P3-C39	1.837(10)
P4-O7	1.508(6)	P4-O8	1.527(7)
P4-C20	1.787(10)	P4-C27	1.808(9)
C2-H2A	0.98	C2-H2B	0.98
C2-H2C	0.98	C3-C8	1.373(13)
C3-C4	1.376(13)	C4-C5	1.392(15)
C4-H4	0.95	C5-C6	1.401(16)
C5-H5	0.95	C6-C7	1.370(15)
C6-H6	0.95	C7-C8	1.386(13)
C7-H7	0.95	C9-C10	1.349(17)
C9-C11	1.409(15)	C10-C64	1.424(19)
C10-H10	0.95	C11-C12	1.388(17)
C11-H11	0.95	C12-C13	1.35(2)
C12-H12	0.95	C13-C64	1.38(2)
C13-H13	0.95	C14-C15	1.383(13)
C14-C19	1.388(13)	C15-C16	1.384(15)
C15-H15	0.95	C16-C17	1.350(15)
C16-H16	0.95	C17-C18	1.420(15)
C17-H17	0.95	C18-C19	1.350(16)
C18-H18	0.95	C19-H19	0.95
C20-C21	1.386(15)	C20-C25	1.391(14)

Table 3 *(cont.)*

C21-C22	1.379(17)	C21-H21	0.95
C22-C23	1.39(2)	C22-H22	0.95
C23-C24	1.38(2)	C23-H23	0.95
C24-C25	1.383(16)	C24-H24	0.95
C25-H25	0.95	C26-F6	1.325(14)
C26-F4	1.322(13)	C26-F5	1.345(13)
C26-S2	1.800(13)	C27-C28	1.389(13)
C27-C32	1.409(13)	C28-C29	1.351(14)
C28-H28	0.95	C29-C30	1.372(16)
C29-H29	0.95	C30-C31	1.394(17)
C30-H30	0.95	C31-C32	1.359(14)
C31-H31	0.95	C32-H32	0.95
C33-C35	1.376(16)	C33-C34	1.404(14)
C33-H33	0.95	C34-C38	1.391(14)
C35-C36	1.375(17)	C35-H35	0.95
C36-C37	1.374(17)	C36-H36	0.95
C37-C38	1.422(16)	C37-H37	0.95
C38-H38	0.95	C39-C40	1.380(15)
C39-C0K	1.388(15)	C40-C41	1.391(17)
C40-H40	0.95	C41-C42	1.40(2)
C41-H41	0.95	C42-C43	1.357(19)
C42-H42	0.95	C43-C0K	1.403(18)
C43-H43	0.95	C45-H45A	0.98
C45-H45B	0.98	C45-H45C	0.98
C46-C47	1.389(13)	C46-C65	1.396(13)
C47-C48	1.373(15)	C47-H47	0.95
C48-C49	1.422(16)	C48-H48	0.95
C49-C50	1.371(14)	C49-H49	0.95
C50-C65	1.390(14)	C50-H50	0.95
C51-F3	1.288(15)	C51-F1	1.331(14)
C51-F2	1.360(14)	C51-S1	1.812(13)
C52-C53	1.395(13)	C52-C54	1.402(14)
C53-C57	1.369(15)	C53-H53	0.95
C54-C55	1.376(14)	C54-H54	0.95
C55-C56	1.398(17)	C55-H55	0.95
C56-C57	1.376(18)	C56-H56	0.95
C57-H57	0.95	C58-C63	1.361(16)
C58-C59	1.389(15)	C59-C60	1.337(17)
C59-H59	0.95	C60-C61	1.33(2)
C60-H60	0.95	C61-C62	1.37(2)
C61-H61	0.95	C62-C63	1.369(18)

Table 3 *(cont.)*

C62-H62	0.95	C63-H63	0.95
C64-H64	0.95	C0K-H0K	0.95
O1-S1	1.413(7)	O2-S1	1.423(7)
O3-S1	1.435(8)	O4-S2	1.436(8)
O5-S2	1.425(7)	O6-S2	1.435(7)

Table 4

*Bond angles (°) for **5**.*

N3-Ag1-O10	152.2(3)	N3-Ag1-O3	109.8(3)
O10-Ag1-O3	82.4(2)	N3-Ag1-O8	124.3(2)
O10-Ag1-O8	80.6(2)	O3-Ag1-O8	84.8(2)
N3-Ag1-Ag2	87.0(2)	O10-Ag1-Ag2	81.26(17)
O3-Ag1-Ag2	163.01(16)	O8-Ag1-Ag2	87.97(14)
O9-Ag2-P3	146.64(18)	O9-Ag2-O7	84.6(2)
P3-Ag2-O7	125.98(16)	O9-Ag2-O6	89.9(2)
P3-Ag2-O6	102.13(17)	O7-Ag2-O6	89.5(2)
O9-Ag2-Ag1	86.92(16)	P3-Ag2-Ag1	85.81(6)
O7-Ag2-Ag1	80.38(16)	O6-Ag2-Ag1	169.60(17)
O8-Ag3-P1	143.35(18)	O8-Ag3-O10	85.6(2)
P1-Ag3-O10	127.94(16)	O8-Ag3-O1	91.3(2)
P1-Ag3-O1	103.60(18)	O10-Ag3-O1	86.7(2)
O8-Ag3-Ag4	87.96(16)	P1-Ag3-Ag4	85.06(6)
O10-Ag3-Ag4	79.25(16)	O1-Ag3-Ag4	165.99(19)
N1-Ag4-O7	145.3(3)	N1-Ag4-O9	130.6(3)
O7-Ag4-O9	81.4(2)	N1-Ag4-O4	108.5(3)
O7-Ag4-O4	84.2(2)	O9-Ag4-O4	84.9(2)
N1-Ag4-Ag3	87.5(2)	O7-Ag4-Ag3	79.32(17)
O9-Ag4-Ag3	88.87(15)	O4-Ag4-Ag3	163.11(17)
C1-N1-C8	106.4(7)	C1-N1-Ag4	128.9(6)
C8-N1-Ag4	124.7(6)	C1-N2-C3	107.2(8)
C1-N2-C2	128.8(8)	C3-N2-C2	123.7(8)
C44-N3-C65	107.2(7)	C44-N3-Ag1	129.7(6)
C65-N3-Ag1	123.1(6)	C46-N4-C44	106.8(8)
C46-N4-C45	124.0(7)	C44-N4-C45	128.8(8)
C1-P1-C14	106.0(4)	C1-P1-C9	100.4(4)
C14-P1-C9	106.2(5)	C1-P1-Ag3	115.8(3)
C14-P1-Ag3	111.7(3)	C9-P1-Ag3	115.6(3)
O10-P2-O9	116.9(4)	O10-P2-C58	106.9(4)
O9-P2-C58	110.3(4)	O10-P2-C52	109.5(4)
O9-P2-C52	107.5(4)	C58-P2-C52	105.2(4)
C44-P3-C34	106.9(4)	C44-P3-C39	102.7(4)
C34-P3-C39	106.0(5)	C44-P3-Ag2	114.5(3)
C34-P3-Ag2	111.0(3)	C39-P3-Ag2	115.1(3)
O7-P4-O8	116.3(4)	O7-P4-C20	106.9(4)
O8-P4-C20	110.7(4)	O7-P4-C27	110.0(4)
O8-P4-C27	107.7(4)	C20-P4-C27	104.6(4)
N1-C1-N2	110.7(8)	N1-C1-P1	122.8(7)

Table 4 *(cont.)*

N2-C1-P1	126.4(7)	N2-C2-H2A	109.5
N2-C2-H2B	109.5	H2A-C2-H2B	109.5
N2-C2-H2C	109.5	H2A-C2-H2C	109.5
H2B-C2-H2C	109.5	C8-C3-N2	106.6(8)
C8-C3-C4	123.6(9)	N2-C3-C4	129.9(9)
C5-C4-C3	114.7(10)	C5-C4-H4	122.7
C3-C4-H4	122.7	C4-C5-C6	121.9(10)
C4-C5-H5	119	C6-C5-H5	119
C7-C6-C5	122.1(10)	C7-C6-H6	119
C5-C6-H6	119	C6-C7-C8	115.8(10)
C6-C7-H7	122.1	C8-C7-H7	122.1
C3-C8-N1	109.1(8)	C3-C8-C7	121.9(9)
N1-C8-C7	129.1(9)	C10-C9-C11	120.9(11)
C10-C9-P1	117.5(9)	C11-C9-P1	121.4(9)
C9-C10-C64	118.9(13)	C9-C10-H10	120.5
C64-C10-H10	120.5	C12-C11-C9	118.7(12)
C12-C11-H11	120.7	C9-C11-H11	120.7
C13-C12-C11	121.5(13)	C13-C12-H12	119.2
C11-C12-H12	119.2	C12-C13-C64	119.5(13)
C12-C13-H13	120.2	C64-C13-H13	120.2
C15-C14-C19	120.2(9)	C15-C14-P1	124.5(8)
C19-C14-P1	115.3(7)	C14-C15-C16	119.2(9)
C14-C15-H15	120.4	C16-C15-H15	120.4
C17-C16-C15	121.3(10)	C17-C16-H16	119.4
C15-C16-H16	119.4	C16-C17-C18	118.9(11)
C16-C17-H17	120.6	C18-C17-H17	120.6
C19-C18-C17	120.5(10)	C19-C18-H18	119.8
C17-C18-H18	119.8	C18-C19-C14	119.8(10)
C18-C19-H19	120.1	C14-C19-H19	120.1
C21-C20-C25	117.6(10)	C21-C20-P4	121.1(8)
C25-C20-P4	121.2(8)	C20-C21-C22	122.8(12)
C20-C21-H21	118.6	C22-C21-H21	118.6
C23-C22-C21	117.0(14)	C23-C22-H22	121.5
C21-C22-H22	121.5	C22-C23-C24	122.9(13)
C22-C23-H23	118.6	C24-C23-H23	118.6
C25-C24-C23	117.9(13)	C25-C24-H24	121.1
C23-C24-H24	121.1	C24-C25-C20	121.8(12)
C24-C25-H25	119.1	C20-C25-H25	119.1
F6-C26-F4	109.7(11)	F6-C26-F5	105.8(10)
F4-C26-F5	105.4(10)	F6-C26-S2	112.0(8)
F4-C26-S2	112.2(8)	F5-C26-S2	111.4(9)

Table 4 *(cont.)*

C28-C27-C32	118.8(9)	C28-C27-P4	120.9(7)
C32-C27-P4	120.3(8)	C29-C28-C27	121.0(10)
C29-C28-H28	119.5	C27-C28-H28	119.5
C28-C29-C30	120.4(11)	C28-C29-H29	119.8
C30-C29-H29	119.8	C29-C30-C31	120.0(10)
C29-C30-H30	120	C31-C30-H30	120
C32-C31-C30	120.1(10)	C32-C31-H31	119.9
C30-C31-H31	119.9	C31-C32-C27	119.7(10)
C31-C32-H32	120.2	C27-C32-H32	120.2
C35-C33-C34	122.0(11)	C35-C33-H33	119
C34-C33-H33	119	C38-C34-C33	118.0(10)
C38-C34-P3	124.9(8)	C33-C34-P3	117.1(8)
C33-C35-C36	120.1(11)	C33-C35-H35	119.9
C36-C35-H35	119.9	C37-C36-C35	119.5(11)
C37-C36-H36	120.3	C35-C36-H36	120.3
C36-C37-C38	121.1(11)	C36-C37-H37	119.4
C38-C37-H37	119.4	C34-C38-C37	119.2(10)
C34-C38-H38	120.4	C37-C38-H38	120.4
C40-C39-C0K	120.7(10)	C40-C39-P3	123.1(9)
C0K-C39-P3	116.2(8)	C39-C40-C41	118.3(12)
C39-C40-H40	120.9	C41-C40-H40	120.9
C42-C41-C40	121.8(12)	C42-C41-H41	119.1
C40-C41-H41	119.1	C41-C42-C43	118.6(12)
C41-C42-H42	120.7	C43-C42-H42	120.7
C42-C43-C0K	120.9(13)	C42-C43-H43	119.6
C0K-C43-H43	119.6	N3-C44-N4	110.8(8)
N3-C44-P3	122.9(7)	N4-C44-P3	126.3(7)
N4-C45-H45A	109.5	N4-C45-H45B	109.5
H45A-C45-H45B	109.5	N4-C45-H45C	109.5
H45A-C45-H45C	109.5	H45B-C45-H45C	109.5
N4-C46-C47	131.1(9)	N4-C46-C65	106.9(8)
C47-C46-C65	122.0(9)	C48-C47-C46	117.1(10)
C48-C47-H47	121.5	C46-C47-H47	121.5
C47-C48-C49	121.1(9)	C47-C48-H48	119.4
C49-C48-H48	119.4	C50-C49-C48	121.3(10)
C50-C49-H49	119.4	C48-C49-H49	119.4
C49-C50-C65	117.7(10)	C49-C50-H50	121.2
C65-C50-H50	121.2	F3-C51-F1	108.9(11)
F3-C51-F2	107.7(12)	F1-C51-F2	104.9(10)
F3-C51-S1	113.8(9)	F1-C51-S1	111.3(9)
F2-C51-S1	109.8(8)	C53-C52-C54	119.6(9)

Table 4 *(cont.)*

C53-C52-P2	120.1(8)	C54-C52-P2	120.3(7)
C57-C53-C52	120.2(11)	C57-C53-H53	119.9
C52-C53-H53	119.9	C55-C54-C52	120.0(10)
C55-C54-H54	120	C52-C54-H54	120
C54-C55-C56	119.1(11)	C54-C55-H55	120.4
C56-C55-H55	120.4	C57-C56-C55	121.0(11)
C57-C56-H56	119.5	C55-C56-H56	119.5
C53-C57-C56	120.0(11)	C53-C57-H57	120
C56-C57-H57	120	C63-C58-C59	118.6(11)
C63-C58-P2	121.4(9)	C59-C58-P2	119.8(9)
C60-C59-C58	121.9(12)	C60-C59-H59	119.1
C58-C59-H59	119.1	C59-C60-C61	120.1(13)
C59-C60-H60	120	C61-C60-H60	120
C60-C61-C62	119.2(13)	C60-C61-H61	120.4
C62-C61-H61	120.4	C63-C62-C61	122.3(14)
C63-C62-H62	118.8	C61-C62-H62	118.8
C62-C63-C58	117.8(13)	C62-C63-H63	121.1
C58-C63-H63	121.1	C13-C64-C10	120.2(14)
C13-C64-H64	119.9	C10-C64-H64	119.9
N3-C65-C50	130.8(9)	N3-C65-C46	108.3(8)
C50-C65-C46	120.8(8)	C43-C0K-C39	119.6(12)
C43-C0K-H0K	120.2	C39-C0K-H0K	120.2
S1-O1-Ag3	132.4(4)	S1-O3-Ag1	137.9(4)
S2-O4-Ag4	136.7(4)	S2-O6-Ag2	131.5(4)
P4-O7-Ag4	118.7(4)	P4-O7-Ag2	124.4(4)
Ag4-O7-Ag2	97.8(2)	P4-O8-Ag3	112.6(3)
P4-O8-Ag1	107.3(3)	Ag3-O8-Ag1	92.2(2)
P2-O9-Ag2	113.2(3)	P2-O9-Ag4	107.4(3)
Ag2-O9-Ag4	93.4(2)	P2-O10-Ag1	117.6(3)
P2-O10-Ag3	122.7(3)	Ag1-O10-Ag3	99.2(2)
O1-S1-O2	114.0(5)	O1-S1-O3	115.3(5)
O2-S1-O3	115.3(5)	O1-S1-C51	101.7(5)
O2-S1-C51	105.1(6)	O3-S1-C51	103.0(6)
O5-S2-O6	114.6(5)	O5-S2-O4	114.9(5)
O6-S2-O4	115.4(5)	O5-S2-C26	103.0(5)
O6-S2-C26	103.3(5)	O4-S2-C26	103.3(5)

Table 5

*Anisotropic atomic displacement parameters (Å2) for **5**.*

	U11	**U22**	**U33**	**U23**	**U13**	**U12**
Ag1	0.0254(4)	0.0200(4)	0.0557(5)	0.0059(4)	0.0135(3)	-0.0040(3)
Ag2	0.0236(4)	0.0176(4)	0.0487(5)	0.0041(3)	0.0110(3)	-0.0041(3)
Ag3	0.0240(4)	0.0177(4)	0.0469(5)	0.0028(3)	0.0108(3)	-0.0034(3)
Ag4	0.0269(4)	0.0188(4)	0.0537(5)	0.0045(4)	0.0126(3)	-0.0056(3)
N1	0.028(4)	0.007(4)	0.044(5)	-0.002(3)	0.014(4)	-0.004(3)
N2	0.029(4)	0.007(4)	0.059(6)	-0.002(4)	0.010(4)	-0.001(3)
N3	0.034(4)	0.016(4)	0.038(5)	0.000(4)	0.018(4)	-0.005(3)
N4	0.016(4)	0.015(4)	0.054(5)	0.001(4)	0.013(4)	-0.002(3)
P1	0.0222(11)	0.0137(13)	0.0384(14)	0.0002(10)	0.0095(10)	-0.0031(9)
P2	0.0264(12)	0.0156(13)	0.0345(13)	-0.0017(10)	0.0134(10)	-0.0027(9)
P3	0.0229(11)	0.0163(13)	0.0388(14)	0.0019(11)	0.0093(10)	-0.0022(9)
P4	0.0259(12)	0.0181(13)	0.0358(14)	0.0005(11)	0.0131(10)	-0.0017(9)
C1	0.023(4)	0.016(5)	0.042(6)	0.001(4)	0.012(4)	-0.002(4)
C2	0.035(5)	0.013(5)	0.060(7)	0.000(5)	0.021(5)	-0.009(4)
C3	0.024(5)	0.022(6)	0.044(6)	0.004(5)	0.007(4)	0.002(4)
C4	0.027(5)	0.028(6)	0.071(8)	0.009(6)	0.007(5)	-0.009(4)
C5	0.021(5)	0.034(7)	0.091(10)	0.004(6)	0.005(6)	0.000(4)
C6	0.045(6)	0.020(6)	0.077(9)	0.005(6)	0.010(6)	0.005(5)
C7	0.037(6)	0.019(6)	0.063(7)	0.005(5)	0.015(5)	0.004(4)
C8	0.026(5)	0.010(5)	0.048(6)	0.004(4)	0.009(4)	-0.002(4)
C9	0.017(4)	0.027(6)	0.067(7)	-0.002(5)	0.025(5)	-0.011(4)
C10	0.095(11)	0.029(7)	0.066(9)	-0.006(6)	0.032(8)	-0.020(7)
C11	0.056(7)	0.021(6)	0.062(8)	-0.005(5)	0.019(6)	0.003(5)
C12	0.089(10)	0.017(7)	0.094(12)	-0.009(7)	0.033(9)	0.007(6)
C13	0.145(16)	0.031(9)	0.082(12)	-0.037(8)	0.033(11)	-0.009(9)
C14	0.030(5)	0.011(5)	0.040(6)	-0.003(4)	0.008(4)	-0.005(4)
C15	0.029(5)	0.031(6)	0.043(6)	-0.005(5)	0.014(4)	0.003(4)
C16	0.044(6)	0.030(6)	0.050(7)	0.001(5)	0.024(5)	0.003(5)
C17	0.047(7)	0.041(7)	0.049(7)	0.009(6)	0.016(5)	0.000(5)
C18	0.032(6)	0.048(8)	0.052(7)	0.011(6)	0.000(5)	0.009(5)
C19	0.028(5)	0.036(7)	0.049(7)	0.008(5)	0.012(5)	-0.005(4)
C20	0.036(5)	0.023(6)	0.035(5)	0.000(4)	0.011(4)	-0.006(4)
C21	0.057(7)	0.025(6)	0.063(8)	-0.010(6)	0.010(6)	0.003(5)
C22	0.115(13)	0.030(8)	0.051(8)	-0.012(6)	0.012(9)	-0.011(8)
C23	0.124(15)	0.058(11)	0.045(8)	-0.006(8)	0.009(9)	-0.037(10)
C24	0.048(7)	0.076(11)	0.056(8)	0.004(8)	-0.014(6)	-0.032(7)
C25	0.041(6)	0.038(7)	0.056(7)	-0.001(6)	0.005(5)	-0.010(5)
C26	0.045(7)	0.034(7)	0.061(8)	0.010(6)	0.016(6)	-0.002(5)

Table 5 *(cont.)*

	U11	U22	U33	U23	U13	U12
C27	0.030(5)	0.018(5)	0.033(5)	-0.006(4)	0.013(4)	-0.002(4)
C28	0.035(5)	0.032(6)	0.029(5)	0.003(5)	0.005(4)	-0.004(4)
C29	0.059(7)	0.040(7)	0.040(6)	0.001(5)	0.021(6)	-0.013(6)
C30	0.058(7)	0.044(7)	0.052(7)	-0.002(6)	0.037(6)	-0.014(6)
C31	0.033(6)	0.034(7)	0.080(9)	-0.012(6)	0.031(6)	-0.012(5)
C32	0.037(5)	0.018(6)	0.047(6)	0.002(5)	0.012(5)	0.002(4)
C33	0.022(5)	0.059(8)	0.060(8)	0.020(6)	0.010(5)	-0.003(5)
C34	0.030(5)	0.013(5)	0.041(6)	0.001(4)	0.005(4)	-0.005(4)
C35	0.035(6)	0.070(10)	0.061(8)	0.030(7)	0.000(6)	-0.011(6)
C36	0.061(8)	0.033(7)	0.042(6)	0.002(5)	0.010(6)	-0.012(6)
C37	0.055(7)	0.046(8)	0.052(7)	-0.015(6)	0.027(6)	-0.007(6)
C38	0.039(6)	0.033(7)	0.050(7)	-0.001(5)	0.020(5)	0.004(5)
C39	0.034(5)	0.015(5)	0.045(6)	0.002(4)	0.013(4)	0.010(4)
C40	0.055(7)	0.025(7)	0.066(8)	0.001(6)	0.023(6)	0.003(5)
C41	0.076(9)	0.018(7)	0.090(11)	-0.009(7)	0.034(8)	-0.004(6)
C42	0.072(9)	0.033(8)	0.090(11)	-0.021(7)	0.032(8)	0.009(6)
C43	0.107(12)	0.063(11)	0.051(8)	-0.006(8)	0.028(8)	0.009(9)
C44	0.022(4)	0.013(5)	0.042(6)	-0.003(4)	0.014(4)	-0.002(4)
C45	0.032(5)	0.018(6)	0.058(7)	0.000(5)	0.015(5)	-0.008(4)
C46	0.028(5)	0.025(6)	0.036(5)	-0.003(4)	0.012(4)	-0.003(4)
C47	0.027(5)	0.025(6)	0.065(7)	0.004(5)	0.016(5)	-0.004(4)
C48	0.027(5)	0.041(7)	0.070(8)	-0.004(6)	0.016(5)	0.000(5)
C49	0.027(5)	0.032(6)	0.060(7)	-0.005(5)	0.007(5)	0.010(4)
C50	0.036(5)	0.027(6)	0.044(6)	-0.003(5)	0.012(5)	-0.007(4)
C51	0.056(8)	0.040(8)	0.060(8)	0.010(6)	0.018(7)	-0.010(6)
C52	0.030(5)	0.015(5)	0.035(5)	-0.003(4)	0.015(4)	0.001(4)
C53	0.033(5)	0.028(6)	0.052(7)	0.003(5)	0.015(5)	0.000(4)
C54	0.041(6)	0.025(6)	0.046(6)	-0.002(5)	0.016(5)	0.000(5)
C55	0.063(8)	0.031(7)	0.048(7)	0.002(5)	0.025(6)	-0.002(5)
C56	0.070(9)	0.029(7)	0.085(10)	-0.016(7)	0.049(8)	-0.017(6)
C57	0.038(6)	0.043(7)	0.066(8)	-0.006(6)	0.024(6)	-0.007(5)
C58	0.044(6)	0.031(6)	0.031(5)	0.003(5)	0.013(5)	-0.013(5)
C59	0.061(7)	0.020(6)	0.051(7)	-0.012(5)	0.026(6)	0.001(5)
C60	0.102(12)	0.029(7)	0.069(9)	-0.018(7)	0.041(9)	-0.016(7)
C61	0.083(10)	0.059(10)	0.058(9)	-0.033(8)	0.018(8)	-0.031(8)
C62	0.068(10)	0.082(12)	0.071(10)	-0.017(9)	-0.009(8)	-0.022(9)
C63	0.044(7)	0.047(8)	0.066(9)	-0.018(7)	0.002(6)	-0.012(6)
C64	0.17(2)	0.058(11)	0.052(9)	-0.017(8)	0.025(11)	0.007(11)
C65	0.019(4)	0.016(5)	0.039(5)	0.000(4)	0.004(4)	0.000(4)
C0K	0.072(8)	0.030(7)	0.048(7)	-0.003(6)	0.025(6)	-0.003(6)

Table 5 *(cont.)*

	U11	**U22**	**U33**	**U23**	**U13**	**U12**
F1	0.094(6)	0.056(5)	0.070(5)	0.021(4)	0.025(5)	-0.009(4)
F2	0.088(6)	0.096(7)	0.067(6)	0.000(5)	0.006(5)	-0.025(5)
F3	0.107(7)	0.086(7)	0.093(7)	0.002(5)	0.062(6)	0.023(6)
F4	0.073(5)	0.123(8)	0.061(5)	-0.020(5)	0.014(4)	-0.036(5)
F5	0.094(6)	0.046(5)	0.067(5)	0.020(4)	0.030(4)	-0.007(4)
F6	0.109(7)	0.083(7)	0.088(6)	0.008(5)	0.061(6)	0.029(5)
O1	0.024(3)	0.042(5)	0.056(5)	0.012(4)	0.005(3)	-0.002(3)
O2	0.031(4)	0.036(5)	0.090(6)	0.006(4)	0.023(4)	0.012(3)
O3	0.037(4)	0.028(4)	0.080(6)	0.022(4)	0.016(4)	-0.004(3)
O4	0.048(4)	0.026(4)	0.065(5)	0.020(4)	0.015(4)	-0.001(3)
O5	0.029(4)	0.034(5)	0.077(6)	0.001(4)	0.016(4)	0.009(3)
O6	0.017(3)	0.045(5)	0.048(4)	0.007(4)	0.005(3)	0.001(3)
O7	0.026(3)	0.022(4)	0.051(4)	-0.003(3)	0.020(3)	-0.001(3)
O8	0.028(3)	0.019(4)	0.040(4)	0.000(3)	0.014(3)	0.000(3)
O9	0.033(4)	0.019(4)	0.041(4)	0.003(3)	0.017(3)	-0.001(3)
O10	0.027(3)	0.014(3)	0.047(4)	-0.007(3)	0.018(3)	-0.005(3)
S1	0.0246(12)	0.0262(15)	0.0579(17)	0.0124(13)	0.0156(11)	0.0054(10)
S2	0.0245(11)	0.0233(14)	0.0513(16)	0.0072(12)	0.0131(11)	0.0027(10)

Note. The anisotropic atomic displacement factor exponent takes the form: -2π2[h2 a*2 U11 + ... + 2 hka* b* U12]

Table 6

Hydrogen atomic coordinates and isotropic atomic displacement parameters (Å2) for **5**.

	x/a	**y/b**	**z/c**	**U(eq)***
H2A	0.2554	-0.0534	0.1936	0.052
H2B	0.2236	-0.0335	0.2451	0.052
H2C	0.3021	-0.0487	0.2586	0.052
H4	0.1331	0.0626	0.1886	0.053
H5	0.0676	0.1876	0.1465	0.061
H6	0.1162	0.3233	0.1338	0.059
H7	0.2312	0.3442	0.1667	0.047
H10	0.3903	0.0529	0.1463	0.074
H11	0.4285	-0.1193	0.2812	0.055
H12	0.41	-0.2405	0.2172	0.078
H13	0.3819	-0.2179	0.1194	0.103
H15	0.3212	0.056	0.3379	0.04
H16	0.3339	-0.0082	0.4281	0.047
H17	0.4333	-0.0716	0.4788	0.054
H18	0.5262	-0.0611	0.4415	0.056
H19	0.5144	0.001	0.3523	0.045
H21	0.5384	0.1405	0.1101	0.059
H22	0.4761	0.0491	0.0361	0.082
H23	0.3639	0.0847	-0.0052	0.095
H24	0.3147	0.2076	0.0253	0.079
H25	0.3803	0.3006	0.0969	0.056
H28	0.4986	0.3992	0.0603	0.039
H29	0.5682	0.4634	0.0137	0.054
H30	0.6825	0.4602	0.0549	0.056
H31	0.7269	0.4023	0.148	0.055
H32	0.6582	0.3308	0.1937	0.041
H33	0.4866	0.6726	0.16	0.057
H35	0.4665	0.7262	0.0671	0.07
H36	0.5492	0.7191	0.0203	0.056
H37	0.6505	0.6525	0.066	0.058
H38	0.6738	0.6015	0.1624	0.047
H40	0.5963	0.7882	0.2295	0.057
H41	0.609	0.908	0.2944	0.071
H42	0.6145	0.8836	0.3914	0.076
H43	0.6009	0.7394	0.4218	0.087
H45A	0.7647	0.7146	0.2971	0.053
H45B	0.7006	0.7116	0.242	0.053
H45C	0.7724	0.687	0.2354	0.053

Table 6 *(cont.)*

	x/a	**y/b**	**z/c**	**U(eq)***
H47	0.8716	0.5907	0.2985	0.046
H48	0.9369	0.4687	0.3419	0.055
H49	0.8876	0.339	0.3675	0.049
H50	0.7725	0.3265	0.3464	0.043
H53	0.3449	0.3499	0.3234	0.044
H54	0.5033	0.2443	0.4442	0.044
H55	0.431	0.1754	0.4887	0.055
H56	0.3157	0.1878	0.4466	0.067
H57	0.2734	0.2782	0.3665	0.056
H59	0.4628	0.532	0.397	0.05
H60	0.5181	0.6213	0.4714	0.076
H61	0.6238	0.5856	0.5244	0.08
H62	0.6732	0.4569	0.5031	0.095
H63	0.6186	0.3628	0.4282	0.066
H64	0.3813	-0.0724	0.0833	0.116
H0K	0.5912	0.6173	0.3585	0.058

* U(eq) is defined as one third of the trace of the orthogonalized Uij tensor.